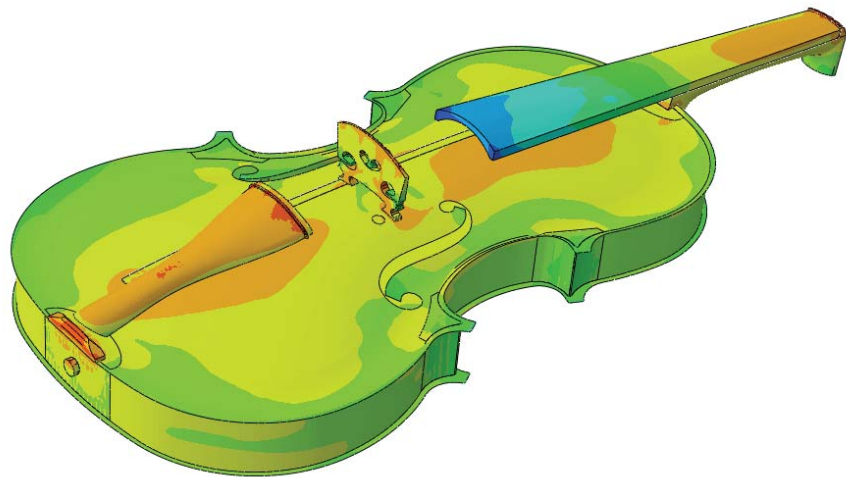# LUND
UNIVERSITY

EXPERIMENTAL CHARACTERIZATION AND COMPUTATIONAL DYNAMIC MODELLING OF A VIOLIN
Analysing the effects of creep and string tension

ERIK TUNLID and JOEL VÄRELÄ

Structural Mechanics

Master's Dissertation

EXPERIMENTAL CHARACTERIZATION AND COMPUTATIONAL DYNAMIC MODELLING OF A VIOLIN

Analysing the effects of creep and string tension

ERIK TUNLID and JOEL VÄRELÄ

Abstract

During the 17th and early 18th century Antonio Stradivari built around 900 violins, that still today are considered some of the best instruments ever created. The theories of how it was possible for a luthier active 300 years ago to create instruments of this quality are many, including unique wood properties and secret building techniques.

The sound of a violin is produced by vibrations from the strings that are transmitted to the top plate and bottom plate through the bridge. The plates and the air in the cavity reverberate within the hollow body, producing the tone characteristic of the violin. Dynamic properties are therefore directly connected to the quality of the instrument.

A top and back plate was provided by luthier Robert Zuger. Experimental modal analysis (EMA) was carried out on the plates using the roving excitation technique to determine their modal parameters. Based on the geometries of the plates FE-models of the plates were created. By studying the results of the EMA, material parameters of the plates could be determined in such a way that the modal contents of the FE-plates matched those of the real plates. The natural frequencies for the first 5 modes, extracted from the FE-model, matched those of the real plates within 7 % and the same mode shapes were prevalent in both the FE-analysis and the EMA.

Based on violin drawings and input from Robert Zuger a FE-model of a complete violin was created which was tuned by tensioning the strings. The model uses non-linear geometry to handle the effects of string tension. A time-hardening creep model is implemented which can be used to study the aging process of violins.

The steady-state response to excitations of the strings were preformed to determine the response of the violin up to 1000 Hz. The mean displacements of the plates were calculated to indicate at which frequencies volume changes of the violin cavity occurred. Each string excitation revealed frequency spans in which the volume change appeared particularly large.

Preface

This master thesis concludes our five years of studies at the Faculty of Engineering at Lund University. The thesis was carried out at the Division of Structural Mechanics and we would like to extend our thanks to both staff members and fellow students at the division for making the last few months both exciting and enjoyable.

We would like to extend a special thanks to Robert Zuger, the initiator of this project. Without his vast knowledge on the subject, and the material he generously lent to us, this thesis could not have been possible.

Lastly, we would like to thank our supervisor Professor Kent Persson for granting us support and guidance, helping us see this thesis through to the end.

Table of Contents

List of Figures

List of Tables

1 Introduction

1.1 Background

During the 17th and early 18th century Antonio Stradivari built around 1100 instruments in Cremona Italy, of those 1110 around 900 where violins. Even today, these violins are considered to be some of the best instruments ever built. Unfortunately, the craftmanship was lost with time and during centuries instruments of the same quality was not built. There have been a lot of theories regarding how a luthier, who lived 300 years ago could create instruments of this quality, ranging from unique properties in the wood to closely guarded trade secrets.

Violins are complicated structures. There are a lot of different parts working together creating a unique sound. The sound of a violin is produced by vibrations from the strings that are transmitted to the top plate and back plate through the bridge. The plates reverberate within the air filled cavity, producing the tone characteristic of the violin. The geometric shape of the violin and the material properties have a large influence on the eigenmodes and resonance frequencies, which in turn determines the harmonic content that gives the violin its unique voice.

Various specimens of wood show very different material properties. The direction of the cut and the position of the specimen in the cross-section of the tree are both factors that contribute to the range of strength seen in wood (Persson, 2000). To add to the complicated geometry and material, the strings induce large stresses on the violin body creating large deformations in the plates, leading to non-linear geometrics (Knot, et al., 1989).

With the introduction of the finite element (FE) method the possibility to model and analyse the unique qualities of the instruments have increased substantially. A lot of research has gone into creating FE-models to research the impact of geometric parameters as well as material properties on the quality of the violin. As early as 1989 FE-softwares were used to perform modal analyses of the different parts of the violin. The modes of frequency from the analysis matched the modes from test results well, both for analysis's performed on the two plates as well as the full violin (Knot, et al., 1989)

How different parameters effect modes of vibration was studied by Gough (2015). The parameters included the effect of boundary conditions, freely supported and edge constrained, the influence of shape, including thickness and arching height as well as material anisotropy. Pyrkosz (2013) used a reverse engineering approach to effectively create a FE-model that represented the *Titian* Stradivari. The model was based on a CT-scan of the actual *Titian* Stradivari violin.

Robert Zuger, violin maker and designer, which this project is done in collaboration with, have through the years come up with some geometric properties that he believes have a large impact on the harmonic content of the violin. It's based on theories regarding the way violins where built in the 17th century. To add to this, the effect of time dependent phenomena such as material creep has to be a factor to consider when understanding the properties of old violins.

All the studies mentioned have contributed to the understanding the dynamic properties of the violin. The aim of this project is to contribute to the previously done research by effectively creating a FE-model of the complete instrument, but to focus on some new factors including creep effects.

1.2 Aim and Objectives

The objective of this study is to create a FE-model of a complete violin, including tensioned strings, that can be used to perform analyses to study the static and dynamic behaviour of the instrument, and to study creep effects. The analyses performed focuses on changes in behaviour in a long-time perspective as well as its dynamic preparties. This is done by modelling the effects of creep and preforming modal and steady-state analyses.

The developed model can be used in future studies to examine the influence of geometric design on total characteristics of the violin

1.3 Method

A FE-model of a violin was created in Abaqus CAE, a software where you can perform FE-calculations. Material parameters of the model was calibrated by performing an experimental modal analysis. With a model of the full instrument created and calibrated different analyses are performed, including steady state dynamics and long-term creep analysis. The process is outlined below:

- Creating a geometric model of a violin in Abaqus. Basis for the model are an actual backplate and a top plate designed by Zuger, cad-models and performed measurements on the provided plates.

- Performing an experimental modal analysis on the top and back plate to obtain the modal characteristics of the plates.

- Calibrating the FE-model from the measured modal parameters of the plates by modifying material properties of the parts.

- Pre-stressing the strings, effectively "tuning" the instrument to obtain a complete FE-model of the violin.

- Performing analyses on the calibrated model to examine the behaviour of the violin. Steady state analysis is done to study the behaviour of the violin when it's being played. Creep analysis is used to study the behavoiur of the violin over time.

1.4 Limitations

- As experimental modal analysis was only preformed on a top and back plate, those are the only parts whose modal characteristics could truly be verified. In order to verify the complete FE-model, a violin would have to be constructed using the plates so that experimental modal analysis could be performed on the complete violin. Given the timescale of this project this was not possible and no comparison with a complete violin was made.

- A violin is composed of many different sorts of wood making the gathering of material parameters which could not be tested troublesome. A single species of wood can display a large variation. Creep parameters for maple and spruce, and strength parameters for ebony and pine are interpreted from previous studies.

- Some of the greatest violins played today were built in the 17th and 18th century. Considering that timescale, the creep model used cannot be guaranteed to accurately reflect the behaviour of a real violin.

- In order to extract accurate amplitudes from a steady-state analysis of the complete violin, damping parameters need to be defined for the participating modes of the whole violin body. As no experimental modal analysis could be performed on a complete violin, these parameters could not be properly defined. 5 % structural damping were used for all modes.

- The force applied to the string by the bow is not a pure sinusoidal force as applied in the present analysis. The repeated process of the string sticking and slipping from the bow causes what is called a Helmholtz motion of the string which was not created for in the strings here.

2 The violin parts and geometric model

2.1 Function of the main violin parts

Before creating a FE-model of a violin it is important to present the different parts of the violin and their function. A sketch describing the different parts of the violin is presented in Figure 2.1.

Every part in the violin has specific functions. Some of the functions are trivial, like the neck is needed to get a certain length of the strings to obtain a playable instrument. The blocks increase the strength of the instrument (Carlö & Sanborn, 1965). The design of the fingerboard is created to achieve an instrument that can be played sufficiently. One must be able to reach the lower part of the strings.

The sound created from the violin starts with the bow stroking the strings causing them to vibrate. The vibration itself does not create much sound, but in a violin the vibration is transmitted through the bridge into the violin body. The bridge is designed to transmit frequencies up to 4 kHz (Wolfe, u.d.). Since the vibration is transmitted through the bridge its position is critical. It is placed between the f-holes, which connects the air inside the instrument with the air outside the instrument. The body itself transmit the vibration from the strings into a vibration of the air around the violin causing the sound. The ribs together with the plates create the violin box. It is the plates that are the main sound generating components. The sound post connects the two plates, it increases the stability of the instrument and couples the vibration of the plates. The bass bar stabilizes the top plate in the longitudinal direction, directly affecting the deformation of the top plate and thereby the tonal content of the violin. The saddles are used to obtain the correct position of the strings.

The type of wood used for the parts are usually spruce for the top plate, bass bar, blocks and sound post. Maple for the back plate, ribs, neck and the bridge. Ebony for the finger board and saddles. The tail piece can be created in plastics or ebony (Dagnell & Sarnell, 1988).
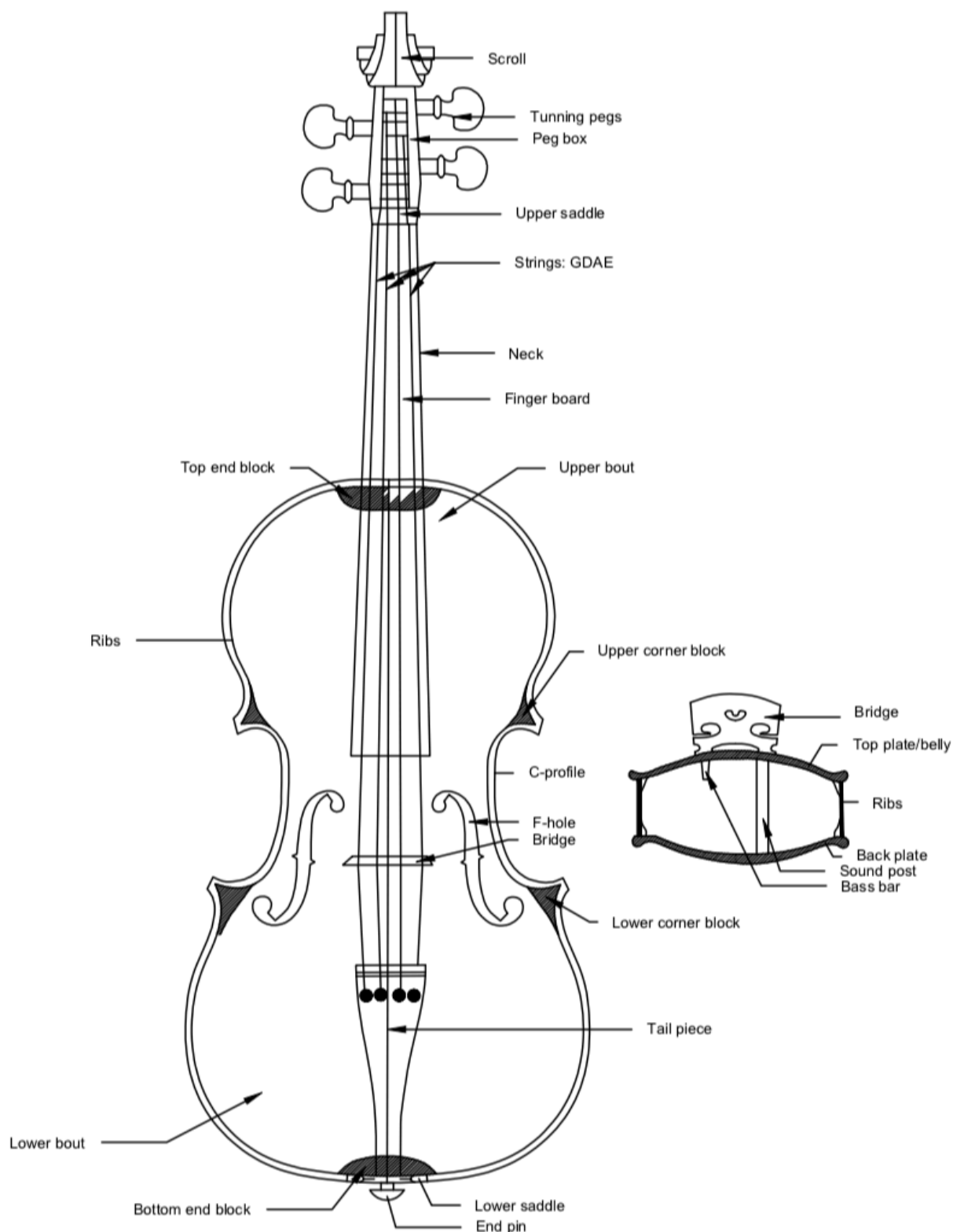
Figure 2.1: Sketch of a violin with the names of the different parts.

A geometric model of the complete violin is to be created in Abaqus. This chapter is divided into subheadings for the different parts. Since the pegbox and scroll don't have any acoustic attributes that effect the analysis done in this project, they are not modelled.

Information regarding the violin parts is gathered from Dagnell & Sarnell (1988), Carlö & Sanborn (1965) and Riechers (1928), three books used by luthiers. Where the information given in the literature is not sufficient enough R. Zuger is asked for his input.

2.2   Geometric models of top and back plate

The basis of modelling the plates are two plates designed by R. Zuger (Figure 2.2). Besides the plates a CAD-model of the inner camber is also provided by R. Zuger. The top and back plate is modelled with shell elements. Since the plates have two surfaces, the interior surface and the exterior surface, a choice has to be made as for which surface to model. In this project the exterior surface is chosen, since the camber profile of the provided CAD-model is of the exterior surface. The interior surface is obtained by inserting the correct thickness of the plates.

Figure 2.2: Violin plates. Created and provided by R. Zuger.

A geometric property that Zuger has found on old violins, including Stradivari violins, is what he calls STLs. STLs are straight lines found on the top and back plate. If the curvature of the plates is created in a certain way a straight line separates the concave from the convex arching shape (Zuger, 2012b). The STLs are found on both the front and back side of the plates. In total there are four STL on each side of a plate. If created correctly, the STLs on the front and back side are to be placed directly on top of eachother. The plates created and provided by Zuger, which was the basis of the model are made so that they have STLs. The STLs are drawn onto the plates in Figure 2.2.

Zuger has performed research regarding the implications of STLs and arching shape on the performance of violins. The implications of arching shape and STLs in particular on the quality of the violin is out of the scope of this project. For information regarding the impact of STL on the violins performance the reader is referred to *The impact of Arching Shape on Structural Deflections* (Zuger 2012b).

2.2.1 The camber shape of the plates
The camber of the plates is made with a special technique produced by R. Zuger. The basis of this technique is described in Zuger (2012a).

The camber shape is built up by six transversal arches and one longitudinal arch. The location of the transversal arches is decided by what Zuger calls the base lines. There are 5 transversal arches in total. The base lines are the red lines in Figure 2.3. Information on how to create the base lines is found in Zuger (2012a).
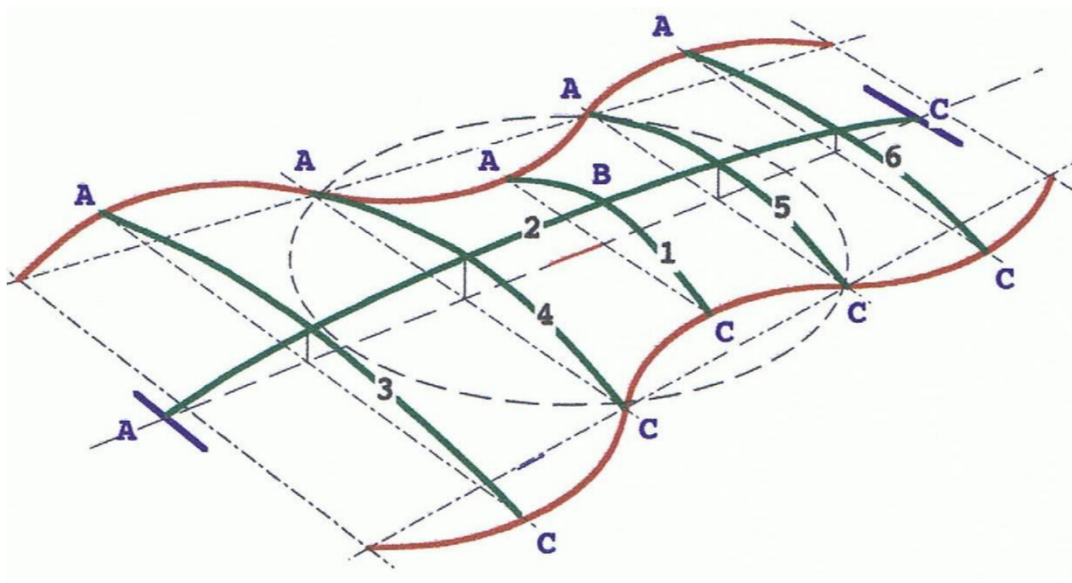
Figure 2.3: Drawing of the arching shape, built up by six transversal arches and one longitudinal. The red lines are what Zuger calls the base lines used for the position of the arches (Zuger, 2012a).

The first arch, at the centre of the plates is obtained by creating an equilateral triangle with the triangle base between the base lines. A circle is created with the height of triangle being the radius to the circle. By putting a compass at the top of the created triangle, where the triangle touch the circle and drawing a circle segment through the other corners of the triangle, the height of the first arch is found (Zuger, 2012a), see Figure 2.4.
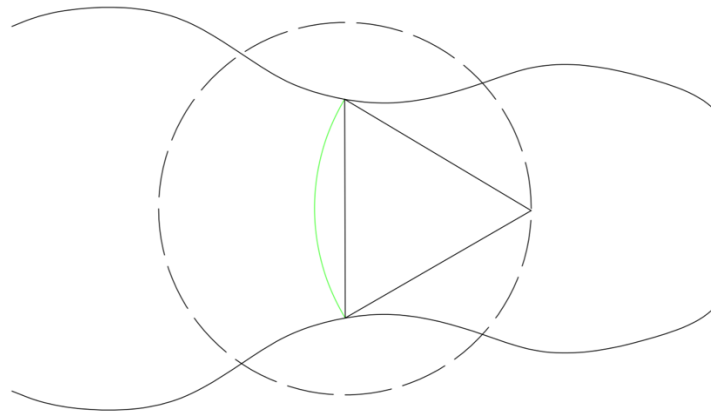
Figure 2.4: The first arch is obtained by creating an equilateral triangle. By drawing a circle segment through the corners of the triangle the arch height is found.

With the height of the middle transversal arch known and the by using the length of the instrument it's possible to create the longitudinal arch by drawing a circle arch. After the longitudinal arch is drawn the rest of the transversal arches are created. The CAD-model provided by Zuger is created by using this technique and it's used as the basis of the model.

Outside the "inner camber" there is a region called the scope (Zuger, 2012a), it's a region, at the outline of the plates where the concave shape of the inner camber turns into a convex shape, see Figure 2.5.

Figure 2.5: Cross-section of one of the plates. The concave shape turns into a convex shape close to the outline.

The position of where the concave shape turns into a convex shape may vary, it does not have to be at an isoline around the instrument (Zuger, 2012a). Close to the C-profile the length of the convex profile is much shorter compared to at the top or base of the plate.

The lowest point and the thickness at the edge are found by using a dial indicator on the provided plates. With the two coordinates known, depicted as red points in Figure 2.5, it's possible to find the convex shape. This method is used around the plates and the coordinates are added to Abaqus.

2.2.2 Outline shape
The outline shape of the plates is created by scanning one of the plates and importing the scan to Autocad. From the scanned profile the outline shape is created by using circle segments. At the intersection of two circles they share the same tangent to create a smooth outline (Figure 2.6). The outline shape is implemented into Abaqus.
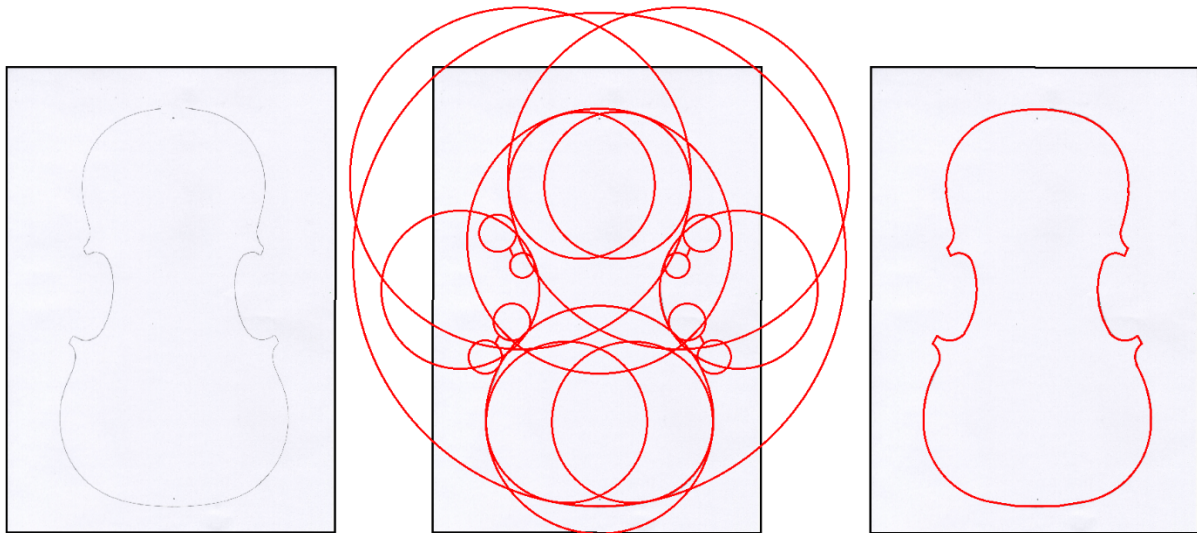
Figure 2.6: The process of creating the outline shape of the plates using circle segments.

2.2.3   Thickness of the plates

The thickness of the violin plates is not constant, instead it varies over the plates. In Knot, et al (1989) a variation from 4.5 mm at the centrum of the back plate to 2.6 mm closer to the edges is used, creating a thickness map over the plates. The same type of maps is presented in Dagnell & Sarnell (1988). Gough (2015) uses both uniform thickness and linear increase of thickness with the thinnest part being 2 mm. There is consensus for some aspects, the back plate is for instance thicker compared to the top plate in general (Dagnell & Sarnell, 1988).

One possibility to model the thickness is to use regions with varying thickness. To obtain a numerical simulation model that behaves close to an actual violin created with the provided plates it is critical that the thickness of the plates in the model is as close to the actual thickness of the plates as possible. Therefore, the thickness was measured using a dial indicator. With the dial indicator the thickness can be measured at a hundredth of a millimetre. Circles, with radius of 20 mm steps are drawn onto both plates, see Figure 2.7. The reason for using circles, and not just a ruler is that it is easier to get an exact position on the plate with a circular coordinate system compared to a rectangular one. The setup used to measure the thickness of the plates is displayed in Figure 2.9.

Figure 2.7: A circular coordinate system is used when determining the thickness of the plates.

Centrum of the circles are at the centre of the plates. Measuring points are added onto the circle borders with the use of a protractor, see Figure 2.8.

Figure 2.8: The position on the circles are measured using a protractor.

Figure 2.9: Dial indicator setup used to measure the thickness of the plates.

The distance between the measuring points on each circle edge is determined by the degrees on the protractor. Different values are chosen to get an even spread of the measuring points over the plates (
Table *2.1*). On the top plate the thickness was measured at 115 points. The thickness of the back plate was measured at 126 points.

Table 2.1: The distance between measuring points on the circles. The centre of the circles is at the centre of the plates in the longitudinal direction.

Radius of the circle [mm]	Degrees between measuring points on the circle edge [°]
20	45
40	30
60	15
80	10
100	10
120	10
140	5
160	5

With the thickness measured in each measuring point a mapped field is defined in Abaqus. From this field the thickness at each nodal point can be defined. Abaqus uses linear interpolation between mapped points to create the full thickness field (Dassault Systèmes, 2012). The resulted thickness for the plates is presented in Figure 2.10.
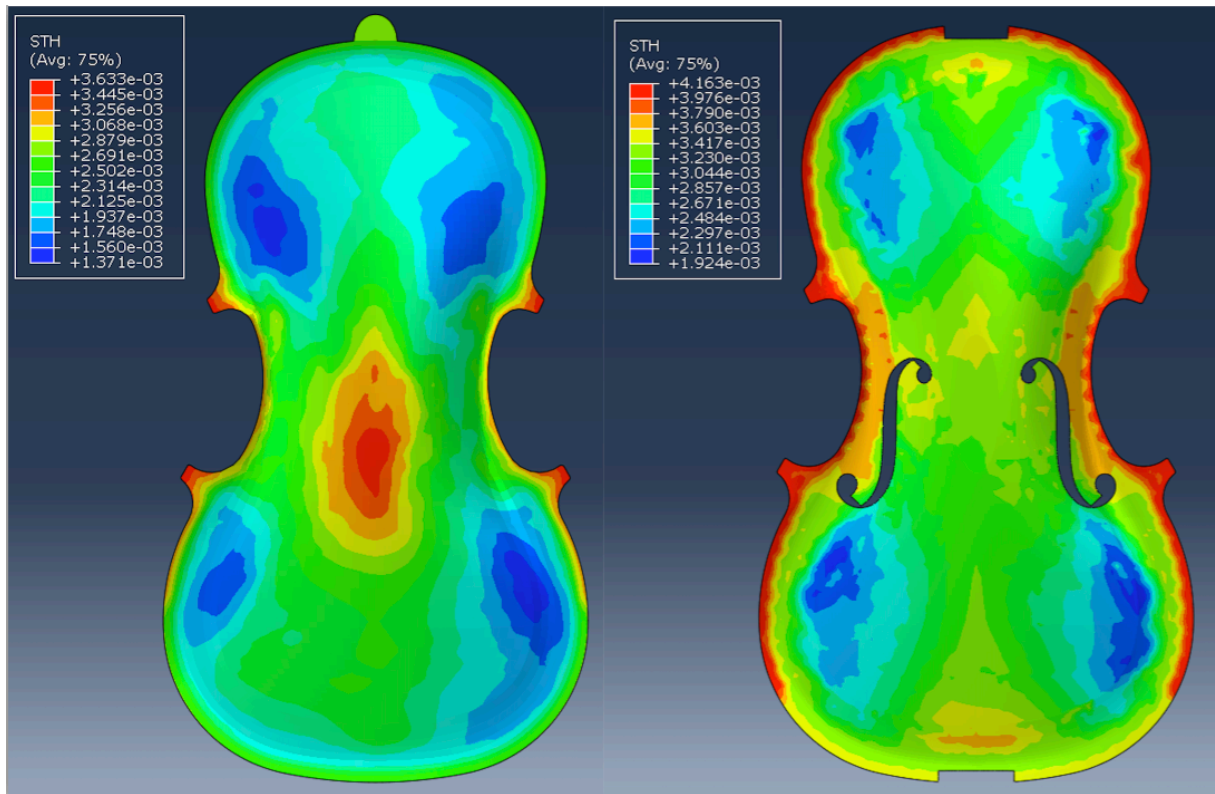
Figure 2.10: Nodal distribution field depicting the thickness of the plates.

The complete geometric model of the plates is presented in Figure 2.11.
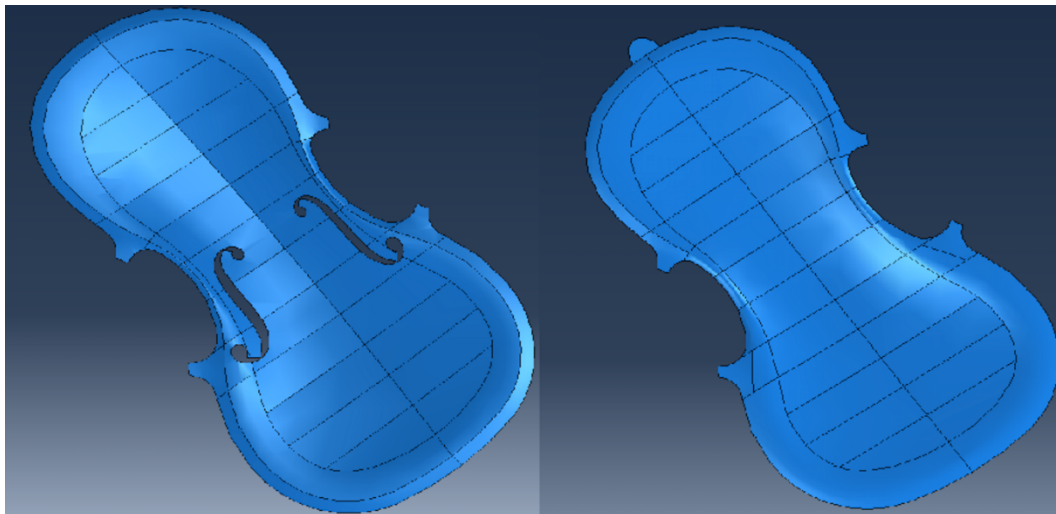
Figure 2.11: Geometric model of the plates.

2.3 Bass bar

There are a couple of rules for the placement and measurements for the bass bar. It's placed under the left foot of the bridge and should be obliquely positioned so it doesn't cover the f-holes. Another benefit of the oblique positioning is to decrease the risk of cracking of the belly around the bass bar (Dagnell & Sarnell, 1988). The length and position in the longitudinal direction is presented in Figure 2.12 below. The measurements are collected from Dagnell & Sarnell (1988).
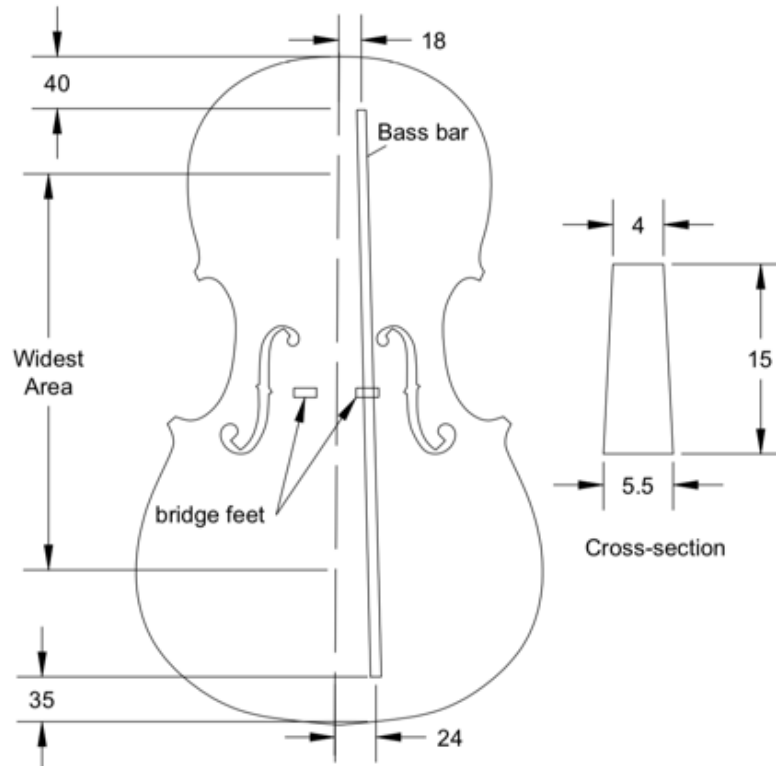
Figure 2.12: Position of the bass bar. All measurements are in mm.

The bass bar must match the curvature of the belly precisely. To obtain the shape, the "footprint" of the bass bar on the belly is the starting point from which the rest of the shape is created, using the measurements presented in Figure 2.12.

The bass bar (Figure 2.13), is modelled as a solid.
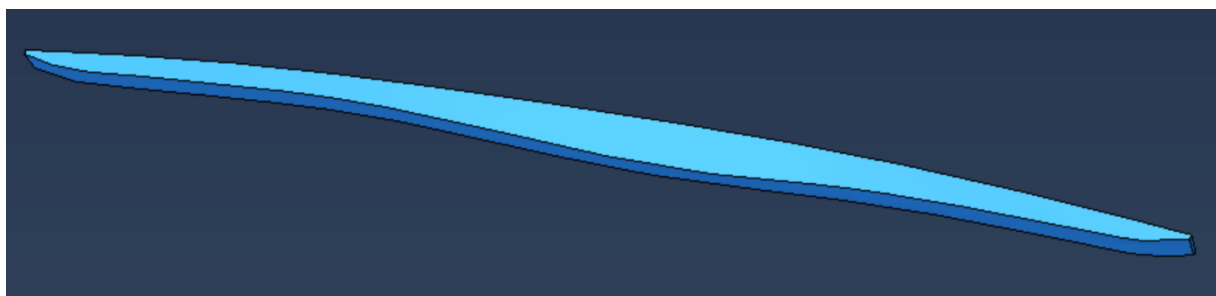
Figure 2.13: Geometric model of the bass bar.

2.4   Sound post

The sound post's shape is cylindrical and is placed behind the right bridge foot, towards the lower bout of the violin. The sound post is 6,0 mm in diameter. The position of the sound post is presented in Figure 2.14 (Dagnell & Sarnell, 1988).
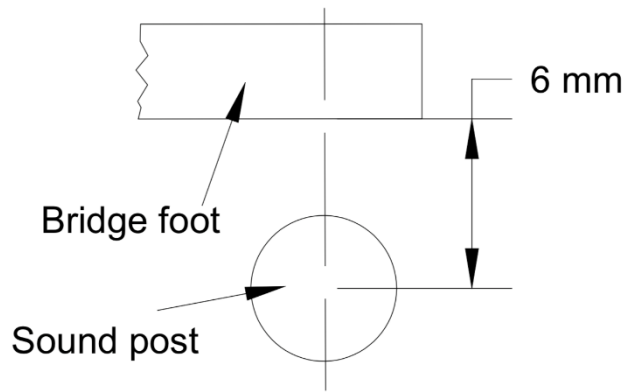
Figure 2.14: Position of the sound post with regard to the bridge foot.

The sound post is modelled as a solid. As done for the bass bar, the sound post has to match the curvature of the belly and back plate exactly. This is obtained in the same manner as for the bass bar. The geometric model of the sound post is presented in Figure 2.15.
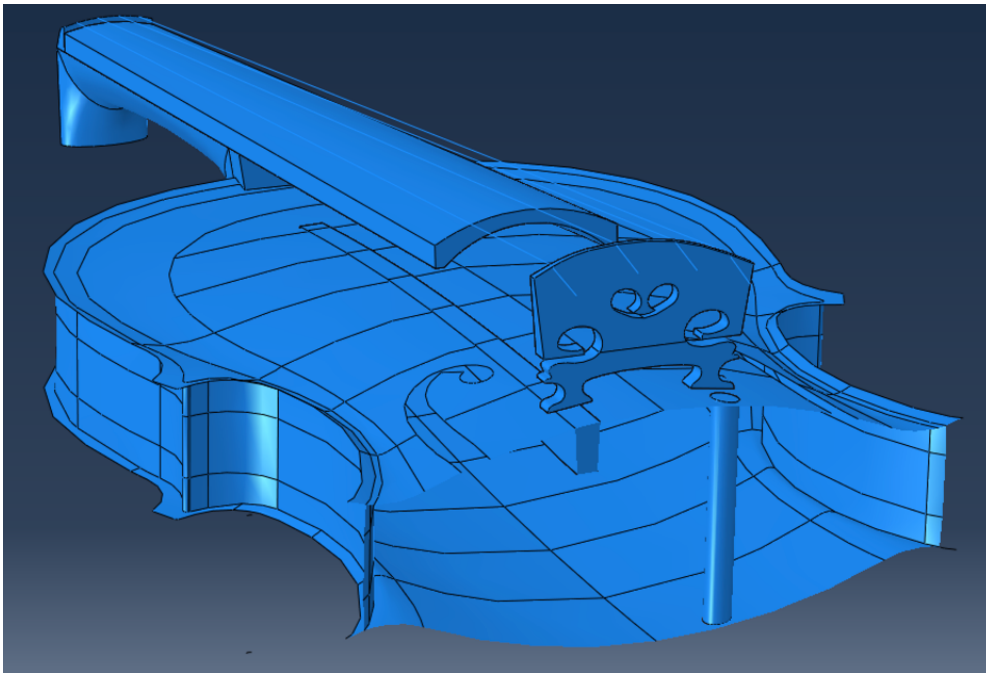
Figure 2.15: Geometric model of the sound post at is position behind the bridge.

2.5   Ribs

The height of the ribs is 28,5 mm. As for the belly and the back plate the ribs are very thin, between 1,0 and 1,2 mm (Dagnell & Sarnell, 1988). Because of this the ribs are modelled as a shell. At the top and bottom of the ribs there is a strip. The shape of the strip is presented in Figure 2.16 (Dagnell & Sarnell, 1988)
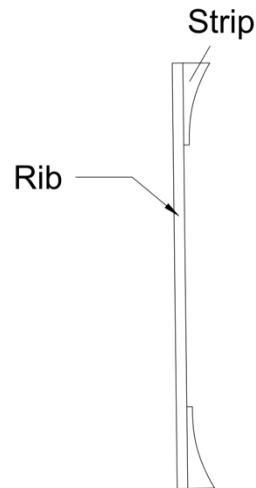
Figure 2.16: Cross-section of the rib and strip structure.

There are different approaches on how to model the strips. The material orientation and type of material of the strip is not the same as the ribs (Dagnell & Sarnell, 1988). Pyrkosz (2013) uses a composite property definition where the rib, strip and the glue in between are modelled. The benefit of using this approach is that no extra geometry needs to be modelled while the effect of the strip is accounted for in the model. Composite property definition is used in this project, the difference from Pyrkosz (2013) is that the glue is not modelled.

The geometric model of the ribs is presented in Figure 2.17.
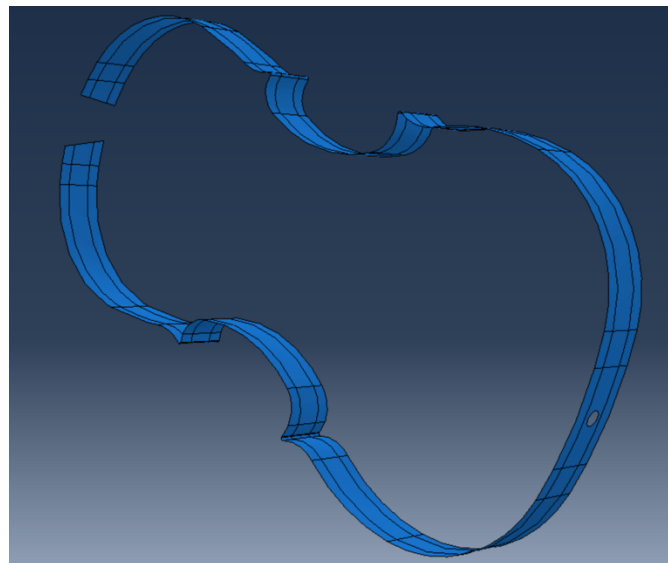
Figure 2.17: Geometric model of the ribs. The strips are modelled using composite property definition

2.6 Bridge

There is not an unambiguous design of the bridge. The design used differ between different luthiers (Dagnell & Sarnell, 1988). In Dagnell & Sarnell (1988) the width at the bridge feet is set to approximately 42 mm, in Carlö & Sanborn (1965) it's set to 43 mm and in Riechers (1928) it's set to 40 mm. The different bridge designs used by luthiers in not only based on the performance of the bridge but also the aesthetics. The bridge should both be functional as well as aesthetically pleasing.

There is consensus on certain aspects. The bridge feet must follow the exact curvature of the top plate. The position of the bridge is 195 mm from the upper bout. The thickness of the bridge varies over the height, at the bridge feet it's 4-4,5 mm (Dagnell & Sarnell, 1988) and at the top 1,5 mm (Riechers, 1928), see Figure 2.18.
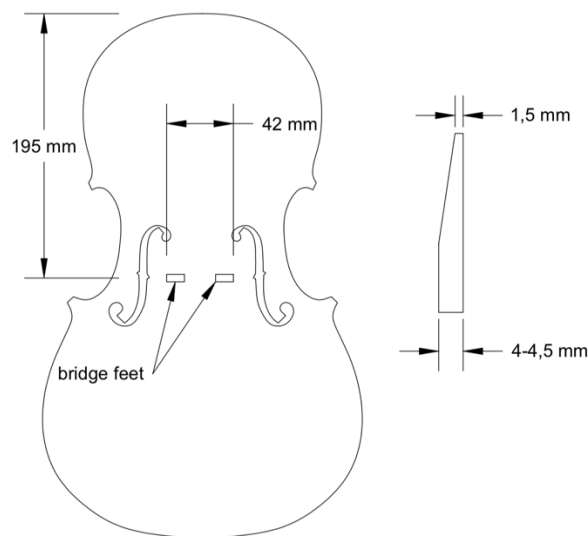
Figure 2.18: The bridge position on the belly and the thickness variation.

The height and curvature of the bridge have a large impact on the playability of the violin. The height of the bridge is determined from the string height above the fingerboard. In Dagnell & Sarnell (1988) the recommendations are 4,5-5 mm for the G-string and 2,5-3 mm for the E-string. This is done to prevent the strings from vibrating against the fingerboard when the violin is played. The mutual distance between the strings should be 11-11,5 mm. The A- and D-string should have a higher position compared to the G- and E-string. The layout from Dagnell & Sarnell (1988) is presented in Figure 2.19.
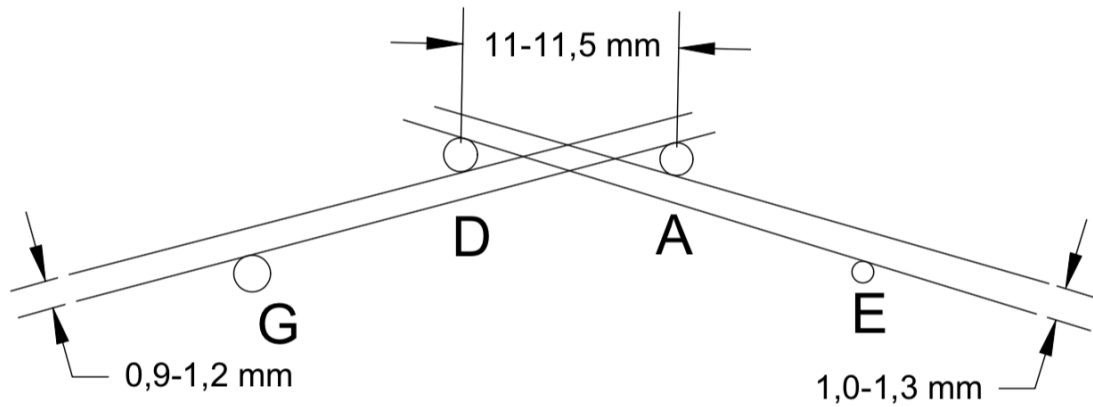
Figure 2.19: Layout from the strings which determines the curvature at the top of the bridge.

The final bridge design is presented in Figure 2.20. It is modelled as a solid.
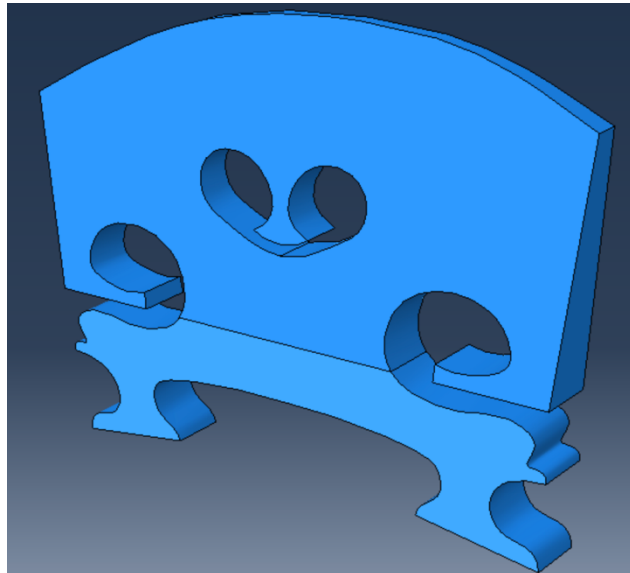
Figure 2.20: Geometric model of the bridge.

2.7 Neck

The length of the neck has to be designed to achieve the correct string length. The full free string length should be 325 mm. Since the bridge is placed 195 mm from the upper edge the neck has to be designed so the free string length over the neck becomes 130 mm. This gives a ratio between the lengths of 2:3 which is desirable (Dagnell & Sarnell, 1988) (Carlö & Sanborn, 1965) (Riechers, 1928). To be able to join the neck to the body, 7 mm are added which is slotted into an indentation on the top end block, the actual length of the neck then becomes 137 mm, see Figure 2.21.
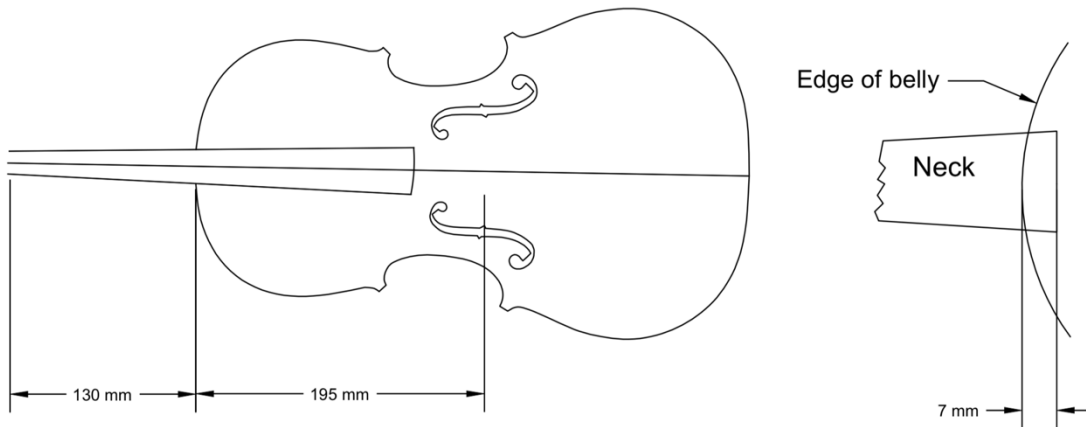
Figure 2.21: The length of the neck. It should be shaped so that the free string length is becomes 325 mm. 7 mm are added to attach the neck to the violin body.

The edge that's attached to the violin body is created with an angle of 86°. The rest of the design of the neck is taken from Dagnell & Sarnell (1988), see Figure 2.22. It should also be mentioned that the shape of the violin neck is critical for the feel of playing the instrument, how it lies in your hand etc. (Carlö & Sanborn, 1965). Of course, this is not as important for a FE-model.
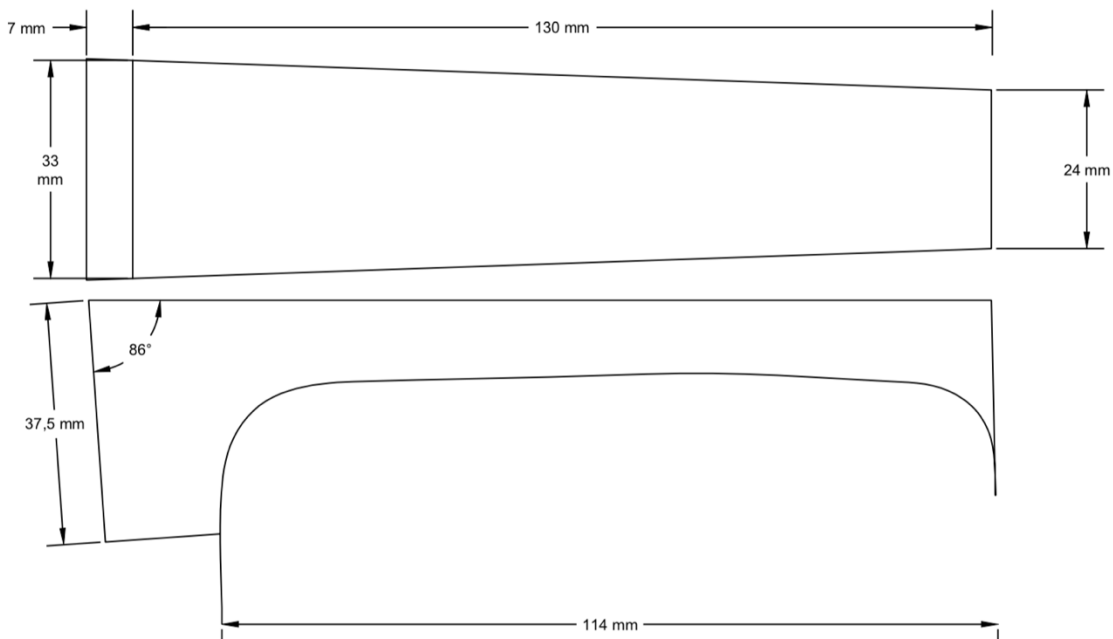
Figure 2.22: Measurements of the neck. The top sketch is a plane view and the bottom sketch is a cut view.

The height, 37,5 mm (Figure 2.22) at the connection to the violin body is a result of a 5 mm free height above the belly (Figure 2.23). Since the ribs are 28,5 mm high and the thickness of the belly is 4 mm at the edge, the resulted height is 37,5 mm.

19
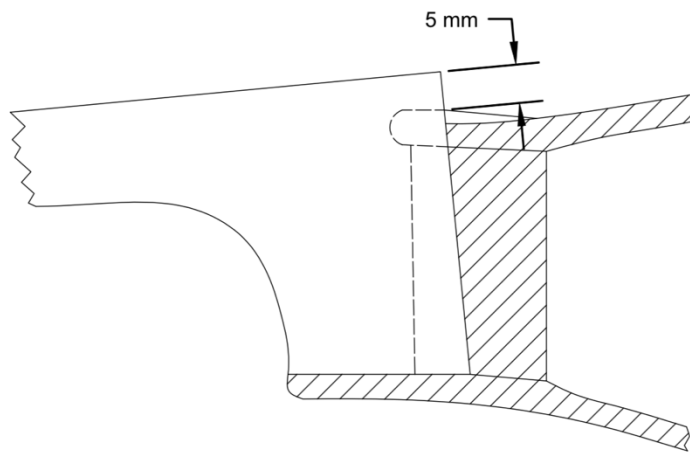
Figure 2.23: The height where the neck is attached to the violin body comes from a 5 mm free height above the belly.

The neck is modelled as a solid, see Figure 2.24 for the geometric model.
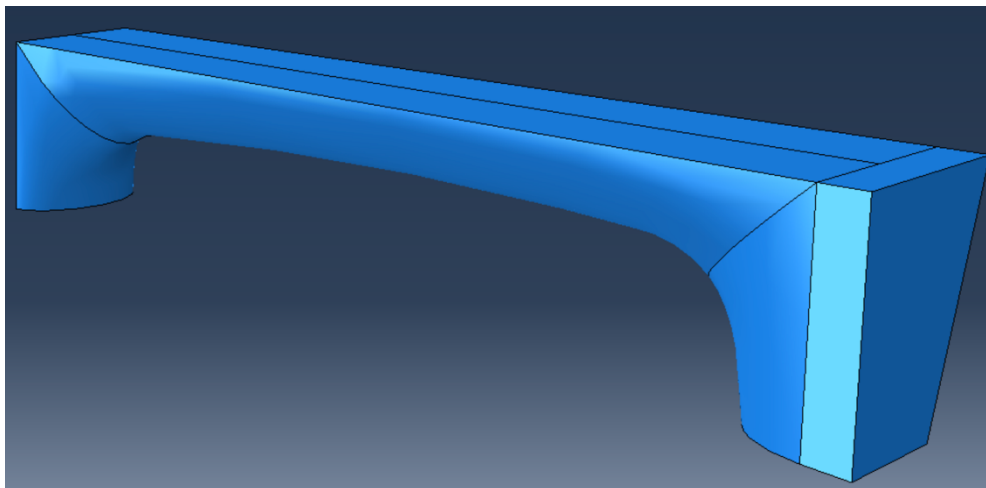
Figure 2.24: Geometric model of the neck.

2.8   Fingerboard

The position of the fingerboard is on the top of the neck. The measurements are collected from Dagnell & Sarnell (1988). A sketch of the cross-sections at the pegs and towards the bridge are presented in Figure 2.25.
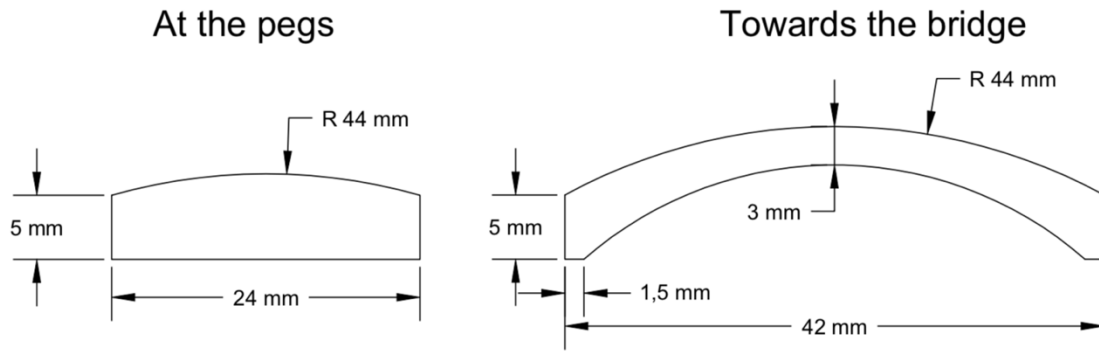
Figure 2.25: Cross-sections of the fingerboard.

In the longitudinal direction the fingerboard follows the shape of the neck. A sketch of the fingerboard in the longitudinal direction is presented in Figure 2.26.
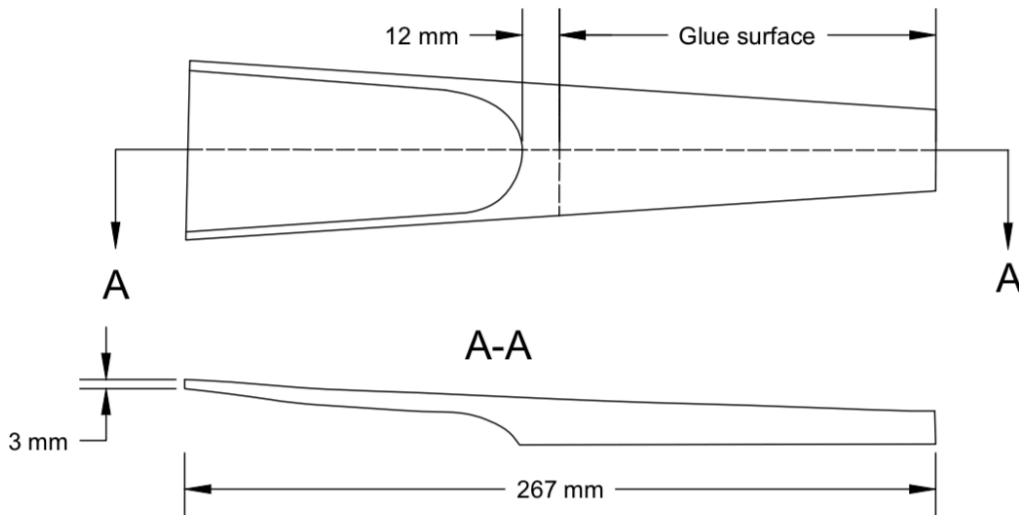
Figure 2.26: Sketch of the fingerboard in the longitudinal direction.

The complete geometric model of the fingerboard is presented in Figure 2.27. It is modelled as a solid.

Figure 2.27: Geometric model of the fingerboard.

21

2.9 Tailpiece

The tailpiece is often factory made, which limits the information regarding the measurements. Some information is available. The curvature closest to the bridge should have the same curvature as the bridge (Riechers, 1928). The distance between the bridge and the tailpiece saddle should be approximately 55 mm, see Figure 2.28.
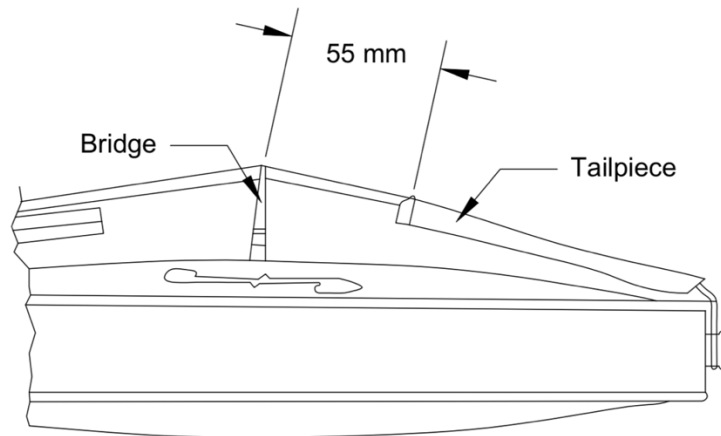
Figure 2.28: The tailpiece is placed so that the distance between the saddle of the tailpiece and the bridge is approximately 55 mm.

The rest of the measurements are obtained from an actual tailpiece and with some consultation with Zuger. The final geometric model of the tailpiece is presented in Figure 2.29. The tailpiece is modelled as a solid.
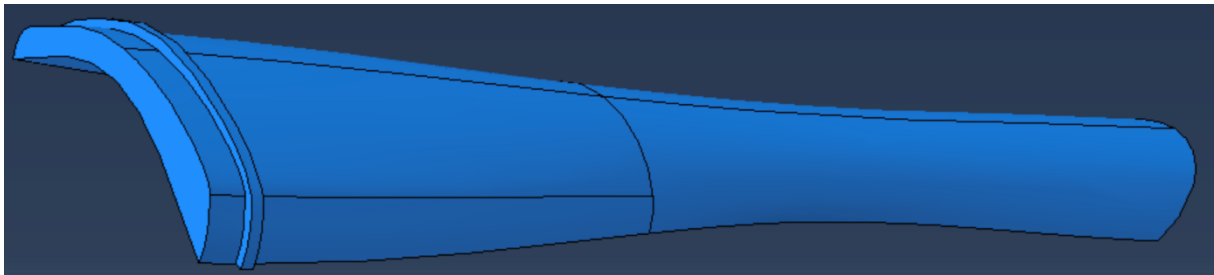
Figure 2.29: Geometric model of the tailpiece.

2.10 Blocks

In total there are six blocks. One at the lower bout, one at the upper bout and four at each corner of the c-profiles (Figure 2.30). The measurements of the blocks are measured from a drawing of a Stradivari violin from 1720.
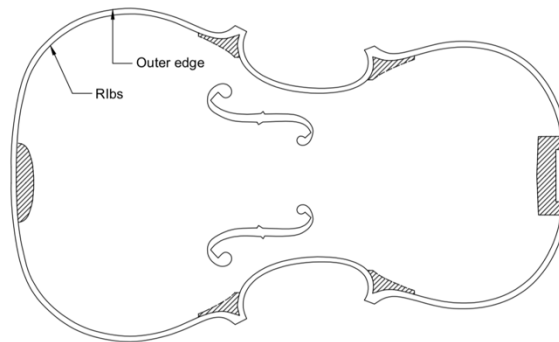
Figure 2.30: The position of the blocks.

Cuts are done in the bottom end block and the top end block to fit the end pin and the neck. For the geometric model of the blocks, see Figure 2.31. They are modelled as solids.
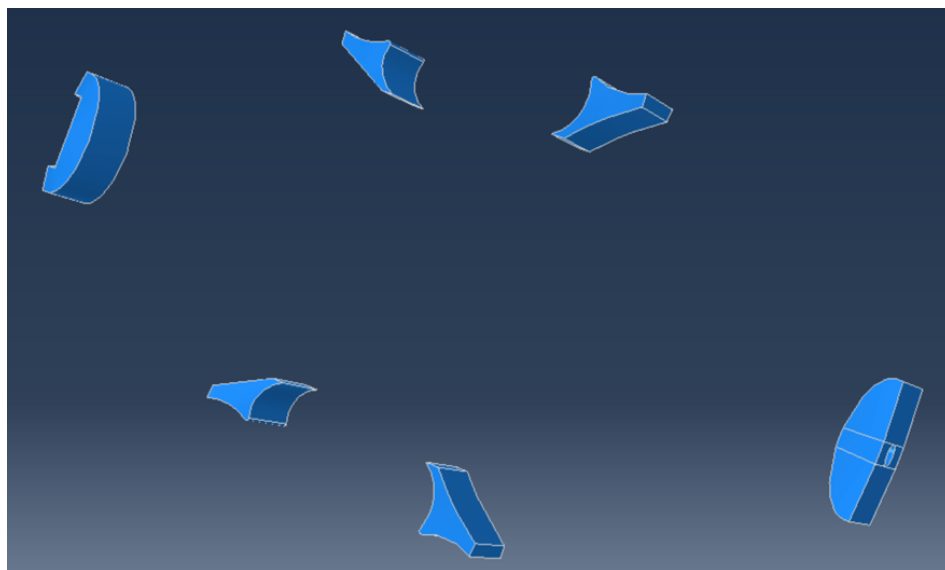
Figure 2.31: Geometric model of the blocks.

2.11 End pin

The end pin is modeled as a solid. It is created to fit the hole in the bottom end block. The geometric model is shown in Figure 2.32.
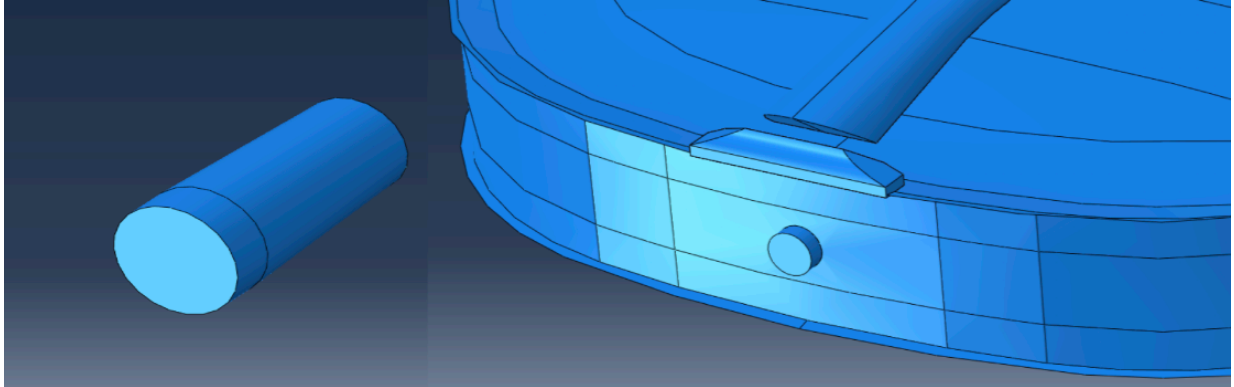
Figure 2.32: Geometric model of the end pin and its position at the bottom end block.

2.12 Upper and lower saddle

Both the upper and lower saddle is modelled using solid elements. The shape and measurements of the saddles are collected from Dagnell & Sarnell (1988). The length of the lower saddle is 38 mm, it's 6 mm thick and 7 mm high (Figure 2.33).
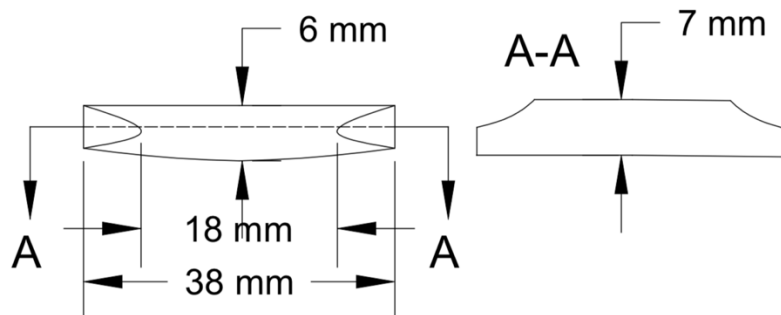
Figure 2.33: Measurements for the lower saddle.

The curvature of the upper saddle should match the curvature of the fingerboard. The height of the upper saddle is set so it's 1,5 mm higher than the fingerboard (Dagnell & Sarnell, 1988). The measurements of the upper saddle are presented in Figure 2.34.
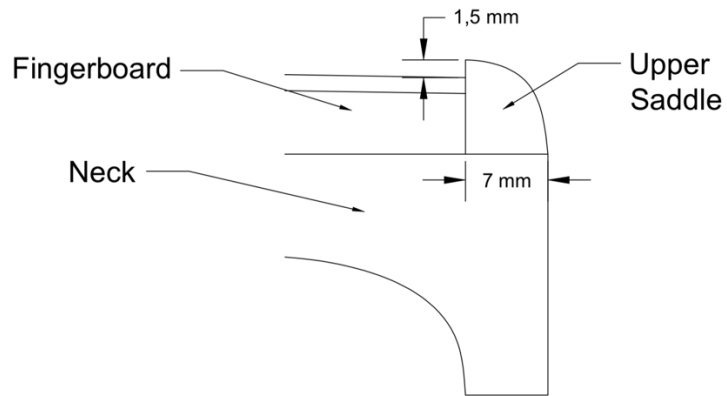
Figure 2.34: Measurements for the upper saddle. The curvature follows the curvature of the fingerboard.

The geometric models of the saddles are shown in Figure 2.35 and Figure 2.36. They are modelled as solids.
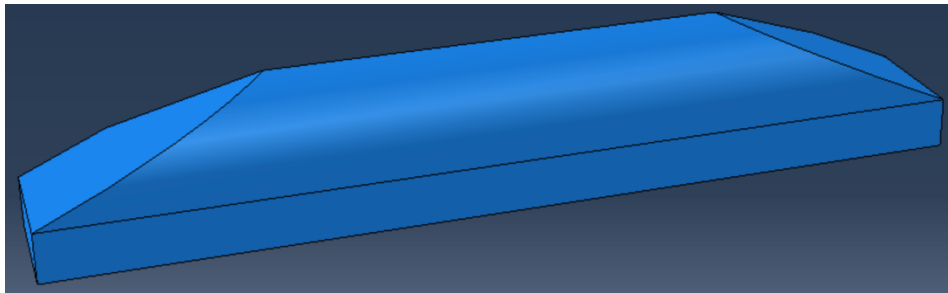
Figure 2.35: Geometric model of the lower saddle.
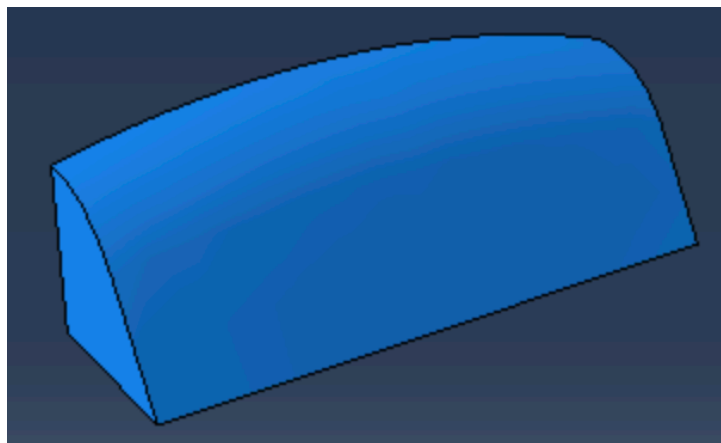
Figure 2.36: Geometric model of the upper saddle.

2.13 Strings

The strings are modelled wires. There are four strings in total G-, D-, A- and the E-string. The total length of the strings is determined from the length between the upper saddle and the bridge plus 55 mm, see Figure 2.28. The core diameter of the strings is collected from Knot, et al (1989) and presented in Table 2.2.

Table 2.2: Core diameter of the strings (Knot, et al., 1989).

String	Core diameter [mm]
G	0,6
D	0,46
A	0,33
E	0,27

2.14 Complete geometric model

With all the parts geometry created, they are assembled and the complete geometric model of the instrument is obtained. The result of the complete model is presented in Figure 2.37. As mentioned in previously the pegbox and scroll are not included in the model.
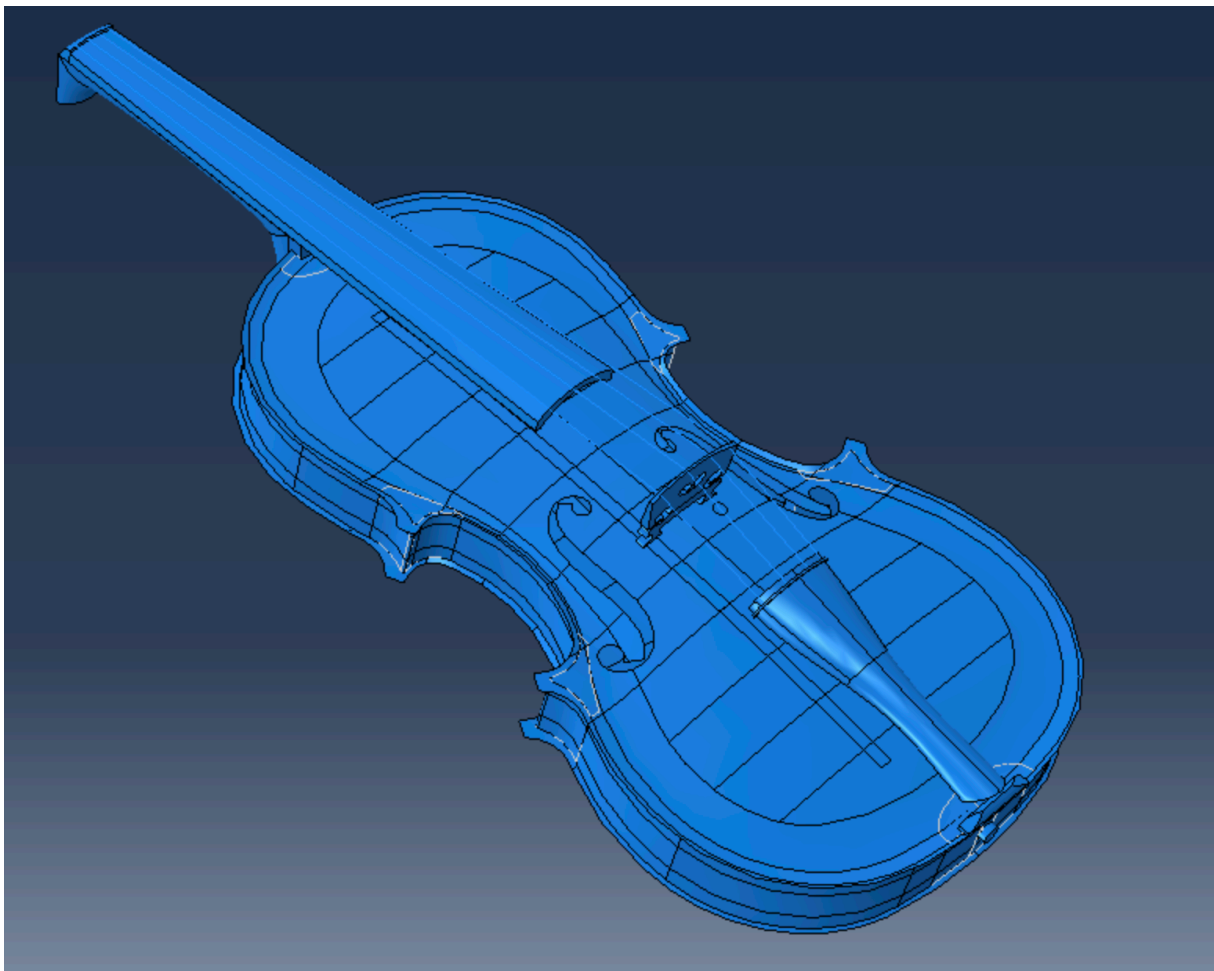
Figure 2.37: The assembled geometric model of the complete violin.

3 Material properties of wood used in violins

In this chapter theory regarding wood is presented and how the choices of wood specimens may affect the material properties of the violin. It also focuses on the types of wood used in violins and what material properties luthiers search for. Material parameters used in previously done studies is also presented.

3.1 General theory regarding material properties of wood

Wood has a complicated material structure, both between different trees and within the same tree material properties can differ substantially. If one looks at a cross section, there are a few macro structures present. In the centre there is the pith, which is encircled by the heartwood. Outside the heartwood there is sapwood followed by the cambium and outmost the bark (Burström, 2007).

The growing process of wood takes place in the cambium. The properties of the new wood differ depending on the growing season leading to annual rings. Growth during the spring is often rapid creating wider sections called springwood. Summerwood is created after the springwood, where the growth is slower. The slower growth leads to better mechanical properties for the summerwood compared to the springwood (Burström, 2007).

The structure of wood materials leads to anisotropic behaviour. There are three main directions that are perpendicular to each other.

1) Longitudinal direction – along the fibres
2) Radial direction – perpendicular to the longitudinal direction and the annual rings
3) Tangential direction – perpendicular to the longitudinal direction but tangential to the annual rings

The directions are presented in Figure 3.1.
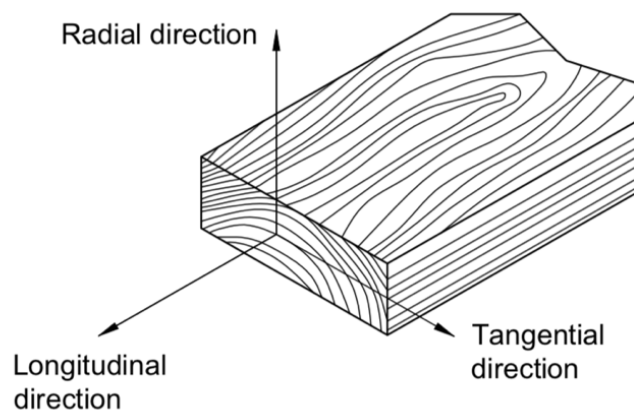
Figure 3.1: Wood has three main directions. Longitudinal, radial and tangential direction.

Because of woods three main directions, leading to three symmetry planes it can be modelled as an orthotropic material that follow Hooke's law below the limit of proportionality (Persson, 2000). A linear elastic orthotropic material has the following compliance matrix, **C**.

$$\boldsymbol{\varepsilon} = \boldsymbol{C} \cdot \boldsymbol{\sigma} \rightarrow \boldsymbol{C} = \begin{bmatrix} \frac{1}{E_L} & -\frac{v_{RL}}{E_R} & -\frac{v_{TL}}{E_T} & 0 & 0 & 0 \\ -\frac{v_{LR}}{E_L} & \frac{1}{E_R} & -\frac{v_{TR}}{E_T} & 0 & 0 & 0 \\ -\frac{v_{LT}}{E_L} & -\frac{v_{RT}}{E_R} & \frac{1}{E_T} & 0 & 0 & 0 \\ 0 & 0 & 0 & \frac{1}{G_{LR}} & 0 & 0 \\ 0 & 0 & 0 & 0 & \frac{1}{G_{LT}} & 0 \\ 0 & 0 & 0 & 0 & 0 & \frac{1}{G_{RT}} \end{bmatrix} \quad (3.1)$$

In total there are 9 material properties required to define the properties of the material:
- Young's modulus in the longitudinal direction, E_L
- Young's modulus in the radial direction, E_R
- Young's modulus in the transversal direction, E_T
- Shear modulus in the longitudinal-radial direction, G_{LR}
- Shear modulus in the radial-transversal direction, G_{RT}
- Shear modulus in the longitudinal-transversal direction, G_{LT}
- Poisson's ratios: v_{LR}, v_{LT}, v_{RT}

As wood is a natural material no two pieces of wood are identical. Besides the differences in the cross-section wood also have imperfections like knots and cracks affecting the mechanical properties between different specimens, even if they are from the same tree. Trees never grows completely straight which can lead to twisting of the grains, meaning that the fibers don't grow in the longitudinal direction.

Another factor that influence the mechanical properties is density. If the annual rings are close together the density increases. In general, the strength increases with increased density (Burström, 2007).

All the factors mentioned above contribute to a high spread in material properties in wood. There are differences in material properties depending on how the cut is done in the cross-section. Persson (2000) did a study on 700 specimens of spruce and tested, among other properties, E_L and density at different positions of the cross-section. The results are presented as growth ring number and the tested property. The results showed that there is a considerable variation of properties in the radial direction depending on the growth ring number. Both the E_L and density increase from the pith out towards the bark and E_L depend both on density and position. Meaning that material properties depend on the sort of wood, variance between logs and position of the cut. The three cuts sketched in Figure 3.2 could therefore have different properties, even though the main directions are the same for each specimen.
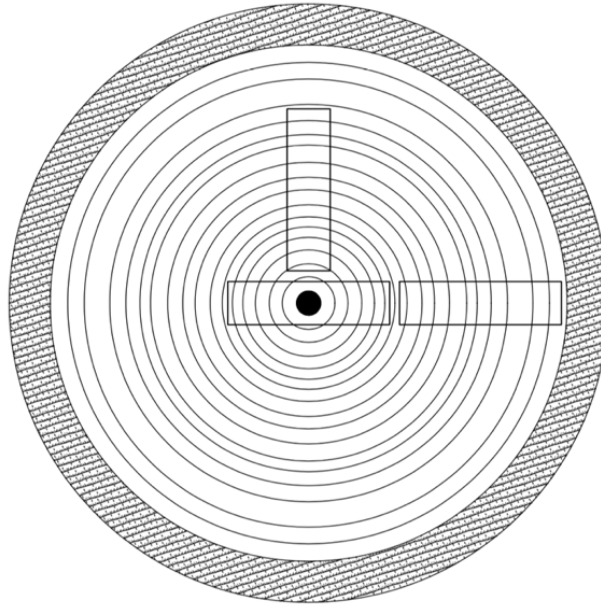
Figure 3.2: Three different cuts is sketched in a cross-section of wood. The position of the cut influence material properties of the specimen.

The moisture content affects strength and deformation properties of wood substantially. The strength reduces with an increase in moisture content (Burström, 2007). For violins the moisture content is not as an essential parameter as for other applications with wood. The wood used in violin building is often placed in humidity-controlled rooms for up to a year to control the moisture (Yamaha, u.d.). A violin can be assumed to be kept indoors in a relatively controlled environment for the majority of its life.

If a structure is subjected to constant load the deformations will increase over time. This time dependent phenomenon is called creep. Different materials are affected various ways. How affected a material is by creep depends on the materials structure, wood is a material that is highly affected by creep.

The amount of creep in wood depends on several different factors (Swedish Wood, 2015):
- A high moisture content leads to a high amount of creep.
- Direction of the load.
- Stiffer wood is affected less compared soft wood.
- Imperfections affect the stiffness of wood and thereby the amount of creep.
- A higher temperature increases creep deformation

Since there are a lot of factors that affect creep deformation it's very complicated to obtain a model that takes all factors into account. There have been a lot of research done with the goal to find expressions that describe creep, both in a short and a long-time perspective. A common approach is to perform experimental tests to find the effects of creep. The obvious problem if the goal is to find the long-time effects is the time aspect.

The creep behaviour differs depending on if the stresses are small or high, with a risk of rupture (Wadsö, 2018). Creep can be divided into three different phases. Primary creep characterized by a high strain rate which decreases with time. Secondary creep characterized by a long period of a near constant strain rate and lastly tertiary creep where cracks and voids

develop in the material, reducing its cross section which accelerates the strain rate and ultimately leads to failure.

A violin is not expected to experience creep failure due to the loads applied from tensioning the strings. Violins have survived stringed up for hundreds of years. Therefore, no effort is made to implement a model for tertiary creep.

Creep-models are usually determined by curve fitting date gathered from experimental measurements. To capture the behaviour of primary creep, the following form of a power law is commonly used. (Wadsö, 2018):

$$\varepsilon_{cr} = a \cdot t^b \qquad (3.2)$$

Where a and b are constants. Creep in the secondary phase can be described with (Wadsö, 2018):

$$\frac{d\varepsilon}{dt} = C\sigma^m \cdot \exp\left(-\frac{E_a}{RT}\right) \qquad (3.3)$$

C and m are constants and the exponential term is Arrhenius law, where E_a is the activation energy, R is the gas constant and T is the temperature.

More information regarding power laws and possible expressions for modelling creep for wood can be found in *Effects of Long-Term Creep on the Integrity of Modern Wood Structures* (Tissaoui, 1996).

3.2   Wood used in violins

There are a few different types of wood which are usually used in violins. Spruce, maple, ebony and lime tree/pine. The type of wood used for the different parts is presented in Table 3.1 (Dagnell & Sarnell, 1988). When it comes to the choice of wood for the plates, spruce is used for the top plate because it's light, but still strong and flexible and maple is chosen for the back plate because it's stable and easy to carve (Waddle, et al., 2014).

Table 3.1: Type of wood used in the different parts of the violin.

Spruce	Maple	Ebony	Lime tree/Pine
Top plate	Back plate	Finger board	Rib strip
Bass bar	Ribs	Upper saddle	
Blocks	Neck	Lower saddle	
Sound post	Bridge	Tail piece *	

* Tail pieces can also be made with plastics

Wood used for violins is of high quality. If one looks at a violin plate it's clear that the annual rings are very close together and appear straight, (Figure 3.3).
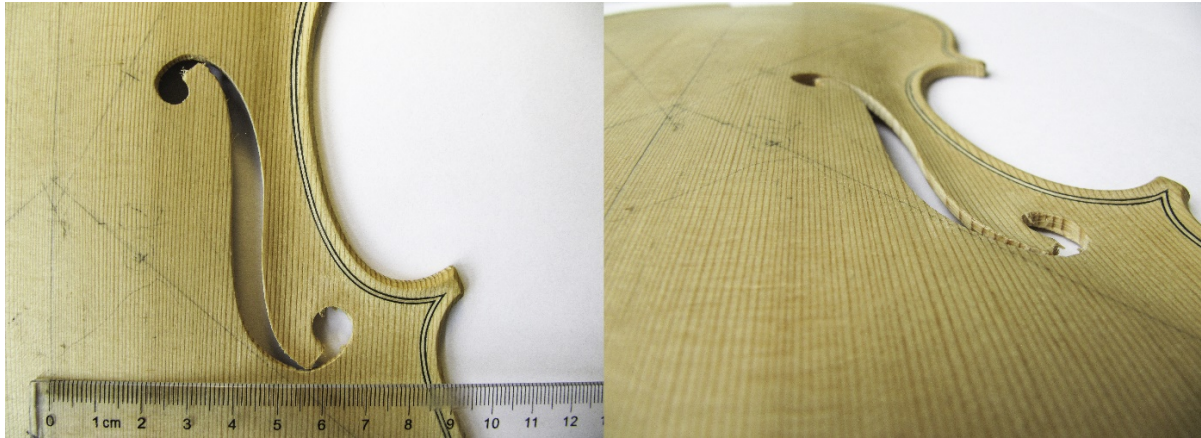
Figure 3.3: The top plate, provided by Zuger. The annual rings are straight and very close together.

As presented previously in this chapter the cut in the cross-section has implications on material properties, i.e. it's very important how the cut is made when creating the parts. Violin plates are either done in one cut or a piece is sawn out, split and glued together. Depending on how the cut is made the radial- and tangential direction differ (Figure 3.4) (Dagnell & Sarnell, 1988). For the plates provided by Zuger, the top plate is glued, and the back plate is created in one piece.
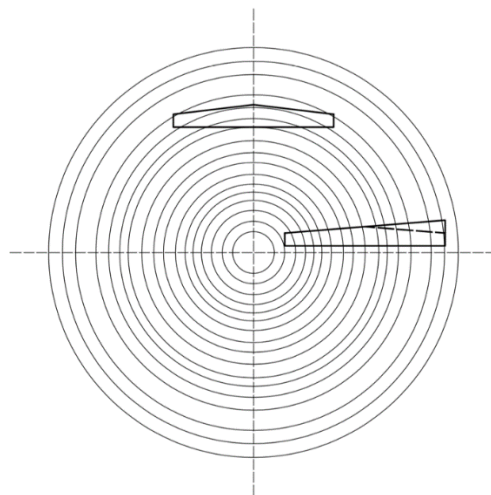
Figure 3.4: The cut when creating the plates is significant for the material properties of the plates. The two cuts depicted here (for a back plate) would have different material orientation.

Material properties for violins have been studied for a long time, as it has been seen as a contributing factor for unique properties of old Stradivari violins. Tests are often performed on the violin plates to research the correlation between material properties and acoustic performance. By performing studies on the violin plates it's possible to obtain knowledge of almost all the parts. As seen in Table 3.1 spruce and maple are used for most of the parts. It's suggested to use wood from the same tree for all the parts made out of the same type of wood (Dagnell & Sarnell, 1988). Of course, it's not a guarantee that the properties are the same in all the parts even if they are created from the same piece of wood, see the theory section of this chapter.

It's difficult to obtain strength properties of already completed instruments since a lot of tests can't be performed on violins without destroying them. A study was performed where 14 luthiers were asked to grade 84 pieces of Norwegian spruce on their suitability for violin building. The study used three criterions. The first criterium was quality, the second was optical and the third was an overall appraisal. The results showed that the luthiers could estimate wood quality related to visible features such as annual ring structure and colour more than mechanical properties (Buksnowitz, et al., 2007). As such there could be a large variation in material properties of the wood used in violins.

3.2.1 Density of wood used in violins

It's clear that the mass of an instrument has major implications on the acoustic properties of the violin and how it vibrates. Since the measurements between violins only differ with a small margin the density has a large impact on the mass and thereby the quality of the instrument.

When it comes to density of a wood specimen it's heavily influenced by the climate of the area where the tree grows. Factors that affect the density include solar exposure, nutrition in the soil and quality of water. Areas with low solar exposure and low nutrition from the soil and water will grow slower leading to denser wood (Stoel & Borman, 2008).

Wood coming from slower growing trees have often been thought to be the wood best suited for building violins, which would indicate that the wood used in violins are dense. CT-scans have been performed on old and new violin plates to research the densities and density variations within violins (Stoel & Borman, 2008). Five classical and eight modern violins where tested. The results from the tests show that there is not a large difference in density between old and new violins. There is a difference in density differentials between the wood grains when comparing the classical and the modern violins. The density differential could have an impact on vibrational efficiency.

The median density found in the study was lower compared other tested samples. For the top plate most of the median densities where in the region of 350-400 kg/m^3 and 550-600 kg/m^3 for the back plate. In Ross (2010) the mean density for sugar maple, at 12 % moisture content is 630 kg/m^3 and for sitka spruce its 400 kg/m^3. The results from the study indicate lighter wood is preferred by luthiers.

3.2.1.1 Densities used for modelling violins found in the literature

There is a significant variation in the densities used in previous models and measurements of violin plates. Densities used to model maple, ebony, pine and spruce in previous FE-analysis, modal analysis or measured from real instruments are presented in Table 3.2. Most of the studies found are focused on the violin plates, i.e. only maple and spruce are needed.

Table 3.2: Density values for spruce and maple used in previous modelling of violins.

	Density Maple [kg/m³]	Density Spruce [kg/m³]	Density Pine [kg/m³]	Density Ebony [kg/m³]
(Pyrkosz, 2013)	570	350		784,9
(Molin, et al., 1988)	609	482	-	-
(Bretos, et al., 1999)	610	420	-	-
(Knot, et al., 1989)	800	460	-	-
(Lu, 2013)	-	420	-	-
(Gough, 2015)**	-	460	-	-
(Fu, et al., 2014)*	510	450	-	-
(Loen, et al., 2005)*	-	368	-	-
	-	382	-	-
	-	427	-	-
(Sproßmann, et al., 2017)				1140
(Ross, 2010)			440	

*Measured values from real violins

** Modal analysis where the density was varied in some of the analyses. 460 kg/m³ was the value used when other parameters were varied. Shape, arching height and anisotropy were among other factors also changed.

3.2.2 Strength parameters of wood used in violins

The high quality of wood used in violins indicate high strength parameters. It's more difficult to measure strength parameters in a violin compared to the density. The issue compared to density is that there are 9 parameters, assuming orthotropy, which are difficult to isolate in tests. There are some studies done which often include modal analysis of the plates to obtain an estimation of the strength parameters.

Molin, et al (1988) present a method using modal analysis on violin plates to determine the strength parameters. The results of the analysis showed a correlation between the frequency of modes and separate parameters. The results of the study are described more in detail in chapter 5.1.

3.2.2.1 Strength parameters used for modelling violins found in the literature

As for the density there are variations in the values of the strength parameters used in the literature. In studies done on violin plates plane stress conditions often apply. The material parameters in the normal direction are neglected. For an orthotropic material this means that the number of material properties used to describe the material goes from 9 to 4 in plane parameters. If one wants to calculate the strain in the normal direction 6 parameters are needed (Ottosen & Petersson, 1992).

Parameter values used in the literature are presented in Table 3.3 and Table 3.4 for maple and spruce respectively.

Table 3.3: Strength parameters used in the literature to model maple. Some studies are done on violin plates, assuming plane stress leading to 6 parameters being enough to describe the orthotropic material.

	(Pyrkosz, 2013)	(Molin, et al., 1988)	(Knot, et al., 1989)
E_L [GPa]	12,32	12	17
E_R [Gpa]	1,63	1,96	1,564
E_T [Gpa]	0,80	-	0,731
G_{LR} [Gpa]	1,37	1,75	1,275
G_{LT} [Gpa]	0,78	-	1,173
G_{RT} [Gpa]	0,41	-	0,187
v_{LR} [-]	0,424	0,2	0,318
v_{LT} [-]	0,476	-	0,392
v_{RT} [-]	0,774	-	0,703

Table 3.4: Strength parameters used in the literature to model spruce. Some studies are done on violin plates, assuming plane stress leading to 6 parameters being enough to describe the orthotropic material.

	(Pyrkosz, 2013)	(Molin, et al., 1988)	(Knot, et al., 1989)	(Lu, 2013)
E_L [Gpa]	9,79	16	13	15,13
E_R [Gpa]	1,25	0,975	0,89	1,2
E_T [Gpa]	0,58	-	0,649	-
G_{LR} [Gpa]	1,21	0,725	1,015	0,7
G_{LT} [Gpa]	1,17	-	0,715	0,059
G_{RT} [Gpa]	0,10	-	0,416	0,7
v_{LR} [-]	0,422	0,03	0,375	0,3
v_{LT} [-]	0,462	-	0,436	0,3
v_{RT} [-]	0,530	-	0,468	0,3

Strength parameters for pine and ebony are more difficult to find. Values for ebony are collected from Pyrkosz (2013) and values for pine are collected from Ross (2010) (Table 3.5).

Table 3.5: Strength parameters for ebony and pine. The values for ebony are the ones used by Pyrkosz (2013) and values for pine are found in Ross (2010)

	Ebony	Pine
E_L [Gpa]	7,65	11,2
E_R [Gpa]	0,85	0,99
E_T [Gpa]	0,38	0,49
G_{LR} [Gpa]	0,67	1,08
G_{LT} [Gpa]	0,45	0,91
G_{RT} [Gpa]	0,16	0,12
v_{LR} [-]	0,297	0,347
v_{LT} [-]	0,641	0,315
v_{RT} [-]	0,604	0,408

4   Experimental modal analysis on top and back plate

4.1   Purpose

The purpose of doing experimental tests of the violin plates are to determine material properties of the back and top plate. The experiment done in this project is an experimental modal analysis. With experimental analysis one can obtain a description of the response of a structure and its properties (Døssing, 1988b). The results from the experimental test can then be compared to results from a modal analysis performed in Abaqus. By modifying material properties in the computer simulation and compare the results it's possible to get an understanding of the plates properties. Since most of the parts of the violin are created with the same type of wood used for the plates it's possible to calibrate the complete violin model.

4.2   Modal Analysis theory

Before describing the process of an experimental modal analysis it's necessary to present some theory regarding modal analysis of a multi degree of freedom (MDOF) system. It's the natural frequencies of the plates that leads to the possibility of determining material properties of the plates. Natural frequencies are obtained through an eigenvalue formulation. The starting point is the equations of motion for an undamped free vibration system. It should be noted that linearity is assumed. The equations of motions are written as:

$$\boldsymbol{M\ddot{u}}(t) + \boldsymbol{Ku}(t) = \boldsymbol{0} \qquad (4.1)$$

Where **M** is the mass matrix and **K** is the stiffness matrix of the structure. $\boldsymbol{\ddot{u}}(t)$ is the acceleration of the structure as a function of time and $\boldsymbol{u}(t)$ is the displacement as a function of time.

The free vibration can be described with the following equation (Chopra, 2015).

$$\boldsymbol{u}(t) = q_n(t) \cdot \Phi_n \qquad (4.2)$$

Φ_n describes the deflected shape, also called natural modes of vibration and $q_n(t)$ is a scalar multiplier that varies with time. It can be described with a harmonic function:

$$q_n(t) = A_n \cos(\omega_n)\, t + B_n \sin(\omega_n)\, t \qquad (4.3)$$

A_n and B_n are constants, determined using initial conditions of the system. ω_n is the natural frequency of vibration. Inserting (4.2) in (4.3) one obtains:

$$\boldsymbol{u}(t) = \Phi_n(A_n \cos(\omega_n)\, t + B_n \sin(\omega_n)\, t) \qquad (4.4)$$

Using this new formulation of $\boldsymbol{u}(t)$ and (4.1), the equation of motion is rewritten as:

$$(\boldsymbol{K}\Phi_n - \omega_n^2 \boldsymbol{M}\Phi_n)q_n(t) = \boldsymbol{0} \qquad (4.5)$$

Equation (4.5) has two types of solutions. The first type is that $q_n(t)$ is equal to zero, this solution is not of interest since it implies that the motion of the structure is equal to zero, see equation (4.2). The second type of solution is that the parenthesis is equal to zero.

$$(\boldsymbol{K}\Phi_n - \omega_n^2 \boldsymbol{M}\Phi_n) = \boldsymbol{0} \quad \rightarrow \quad (\boldsymbol{K} - \omega_n^2 \boldsymbol{M})\Phi_n = \boldsymbol{0} \quad (4.6)$$

Equation (4.6) is a set of equations. A vibrating system with N DOFs has N natural frequencies of vibration, ω_n. The solution provided by Φ_n again applies no motion. Equation (4.6) is written as a matrix eigenvalue problem.

$$det[\boldsymbol{K} - \omega_n^2 \boldsymbol{M}] = 0. \quad (4.7)$$

If $\boldsymbol{K}$ and $\boldsymbol{M}$ are positive definite and symmetrical (4.7) has N real solutions for ω_n^2 . For each ω_n there is an independent vector Φ_n (Chopra, 2015). In a free vibration system with no damping Φ_n depend only on the mass and stiffness of the system.

4.3   Measurement techniques

In an experimental modal analysis, Φ_n are triggered using an impact hammer. The response from the structure is measured in motion. Either displacement, velocity or acceleration can be used (Døssing, 1988a). The most common approach is to use accelerometers and measure the acceleration of the structure.

There are two main techniques for performing an experimental modal analysis using an impact hammer and accelerometers.

The first option is roving excitation. Accelerometers have a fixed position and the hammer is roved over the structure. The main benefit of using this approach is that the mass from accelerometers are not moved around. The main downside is that the approach is time consuming (Manege, 2018).

The second option is roving response. Accelerometers are roved over the structure and the impact is performed in a specific node. This approach would reduce the test time if the test is done with more than one accelerometer. The disadvantage is that the mass of the system is rearranged for every impact, since the accelerometers are moved. Therefore, roving response is more suitable when the mass of the accelerometers is deemed insignificant in comparison to the mass of the structure measured. (Manege, 2018).

The goal with the experimental modal analysis is to find the response of the structure in a span of frequencies. The software used is BK connect, which is a sound and vibration software. In BK connect ω_n can be found from a frequency response function (FRF).

4.4   Frequency response function

Frequency response function (FRF) is a function that describes the relationship between input and output in a system. Different parameters of motion can be used to measure an FRF, in this project acceleration is used. The relationship between input and output is weighted with a system descriptor, which is a function of frequency, A(ω). The input could be a force from an impact, F(ω) and the output could be the resulted acceleration $\ddot{u}(w)$ measured with accelerometers (Døssing, 1988a).

$$\ddot{u}(w) = A(\omega) \cdot F(\omega) \rightarrow A(\omega) = \frac{\ddot{u}(w)}{F(\omega)} \quad (4.8)$$

The function A(ω) has both a magnitude |A(w) | and a phase $\sphericalangle A(\omega)$.

In an MDOF system all DOFs vibrate at the same time (Chopra, 2015). A displacement in a structure is a combination of all modes of frequency. When a structure vibrates it can be seen as a collection of single degree of freedom (SDOF) system vibrating together (Døssing, 1988b).

If a FRF measurement is done and plotted the response will be shown as a series of peaks, in an MDOF system the FRF will be the sum of every SDOF FRF (Døssing, 1988b). The peaks will correspond to the ω_n of the structure.

If you place accelerometers on a structure and rove an impulse hammer over the structure each hit of the hammer will produce an FRF for each of the accelerometers. By combining the FRFs one obtains a plot describing the dynamic behaviour of the structure (Døssing, 1988b).

In BK connect complex mode indicator function (CMIF) can be used as well as FRFs to visualize ω_n. A CMIF uses all FRFs and singular value decomposition to find the number of eigenvalues that exists in the FRFs. For the theory behind CMIF the reader is referred to *Performance of Various Mode Indicator Functions* (Radeş, 2010).

4.5   Curve fitting

Besides finding ω_n and Φ_n the damping ratio, ζ of the structure is essential information. When determining material properties of the violin, the results from the experimental analysis have to be compared to the results from Abaqus. In Abaqus the modal analysis is performed on an undamped system, meaning that the undamped frequencies must be approximated from the experimental analysis. To obtain the undamped behaviour, ζ has to be found.

FRFs are complex functions. To determine ζ and Φ_n the complex functions have to be described with analytical expressions. The method often used is curve fitting (Richardson & Formenti, 1982). There are many different types of curve fitting algorithms to choose from. All tries to obtain analytical expressions of the FRFs (Richardson, 1986).

The curve fitting algorithm used in this project is called Rational Fraction Polynomial (RFP). The method fits an RFP, which is the ratio between two polynomials to the FRF curve. The ratio between the polynomials are independent of each other. The theory behind the algorithm

is presented and discussed in Richardson & Formenti (1982) and Richardson & Formenti (1985).

Another important choice is whether local or global curve fitting is used. In local curve fitting every measurement is curve fitted separately. Frequency, damping and the residue are estimated for each node (Richardson & Formenti, 1985). The residue is not a physical parameter but a mathematical one that controls the magnitude of the FRF and is related to finding the correct modal shape (Døssing, 1988b). The downside of using local curve fitting is that when the parameters are estimated for every node it leads to a lot of unknowns which increase the risk of errors (Richardson & Formenti, 1985).

In global curve fitting the process is divided into two steps. First frequency and damping are estimated by using all FRFs. The estimations are then used to find the residue and the modal shape. The main advantage is that by using all the measurements the accuracy of the frequency and damping increases (Richardson & Formenti, 1985).

It should be noted that for lightly coupled modes the choice of local and global curve fitting is not as large as for coupled modes (Richardson & Formenti, 1985). Since a violin plate is lightly damped structure the impact should not be substantial regardless of method.

4.6   Support conditions

One large aspect in performing an experimental modal analysis is to achieve the correct support conditions. To correlate the FE-analysis to the experiment data the conditions have to as similar as possible between the two analyses. The goal is to obtain supports as close to free-free boundary conditions as possible. In practice this means that the support conditions should not influence the natural modes of vibration of the plates themselves.

There are several ways to create appropriate support conditions. Lu (2013) used a nylon string strung from the ceiling. Another common approach is to use rubber bands. When doing an experimental modal analysis on the complete instrument it can be hung in the c-profile vertically (Marshall, 1985) (Pyrkosz, 2013). Rubber bands can also be used when doing tests on the plates. Pyrkosz (2013) used rubber bands in a cross and placed the plate in the nodal lines for the expected first natural mode of frequency

4.7   Modal Assurance Criterion

It's necessary to compare the deflected shapes to each other to distinguish the differences between them. A way to do this is with a modal assurance criterion (MAC). A MAC test is a statistical indicator that is bounded between 0 and 1, where 0 describes no consistency between the modal shape and 1 describes modes complete consistency A MAC can be performed both within a mode set (Auto MAC) or between two different mode sets (Cross MAC). Since MAC only describes the consistency in modal shape it's only based on the modal vectors, Φ_n. The results are often presented in a matrix format (x,y). There are MAC criterions for both complex and non-complex modes. Below the complex MAC is presented, since the results from an experimental modal analysis are complex modes (Pástor, et al., 2012).

$$MAC(x, y) = \frac{\left|\{\Phi_a\}_x^T \{\Phi_b\}_y^*\right|^2}{\left(\{\Phi_a\}_x^T\{\Phi_a\}_x^*\right) \left(\{\Phi_b\}_y^T\{\Phi_b\}_y^*\right)} \qquad (4.9)$$

Where:
- $\{\Phi_a\}_x$ is an eigenvector for the complex damped mode, for mode x.
- $\{\Phi_b\}_y$ is an eigenvector for the complex damped mode, for mode y.
- $\{\Phi_a\}_x^*$ is the complex conjugate of $\{\Phi_a\}_x$
- $\{\Phi_b\}_y^*$ is the complex conjugate of $\{\Phi_b\}_y$

4.8   Assumptions

The main assumption done in this type of analysis is linearity. The impact from the hammer must be proportional to the response of the plate.

Since the movement of a structure is a combination of all modes of frequency its critical to distinguish that the mode obtained is not influenced by the other modes. If the structure is lightly damped the modes of frequency should be well separated (Døssing, 1988b). For the violin plates both the shape and reasonable associated frequency is known. Gough (2015) shows a table with frequencies for the first five modes of vibration from previously done research. Even though there is a clear variation between the frequencies between the modes there should not be a risk of modal coupling, since no modes of frequency are close.

Another important aspect is the number of DOFs needed to obtain the number of modes of interest. There are a few factors to consider when deciding the number of nodes used in the test geometry.

One factor is the complexity of the modes. If there are modes with a lot of oscillation on a small area, a higher node density is needed to differentiate the modal shape compared to a mode of a simpler shape. The first five modes for both the top and back plate have a relatively simple shape, meaning a smaller number of nodes should be sufficient. Another important factor is that the maximal number of modes predicted cannot be more than the number of nodes in the model (Døssing, 1988b).

4.9   Coherence function

The coherence function is a measurement of the linearity between the input and output of the system for each frequency in the studied frequency range. The function ranges from 0 to 1, where 1 is a perfect coherence between the input and the output (Døssing, 1988a).

Reasons for a low value of the coherence could be outside disturbance like unintentional vibrations or poorly executed impact hits. If the coherence is low at antiresonance it does not affect the result of the measurement. To ensure that the coherence is sufficient enough, meaning close to 1, hits in each node is performed more than one time and the coherence between the hits is assessed.

4.10 Method

The goal of this experimental analysis is to find the structures natural frequency ω_n and the associated mode shape vector Φ_n of the first 5 natural modes of vibration. The reason for choosing the first 5 is that there is a wide basis of information in the literature to compare and get validation in the results. The software used is BK connect.

4.10.1 Creating the test geometry
The first step in performing the experimental modal analysis is to build up the test geometry in BK connect. The test geometry should include the nodes where the plates are hit with the impact hammer. Like a FE-software the geometry in BK connect is based on nodes and elements. As mentioned in the theory section of this chapter, there is no need for the mesh to be very fine to obtain natural modes of frequency where most of the plate is active, which is the case for the first 5 modes. The FE-model of the plates, built in Abaqus, including the mesh is imported to BK connect. The test geometry is built from the imported FE-model. It has to be reduced to obtain a suitable number of nodes. This is done in the *geometry module* for both the back and the top plate. The number of nodes for the back and top plate are 35 and 41 respectively, see Figure 4.1.
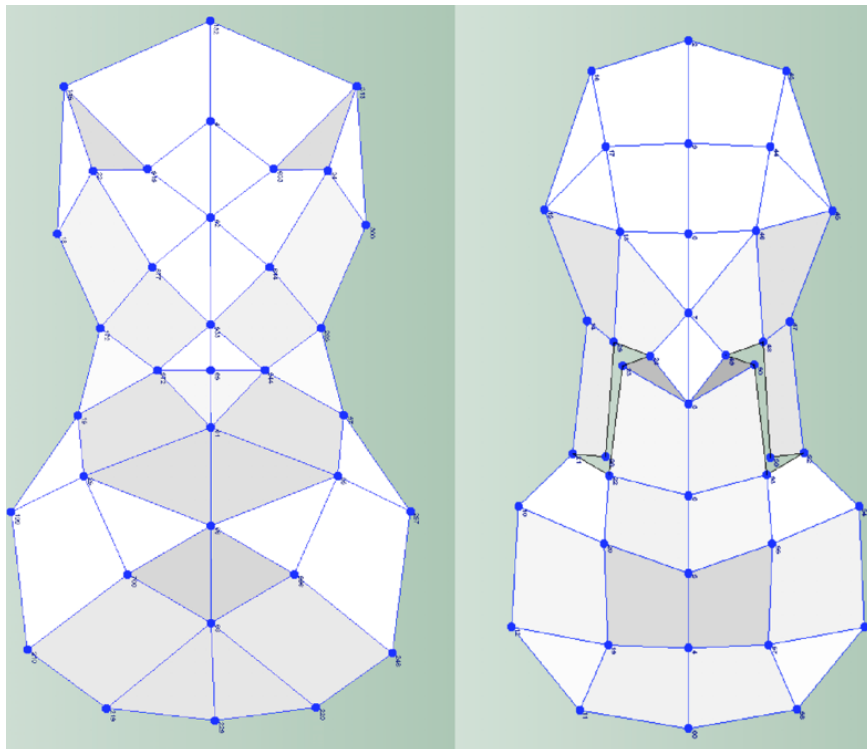
Figure 4.1: Test geometry used in the experimental modal analysis. There are 35 nodes for the back plate and 41 for the top plate.

Each node in the test geometry is marked on the actual plates. The coordinates for the nodes are collected from BK connect and measured on to the plates. The positions are marked using pieces of tape (Figure 4.2).

*Figure 4.2: The coordinates of every node from the test geometry is transferred to the plates.
The position is marked using a piece of tape.*

4.10.2 Hammer and accelerometers

The roving technique chosen is the roving excitation. The number of nodes in the test is quite small, so the added time of this approach is not a problem, also the available accelerometers used are quite heavy compared to the mass of the plates.

The impact hammer used is a miniature impact hammer – type 8204, manufactured by Brüel & Kjær. It's designed for measurements where a small excitation force is desirable. It's a compact hammer with low weight, 121,6 mm long and weighs 2 grams. The low mass combined with a tip of stainless steel gives the hammer the possibility to reach high frequencies, well above the needed frequency range (Brüel & Kjær, 2008).

The accelerometers used are piezoelectric accelerometers – type 4507-001, manufactured by Brüel & Kjær. This type of accelerometers is uniaxial, which is sufficient enough, since the motion mainly is perpendicular to the plates for the first 5 modes. They are quite large for this type of measurement but are the only ones available. The measurements are 10x10x10 mm titanium casing and the weight is 4,8 grams. The design is done for larger structure than violin plates, but as for the impact hammer the frequency range is well above the needed one (Brüel & Kjær, 2018).

4.10.3 Experiment setup

To obtain free-free boundary conditions a similar set up to Pyrkosz (2013) is chosen, where the plate is placed on rubber bands (Figure 4.3). Three accelerometers are used. The placement is presented in Figure 4.3. Two accelerometers are placed in corners close to the lower and upper bouts. The third accelerometer is placed in the centre of the plates. The reason for the positioning of the accelerometers are that the first four modes of vibration are active around the corners and the fifth is active in the middle part of the plate. The position is important, since a poor choice can lead to a mode being completely missed (Pyrkosz, 2013).

Figure 4.3: Experimental setup for the top plate. Three accelerometers are used. Two are placed close to the corners and the third is placed in the center of the plate to cover all of the first five modes of vibration. The white squares mark the position of the hammer hits.

4.10.4 Performing the experimental modal analysis

Before performing the measurements, the hammer has to be calibrated to find the impact force magnitude that should trigger a hit. In BK connect this is done in the *set-up module*. A few test hits are performed around the plate to find a suitable magnitude. The required force depends both on the type of hammer and the material of the specimen. 0,5 N was a good threshold for both the top and back plate. Besides the trigger level the pre-delay is set so that the response of the full hit is recorded. The response, measured with the accelerometers are set up to minimize noise, which otherwise could impact the results.

The setup is controlled by performing a pre-test. The plate is hit with the impact hammer at a specific DOF a few times and the response from accelerometers are checked. Also impact validation of the hammer is controlled, to observe that the settings from the hammer calibration is correct and that double and soft hits are avoided.

With the settings determined the measurements themselves are carried out in the *measuring module*. The impact hammer is hovered over the measuring points, see Figure 4.4. For each hit the coherence and FRF curves are studied to check for clear hits. Three hits are performed in each measuring point and a linear average of the FRF is calculated. In total there are three FRFs for each node, measured at each accelerometer. Both the plate and the rubber band setup will continue to vibrate for a period after striking a plate with the hammer. It's therefore critical to wait a while between hits. Otherwise the residual vibrations will be picked up in the next measurement.
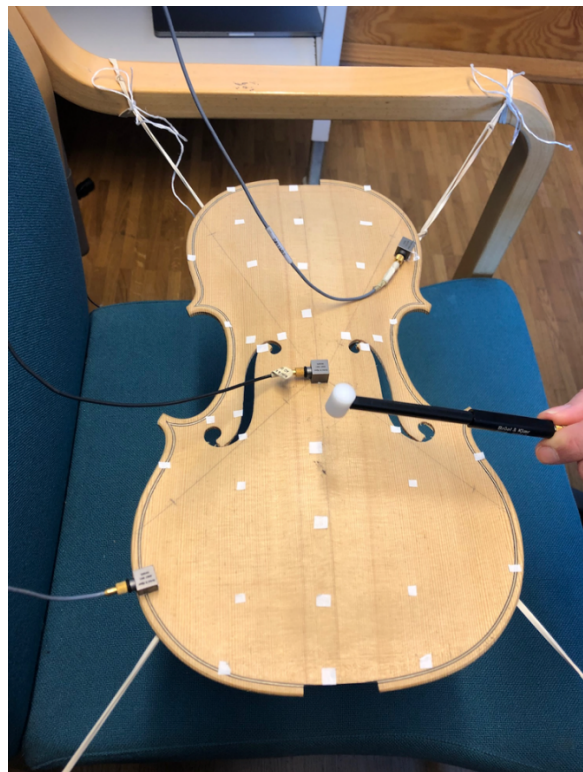
Figure 4.4: The impact hammer is hovered over the plates. Three hits per node and a linear average is saved for each.

The resulted FRF values are then put in to the *analyze module*, where the modes of frequency are calculated. The first step in the *analyze module* is measurement validation where the quality of the data is checked before the rest of the analysis. All FRFs and Coherence functions are controlled to get an overview of any faulty measurements.

The next step is the parameter estimation setup. The functions for determining the natural modes of vibration are decided in this step, as well as the frequency range for the modes. RFP is chosen with global curve fitting. CMIF is used to visualize ω_n. The frequency range is set from 50 Hz to 500 Hz, which is sufficient to cover the first 5 natural modes of vibration.

After the parameter estimation setup, the mode selection is done. BK connect estimates the frequency, damping and modal shape from the functions determined in the previous step. The automated mode selection is used, where BK connect finds the frequency, damping and modal shape based on the curve fitting method chosen. The undamped-, damped frequency and modal shapes are saved and stored.

The last step is analysis validation. Auto MAC is calculated to secure that consistency between the modal shapes is not too large.

4.11 Results

4.11.1 Back plate
As an example, FRF-curves for a node at the bottom right corner of the back plate and the associated coherence function is presented in Figure 4.5.
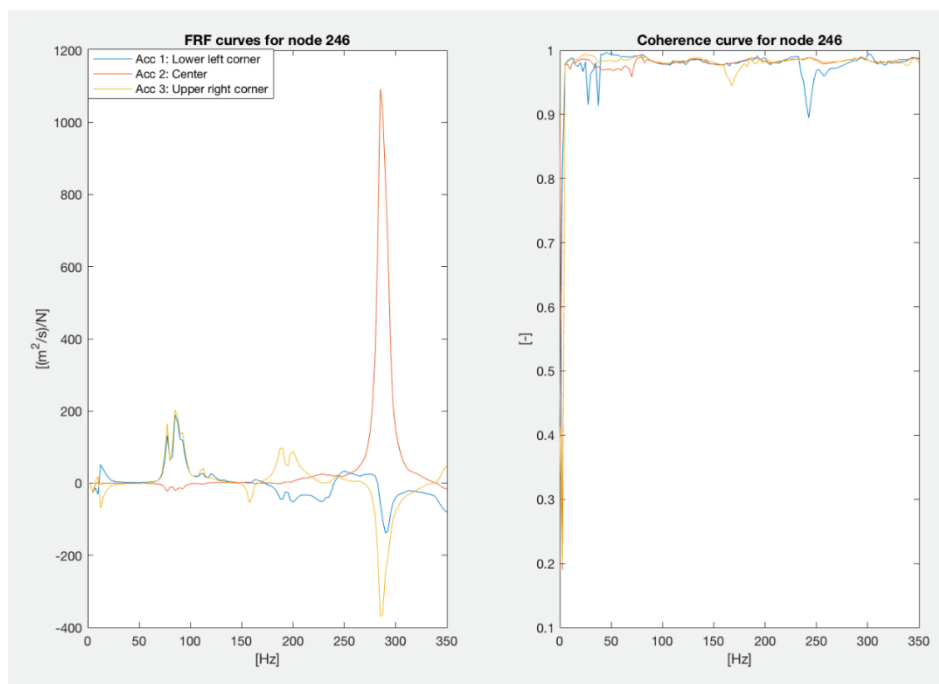
Figure 4.5: FRF-curves, one for each accelerometer and associated Coherence function for hammer impact at node 246. Back plate.

The CMIF-curves obtained for the back plate are presented in Figure 4.6.
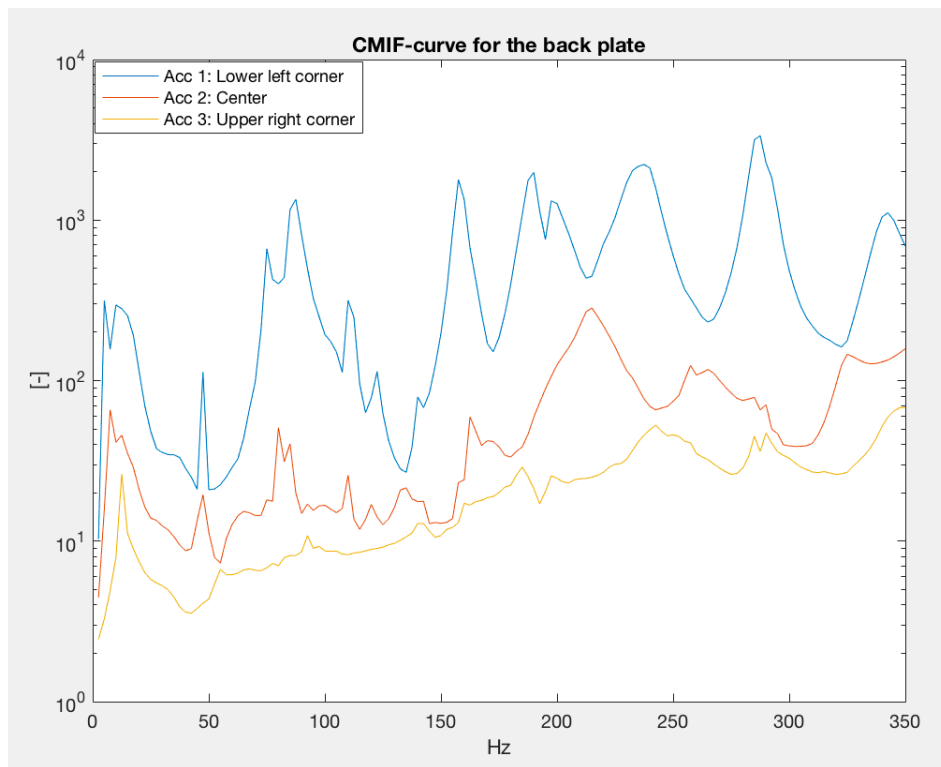
Figure 4.6: CMIF for the back plate.

Damped and undamped frequencies for the first five modes of vibration is presented in Table 4.1.

Table 4.1: Frequencies for the first five modes of vibration for the back plate.

Mode number	Undamped Frequency [Hz]	Damped Frequency [Hz]
1	86,8	86,7
2	157,8	157,8
3	192,0	191,9
4	235,4	235,3
5	286,9	286,9

The modal shapes for the back plate are presented in Figure 4.7 to Figure 4.9. Note that this is with weight of the accelerometers included that effects the eigenfrequencies and modal shape.
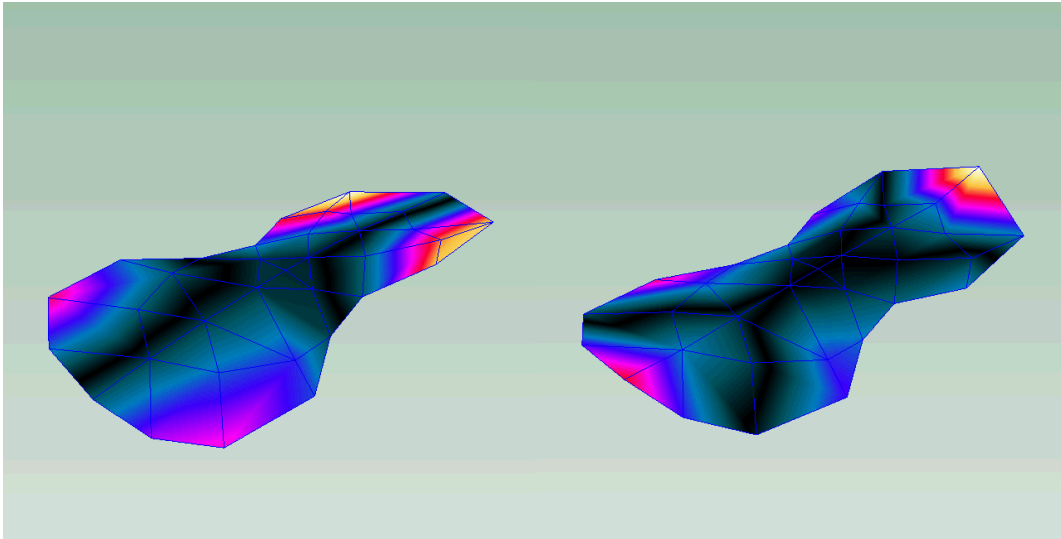
Figure 4.7: Modal shape for the 1st and 2nd mode of vibration.
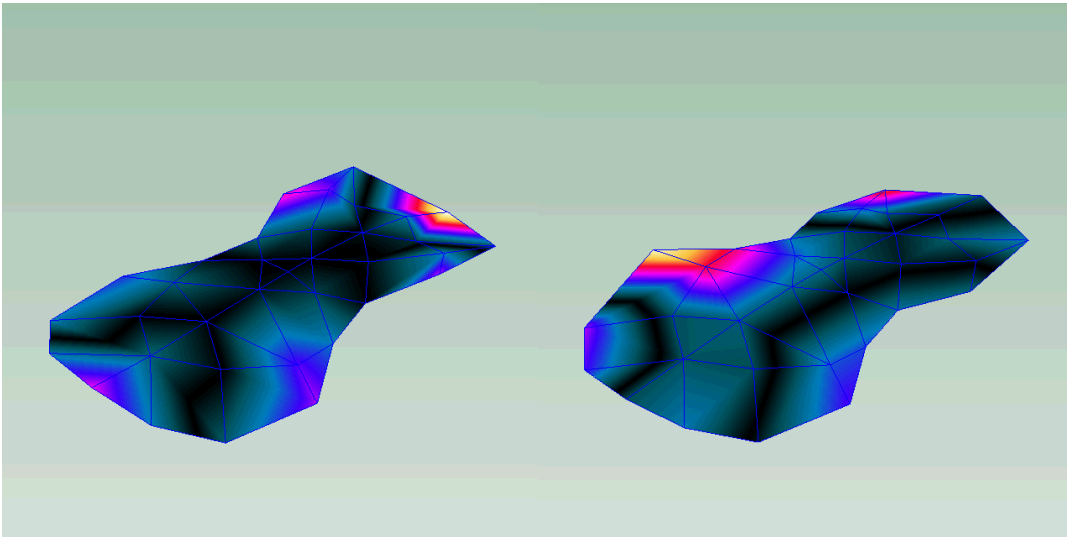
Figure 4.8: Modal shape for the 3rd and 4th mode of vibration.
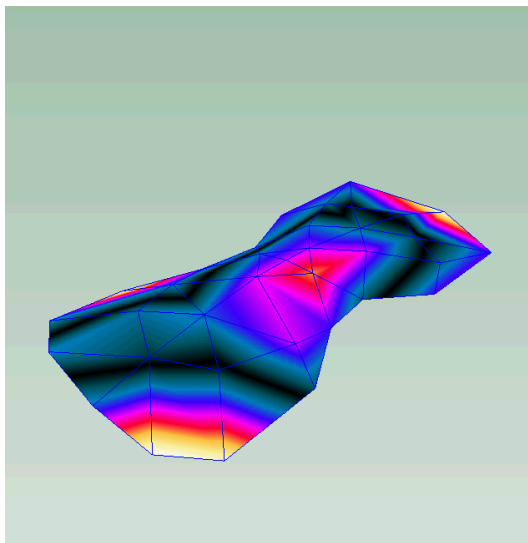
Figure 4.9: Modal shape for the 5th mode of vibration.

The Auto Mac for the modal shape of the first five modes is presented in Figure 4.10.
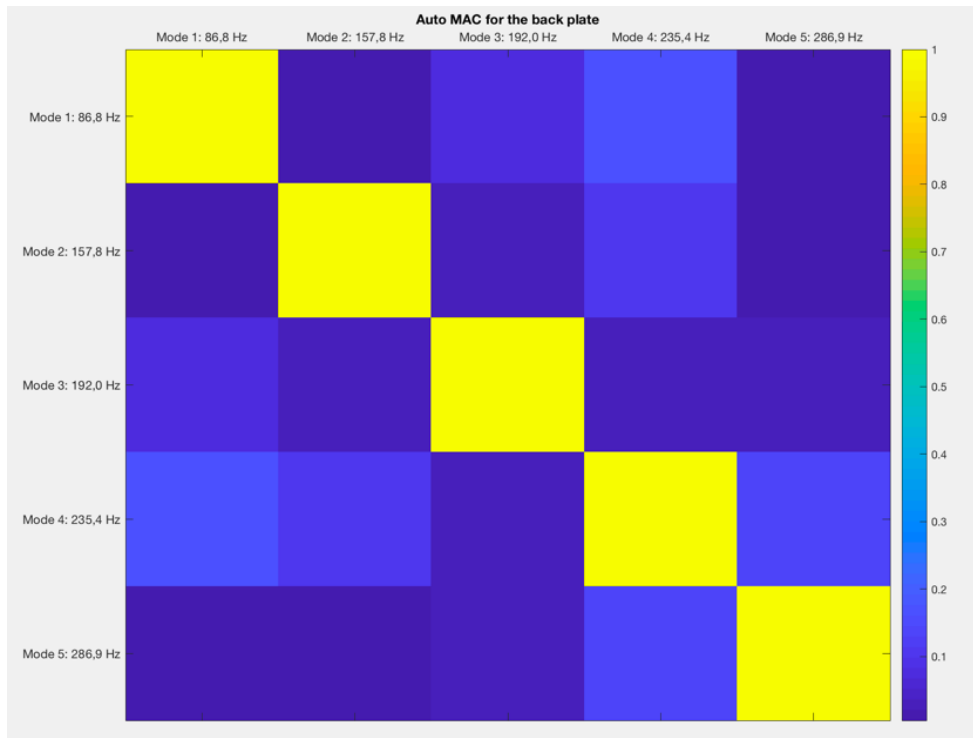
Figure 4.10: Auto MAC of the first five modes of vibration for the back plate.

4.11.2 Top plate

As an example the FRF curves for node 58 (right bottom corner) and associated coherence curve for the top plate is presented in Figure 4.11.
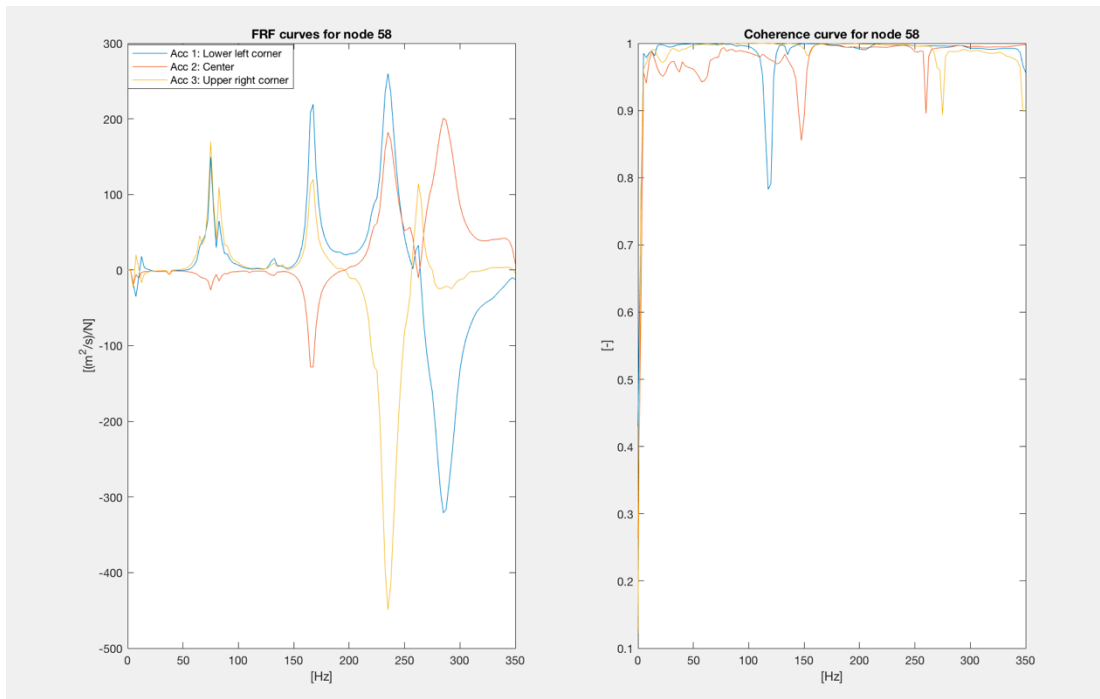
Figure 4.11: FRF-curves, 1 for each accelerometer and associated Coherence function for hammer impact at node 58 Top plate.

The CMIF obtained for the top plate is presented in Figure 4.12.
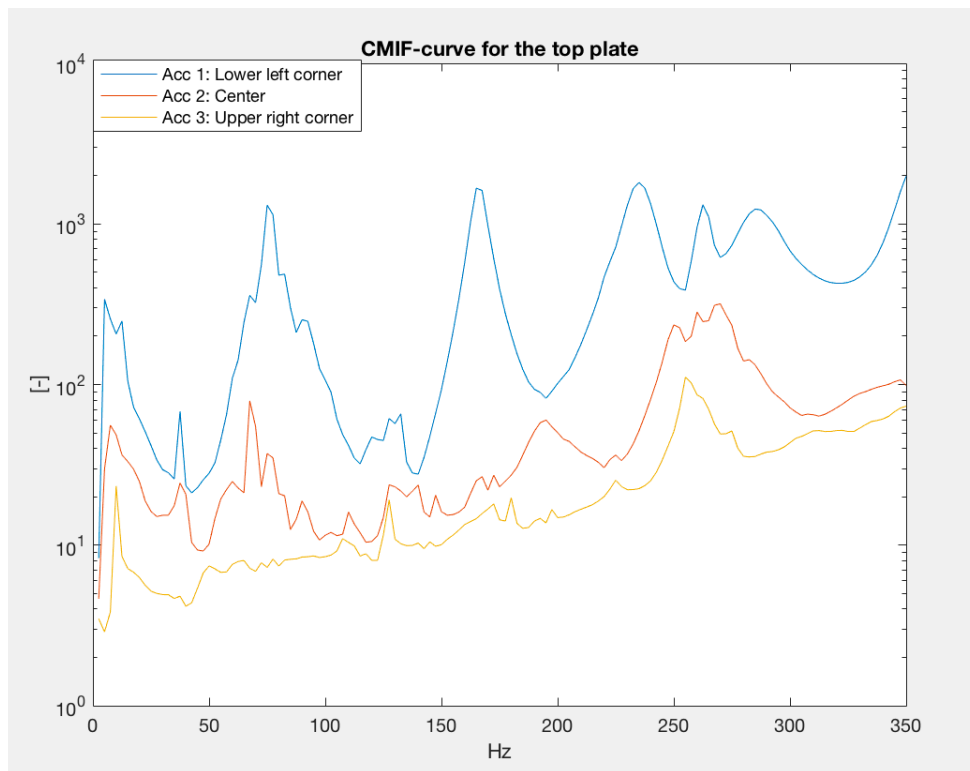
Figure 4.12: CMIF for the top plate.

Damped and undamped frequencies for the first five modes of vibration is presented in Table 4.2.

Table 4.2: Frequencies for the first five modes of vibration.

Mode number	Undamped Frequency [Hz]	Damped Frequency [Hz]
1	76,8	76,5
2	166,0	165,9
3	234,0	233,8
4	261,6	261,5
5	282,4	282,0

The modal shapes for the top plate are presented in Figure 4.13 to Figure 4.15. Observe that the weight of the accelerometers effects the modal shape.
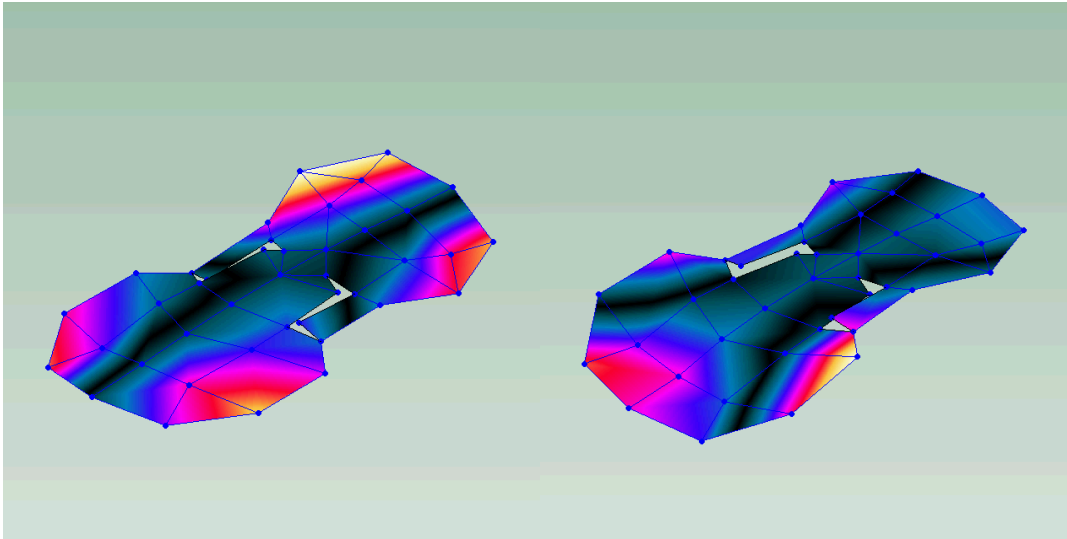
Figure 4.13: Modal shape for the 1ˢᵗ and 2ⁿᵈ mode of vibration.
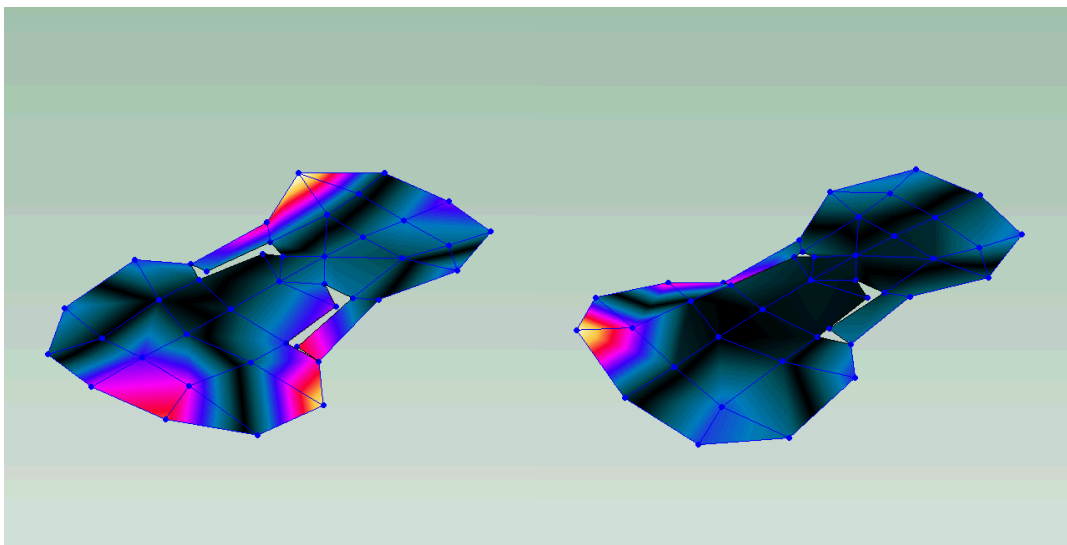
Figure 4.14: Modal shape for the 3ʳᵈ and 4ᵗʰ mode of vibration
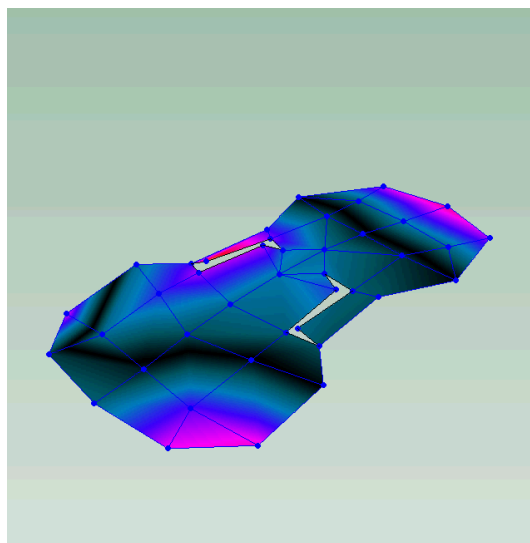
Figure 4.15: Modal shape for the 5th mode of vibration.

The Auto Mac for the modal shape of the first five modes is presented in Figure 4.16.
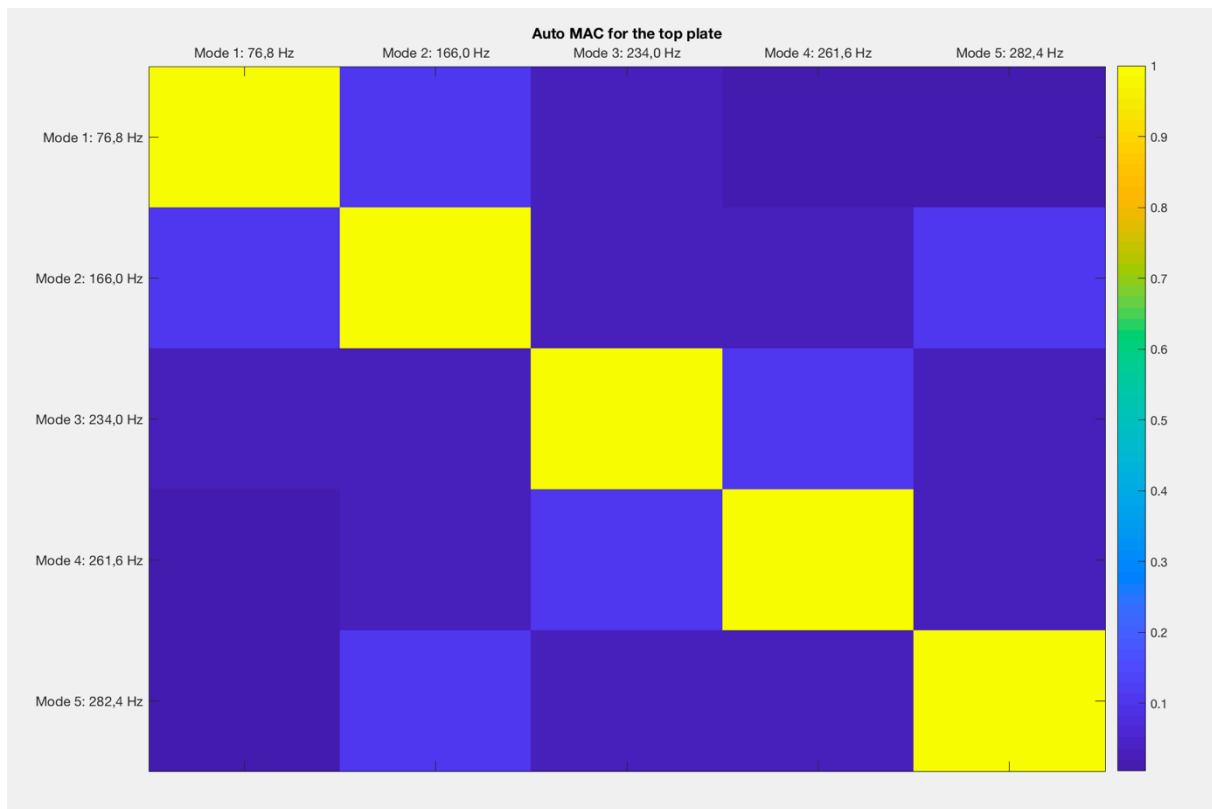
Figure 4.16: Auto MAC of the first five modes of vibration for the top plate.

4.12 Discussion

The natural frequencies for the first 5 modes of vibration (Table 4.1 and Table 4.2) are within a range that is reasonable. Gough (2015) presents results from other studies done on plate modes. It's more difficult to verify the results of the top plate, since most studies done exclude the bass bar. How the presence of the bass bar effects the natural frequencies is different depending on the mode, since it both increases the mass and the stiffness of the system, see equation (4.7). For modes where the bass bar is active in bending, for example mode 5, the stiffness of the system should increase leading to a higher natural frequency. Mode 1, where most of the oscillation is at the corners of the plate the mass probably effects the frequency more than the stiffness of the bass bar, leading to a lower natural frequency. The same reasoning is valid for the accelerometers.

The modal shapes of both the back and top plate are presented in Figure 4.7 to Figure 4.9 and Figure 4.13 to Figure 4.15. The first 3 modal shapes are close to the shapes presented in the literature (Pyrkosz, 2013) (Lu, 2013) (Gough, 2015). The presence of the accelerometers has some effect on the modal shape, making them less symmetrical, but it's clear that the shape is the same. The 4th and 5th modal shapes display larger differences. The accelerometers might have a larger impact on these compared to the first 3 ones. When the modal analysis is performed in Abaqus the hope is that by removing the accelerometers the 4th and 5th modal shape will be closer to shapes found in the literature.

The Auto MACs (Figure 4.10 and Figure 4.16) show that the modal shape of the first 5 modes are close to being orthogonal, i.e. the modes are independent from each other.

From the FRF curves and associated coherence functions (Figure 4.5 and Figure 4.11) the peaks showing the frequencies for the natural modes of vibration are clear. The reason for showing theses specific nodes are that the hammer impact in these nodes have triggered all the first 5 natural modes of vibration. If one looks at the last peaks, at 282,0 Hz for the top plate and 286,9 Hz for the back plate only the accelerometer placed at the centre of the plate has provided a peak for this mode. As mentioned previously, this was the reason for using an accelerometer at the centre, without it the mode would have been missed. The dips in the coherence function are at positions where there are no modes, i.e. the low coherence at these positions do not affect the results. Besides the dips the coherence is above 95 % for the range of interest.

The frequency for the natural modes of vibration are also clear from the CMIF-curves (Figure 4.6 and Figure 4.12).

To hit the plates perfectly with the hammer was difficult at some positions. To hit the plates with the same force and at a correct angle to the surface is hard and did affect the results, both the FRF-curves and the coherence. Lu (2013) used a pendulum setup which allows greater control over the hammer hits. To use a pendulum would have been desirable but was difficult to achieve given the experimental setup used.

5 FE-analysis of top and back plates

The purpose of this chapter is to set up the model in Abaqus that is used in the process of obtaining the material parameters of the plates by correlating the FE-results to the experimental modal analysis.

5.1 Element types

In Abaqus the geometry is built up by elements. The model contains a few different types of elements depending on the geometry of the part. Below is a description of the elements used.

Thin parts, like the plates and the ribs are modelled using shell elements. The type of shell elements is S4R elements. The S4R element is a quadrilateral ,4 node 3-dimensional element. Each node has 3 translational degrees of freedom (DOF), which allow for deformation in x-, y- and z-direction it also has 2 rotational DOFs for rotation in the plane. The third rotational DOF can be activated if required, for example by rotational boundary conditions (Dassault Systèmes, 2012). A sketch of the S4R element is presented in Figure 5.1.
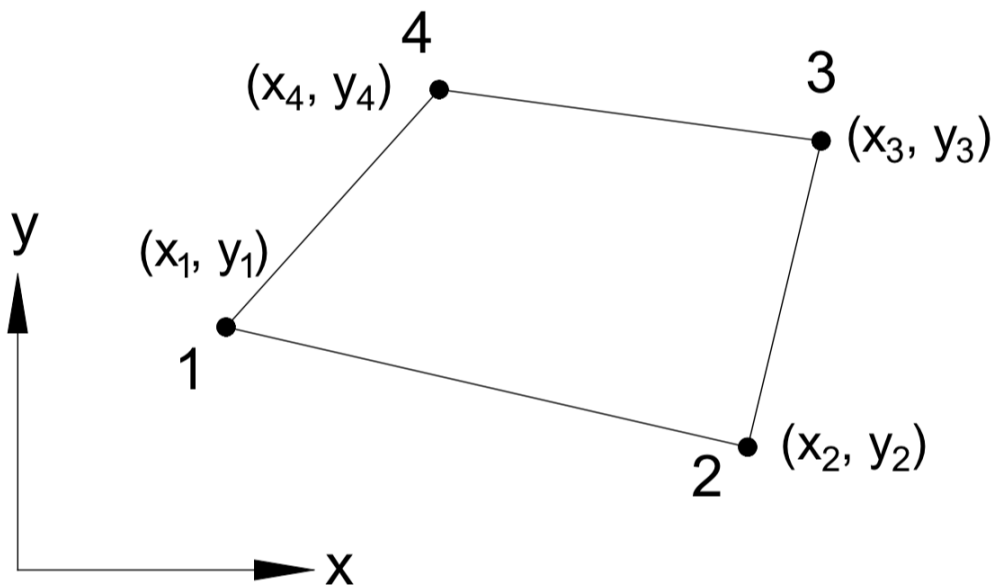
Figure 5.1: A sketch of a quadrilateral shell element.

Shell elements are the natural choice for a part where the thickness is small compared to the area of the parts. Shell elements also require less computational cost compared to solid elements.

For the other parts of the violin, excluding the strings solid elements are used. The element type used is called C3D8R, which is a linear isoparametric brick element with 8-nodes. The solid element has 3 translational and 3 rotational DOFs per node. A sketch of the C3D8R element is presented in Figure 5.2.
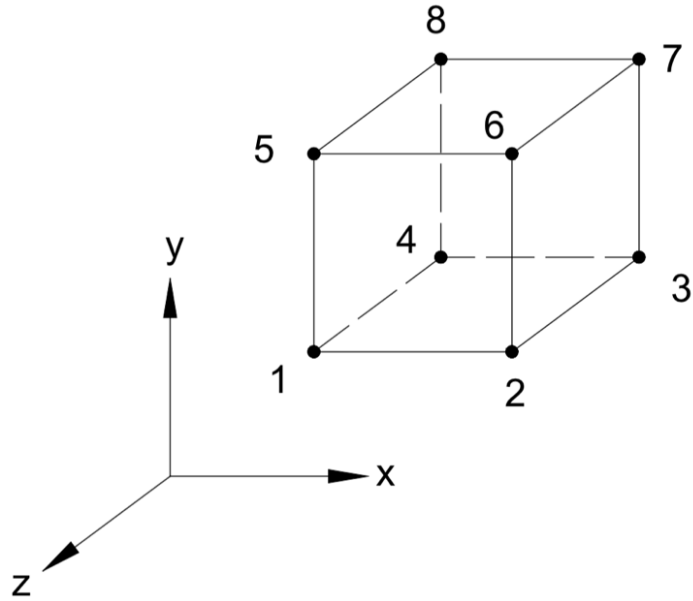
Figure 5.2: A sketch of an isoparametric brick element with 8-nodes.

For the strings linear 2-node beam elements are used. In Abaqus this type of element is called B31. Both translation and rotation are possible, i.e. 6 DOFs per node. Timoshenko beam theory is the standard approach in Abaqus and is also used in this project. For more information regarding beams in Abaqus, the reader is referred to *Abaqus/CAE User's Manual* (Dassault Systèmes, 2012). A sketch of a 2-node beam element is presented in Figure 5.3.
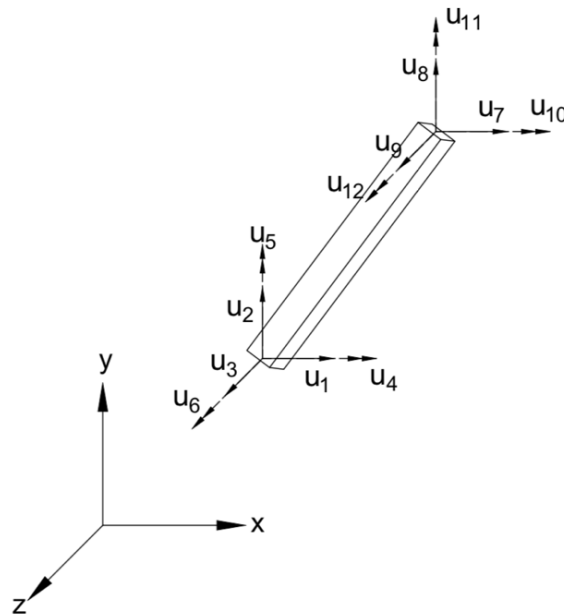
Figure 5.3: a sketch of a 3D linear beam element with 2 nodes. In total 12 DOFs.

5.2 FE-theory

FE-analysis is a numerical method used to solve problems containing differential equations that cannot be solved analytically. Physical mechanical problems can be described using differential equations, leading to the method being very versatile. The differential equations are assumed to hold over a defined region. The region is split into finite elements where the approximation of the solution to the differential equations are solved numerically. The approximation of the solution within an element can for instance be a polynomial of a certain power. The collection of elements is called the mesh. Since the approximation is solved over an element the number of elements that the region is split up into is crucial. If the number of elements goes towards infinity the approximated solution should go towards the correct one, i.e. a finer mesh should lead to a more correct solution (Ottosen & Petersson, 1992).

Each element is built up with nodes and the nodes are assigned with DOFs. The number of DOFs per node depend on the dimension of the problem and the type of element used. It's at the nodes that the displacement and forces are calculated. From the mesh a global equation system is set up, equation (5.1), the size of the system is the same as the number of DOFs.

$$Ka = f_b + f_l \qquad (5.1)$$

Where K is the stiffness matrix, a is a vector containing nodal displacements, f_b is the body force vector and f_l is the load force vector. To solve the equation system, either forces or displacement have to be known, this is obtained by inserting boundary conditions, either by applying forces or initial displacements (Ottosen & Petersson, 1992). For more information regarding FE-analysis one is referred to *Introduction to the finite element method* (Ottosen & Petersson, 1992).

5.3 Modal analysis in Abaqus
Modal analysis in Abaqus follow the theory presented in chapter 4.2 where the modal shapes and frequencies are obtained by solving the eigenvalue problem. So this section is focused on how to set up a modal analysis in Abaqus.

5.3.1 Modules in Abaqus
To understand the procedure of creating a FE-model in Abaqus some information about the software is necessary. Abaqus CAE is divided into different modules. Each module defines a part of the modelling procedure. Below is a list explaining the purpose of each module used.

Part module: The geometry of the different parts of the model is defined here, as well as which type of elements can be assigned to the geometry (solid, shell, beam, etc.), see chapter 5.1.

Property module: Defining material properties of the parts created. Including choosing material properties and assigning them to different regions of the parts.

Assembly module: Assemble all the created parts into the full structure. Only the position of different parts to one another is defined here.

Step module: Define the type of analysis to be performed. Each step is associated to specific procedure, for example a modal analysis. It's possible to have more than one step if more than one type of procedure is wanted.

Interaction module: Here the interaction between the different parts, assembled together in the *assembly module,* is set. Without interaction the parts would act as if they are not connected to each other.

Load module: External loads, boundary conditions and predefined fields are set here.

Mesh module: Defining the mesh of the global structure. There are different types of meshing controls. Structured meshing, free meshing and swept meshing (there are others as well). In structured meshing meshes are predefined on a regularly defined shape, like a cube and then transferred over to the selected geometry. In free meshing there are no preestablished mesh patterns. Swept meshing is more complicated. First the mesh is created on one side of the part, that mesh is then copied in layers until the whole part is meshed (Dassault Systèmes, 2012).

Job module: Submitting the model for analysis. There is also possibility to monitor the progression.

Visualization module: View and save the results of the analysis.

5.3.2   Setting up the modal analysis in Abaqus

With the geometry is created the next step is to set up material parameters and thickness distribution for the plates. The orthotropic behaviour of wood is defined using "engineering constraints" where the 9 material parameters, presented in chapter 3.1 are implemented individually. Material orientation is set so that the longitudinal direction follows the length of the plate, the radial direction is in the plane of the plate and the tangential direction is perpendicular to the plate.

In the *assembly module* either the back plate or top plate is selected, depending on which plate is analysed. In the case of the top plate also the bass bar is selected, since the experimental modal analysis where done with the bass bar. Since the results from the FE-analysis is to be compared to the results from the experimental modal analysis the weight of the accelerometers is added as a non-structural mass at their positions.

The procedure type selected in the *step module* is Linear perturbation frequency, i.e. a linear analysis to obtain the frequencies.

No interactions are added in the *interaction module* for the back plate since it's the only part that's analysed. For the top plate – bass bar interaction a tie constraint is set, i.e. the two surfaces have no relative motion between each other.

No loads or boundary conditions are added in the *load module*. By not adding any boundary conditions free-free boundary conditions are obtained, i.e. the plates hovers in space.

The elements selected in the *mesh module* are S4R for the plates and C3D8R for the bass bar. The type of element and number of elements are presented in Table 5.1. The mesh is improved to avoid elongated elements. Structured meshing is used in the regions where it's possible, in regions where the geometry is too complicated free meshing is used.

Table 5.1: Type and number of elements used in the modal analysis in Abaqus.

Part	Type of element	No. of elements
Back plate	S4R	6517
Top plate	S4R	6706
Bass bar	C3D8R	577

With the mesh completed the plates are ready to be analyzed. A job is created in the *job module* and submitted for analysis.

5.4 Model correlation

The model correlation is performed to find material properties of the violin plates. The results from the experimental analysis show the frequencies that wanted to be achieved in the Abaqus model. To correlate the model to the experimental modal analysis results, some insight in how modifying the parameters is expected to change the results are necessary, i.e. what parameters affect which modes of vibration.

5.4.1 Parameters affecting the first five modes of vibration

The five first of modes of vibration are five very characteristic modes for the violin plates. The naturel frequencies of violin plates have been used as a tool for hundreds of years for assessing the quality of the plates. A common technique for luthiers is to tap the plates at certain position and listen to the sound created by the plate (Molin, et al., 1988) (Curtin, 2006).

There are a lot of factors that influence the modal shape and the frequencies. There is a variation in frequencies between different plates, but the shape tends to be more or less the same (Curtin, 2006). Acoustic properties are related to the modes of vibration of the plates since the vibration created in the strings are transmitted to the top plate through the bridge and further to the back plate through the sound post and the ribs, i.e. it's very important for the quality of the instrument.

There are studies done with the goal to find which factors, material or geometrical that influence which modes and in what way (Gough, 2015) (Molin, et al., 1988) (Curtin, 2006). Material factors include strength parameters and density. Geometrical factors include the shape of the plates, arching height and thickness.

It should be noted that (Molin, et al., 1988) used plane stress conditions when determining the correlation between shape and material parameters, i.e. no information regarding out of plane

parameters are examined. The out of plane material parameters are expected to have a small impact on the modal parameters.

In this project where two actual plates have been tested, some of these factors are already set or have been measured, namely all geometrical parameters. By weighing the plates, the density is easily calculated since the volume of the plates are known from the thickness measurements, see chapter 2.2.3. Meaning that only material properties are relevant to study to match the FE-analysis to the experimental modal analysis.

The shape of the modes of the top and back plate are similar if the bass bar is excluded. In the experimental modal analysis, the bass bar was included which will change the modal shape of the top plate. The parameters affecting the different modes are not expected to change by a large margin though. Therefore, the parameters affecting the modal shapes for the back plate, or the top plate excluding the bass bar is presented below.

1st mode of vibration
The first mode of vibration is a twisting mode, where the corners of the plate oscillate. The longitudinal centre line is a nodal line. The vibration is asymmetrical where the diagonal corners of the plate move in the same phases. The mode is very dependent on the torsional stiffness of the plate. The parameter that effect the frequency of the mode the most is G_{LR}, but an effect from modifying E_L and E_R is also expected (Molin, et al., 1988)

2nd mode of vibration
This is a symmetrical mode, around the centre lines of the plate. Most of the oscillation takes place around the edge of the plate, most movement is around the C-profile. The nodal lines form a u-shape at the lower and upper bout of the plate, there is also a nodal line along the centre line of the plate but some oscillation at the top and lower edge. The mode has a bending behaviour in both in plane directions, i.e. the material parameters that's expected to influence the frequency the most are E_L and E_R (Molin, et al., 1988).

3rd mode of vibration
The 3rd mode of vibration is more complex compared to the 1st and the 2nd one, making a clear relationship between shape and material parameters more difficult. The behaviour includes both twisting and bending. The oscillation is symmetrical. The nodal lines are similar to the 2nd mode with u-shapes in the lower and upper bout as well as at the middle part of the centre line. The outer parts of the plate oscillate the most. The complex behaviour leads to E_L, E_R and G_{LR} all affecting the frequency. Most effect from modifying E_L (Molin, et al., 1988).

4th mode of vibration
As the 1st mode the 4th mode is a torsional mode. The mode is more complex compared to the 1st one and like the 3rd mode it complicates the relationship between shape and material parameters. The mode is nonsymmetric, but there is a nodal line along the centre line of the plate. Since it's a twisting mode it's intuitive to think that G_{LR} is the material parameter affecting the frequency the most, but the complexity of the mode leads to also E_L and E_R having an impact (Molin, et al., 1988).

5th mode of vibration

The 5th mode is called the ring mode. Unlike the 1st-4th there is clear oscillation in the middle part of the plate. The mode is symmetrical, and the middle part vibrates out of phase compared to the edges. There is both twisting and bending. The bending is in both in plane directions. Since there is both twisting and bending all parameters effect the frequency of the plate (Molin, et al., 1988).

5.4.2   Method

Material parameters are chosen for the first iteration. The density is easily calculated by weighing the plates by collecting the volume of the plates from Abaqus. The strength parameters selected are the ones used by Knot, et al. (1989), see Table 3.3 and Table 3.4

A job is summited, and the results are compared to the results from the experimental modal analysis. The percental difference between the frequencies are checked. The parameters are modified using the theory about the modes presented above. First G_{LR}, E_L and E_R are varied to find a match of the first mode of vibration. The procedure continues with matching the other 4 modes. The study stops when a variation of a parameter has more negative than positive impact on the differences in frequency.

Auto MACs are calculated to control the difference in modal shapes between the modes in Abaqus.

5.4.3   Results

Material parameters found from the model correlation is presented in Table 5.2.

Table 5.2: Material parameters determined from the model correlation.

	Back Plate	Top Plate
Weight [g]	81,0	83.6*
ρ [kg/m^3]	628	467
E_L [GPa]	15	13
E_R [GPa]	2.1	1.5
E_T [GPa]	0.73	0.65
G_{LR} [GPa]	1.6	0.6
G_{LT} [GPa]	0.12	0.72
G_{RT} [GPa]	0.19	0.42
ν_{LR} [-]	0.2	0.375
ν_{LT} [-]	0.392	0.436
ν_{RT} [-]	0.703	0.468

* Includes the weight of the bass bar

The comparison in frequencies between the experimental modal analysis and the modal analysis performed in Abaqus is presented in Table 5.3 and Table 5.4.

Table 5.3: Comparison of frequency between experimental modal analysis and modal analysis in Abaqus for the first five modes. Back plate.

Mode	Back plate		
	Frequency Experiment [Hz]	Frequency Abaqus (incl. Acc.) [Hz]	Percentual difference [%]
1	86,8	80,9	-7
2	157,8	148,6	-6
3	192	183,8	-4
4	235,4	253,0	7
5	286,9	305,4	6

Table 5.4: Comparison of frequency between experimental modal analysis and modal analysis in Abaqus for the first five modes. Top plate.

Mode	Top plate		
	Frequency Experiment [Hz]	Frequency Abaqus (incl. Acc.) [Hz]	Percentual difference [%]
1	76,8	73,2	-5
2	166,0	161,8	-2
3	234,0	233,8	0
4	261,6	273,9	5
5	282,4	282,6	0

Frequencies for the first 5 modes of vibration from the modal analysis performed in Abaqus, excluding the accelerometers are presented in Table 5.5.

Table 5.5: Frequencies for the first 5 modes of vibration from the modal analysis in Abaqus without accelerometers.

Mode	Back plate	Top plate
	Frequency (excl. Acc.) [Hz]	Frequency (excl. Acc.) [Hz]
1	98.5	89.6
2	162.6	182.0
3	239.5	270.5
4	292.8	285.1
5	366.0	338.7

The modal shapes of the first five modes of vibration for the back and top plate, both with and without accelerometers are presented in Figure 5.4 to Figure 5.13.
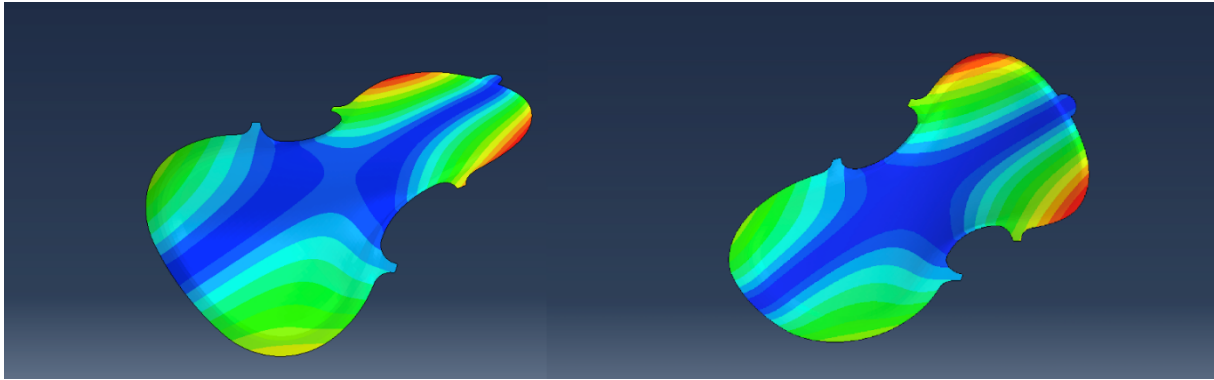
Figure 5.4: Modal shape for the 1st mode of vibration for the back plate. To the left with accelerometers and to the right without accelerometers.
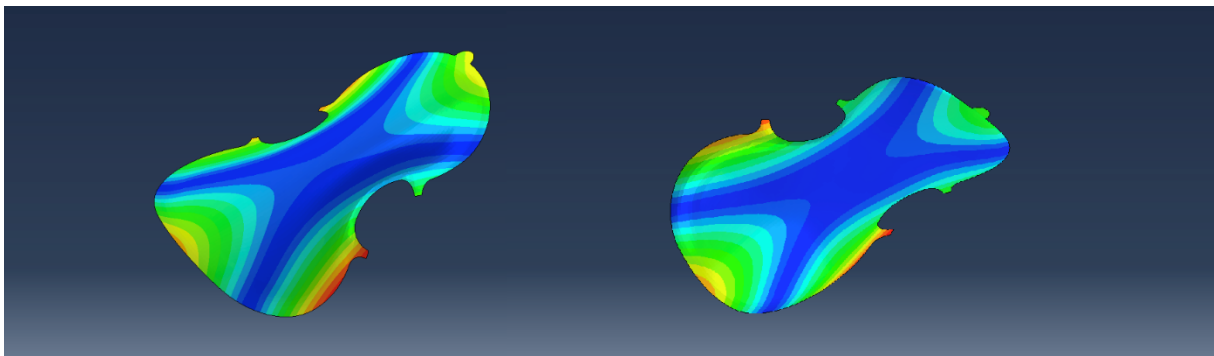
Figure 5.5: Modal shape for the 2nd mode of vibration for the back plate. To the left with accelerometers and to the right without accelerometers.
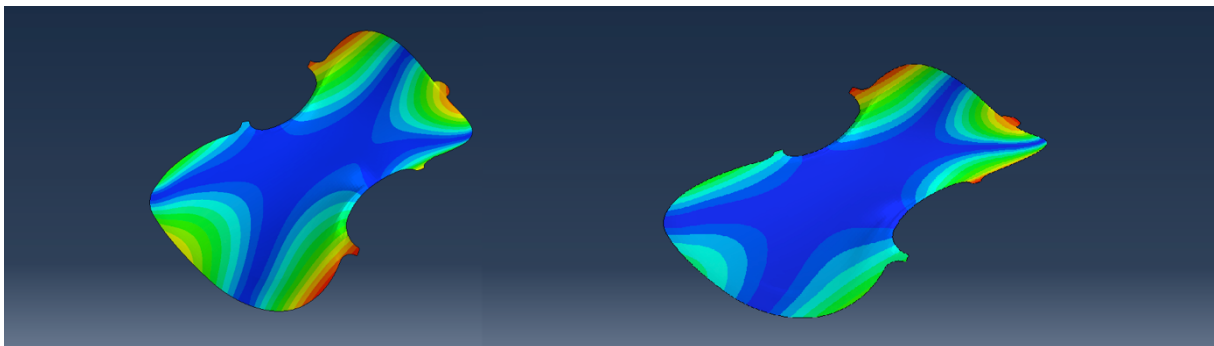
Figure 5.6: Modal shape for the 3rd mode of vibration for the back plate. To the left with accelerometers and to the right without accelerometers.
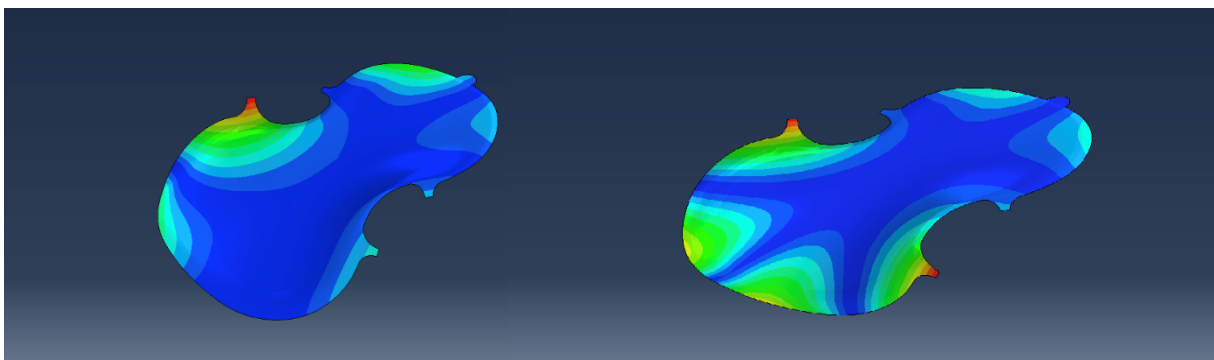
Figure 5.7: Modal shape for the 4th mode of vibration for the back plate. To the left with accelerometers and to the right without accelerometers.
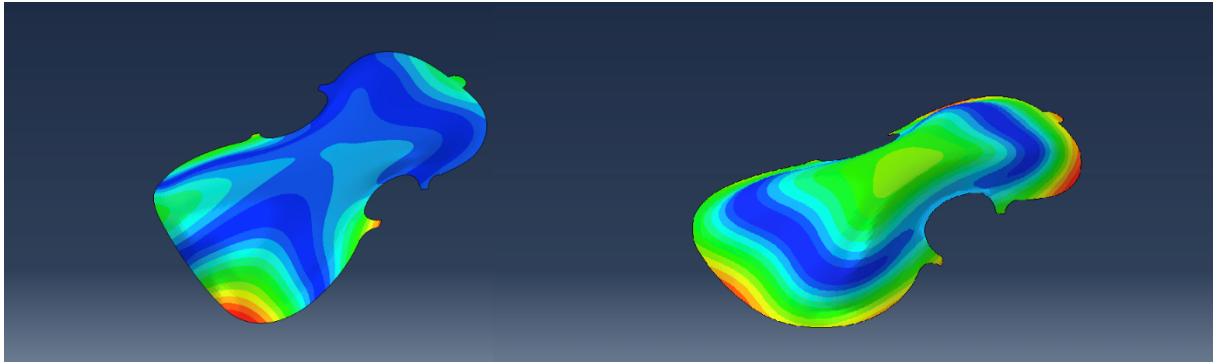
Figure 5.8: Modal shape for the 5th mode of vibration for the back plate. To the left with accelerometers and to the right without accelerometers.
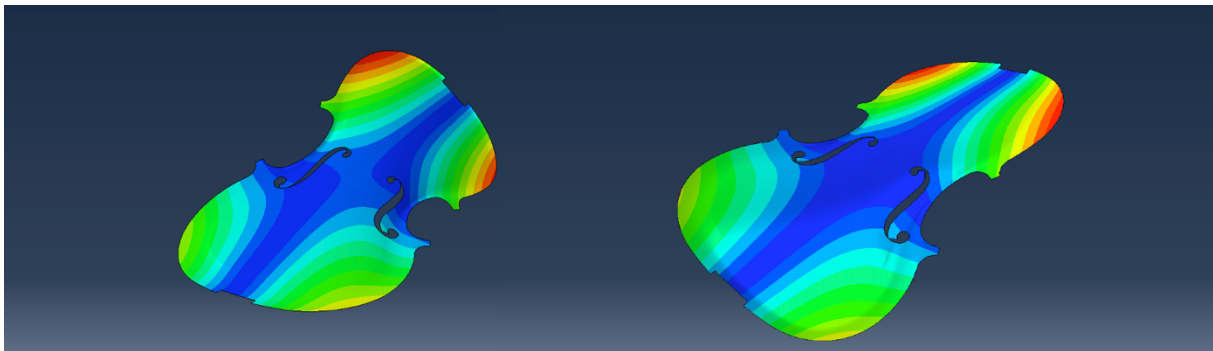
Figure 5.9: Modal shape for the 1st mode of vibration for the top plate. To the left with accelerometers and to the right without accelerometers.
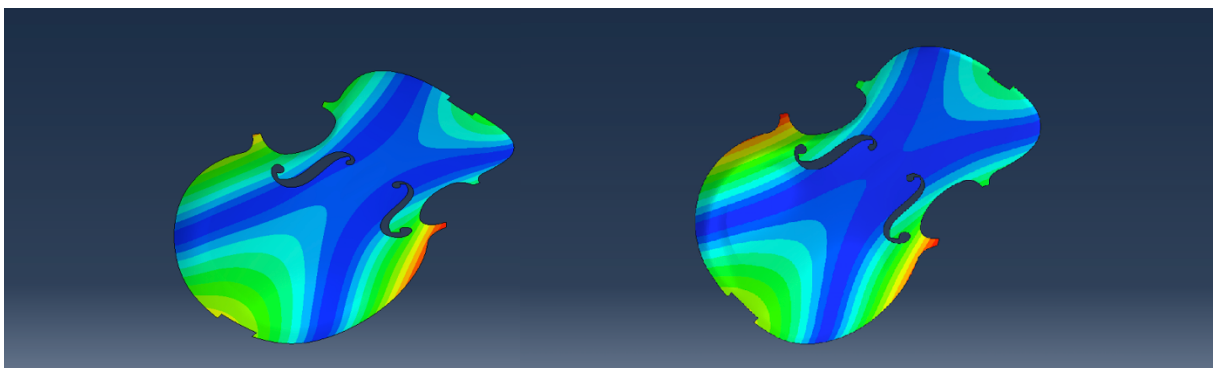
Figure 5.10: Modal shape for the 2nd mode of vibration for the top plate. To the left with accelerometers and to the right without accelerometers.
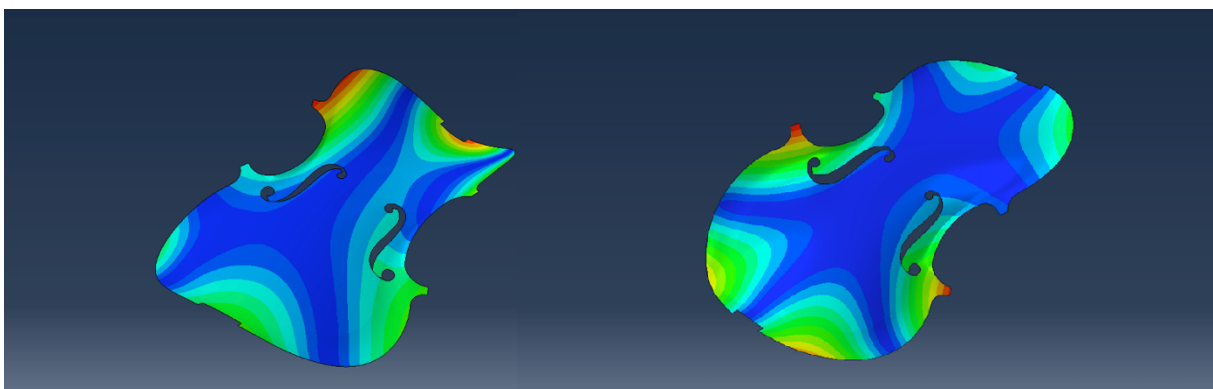
Figure 5.11: Modal shape for the 3rd mode of vibration for the top plate. To the left with accelerometers and to the right without accelerometers.
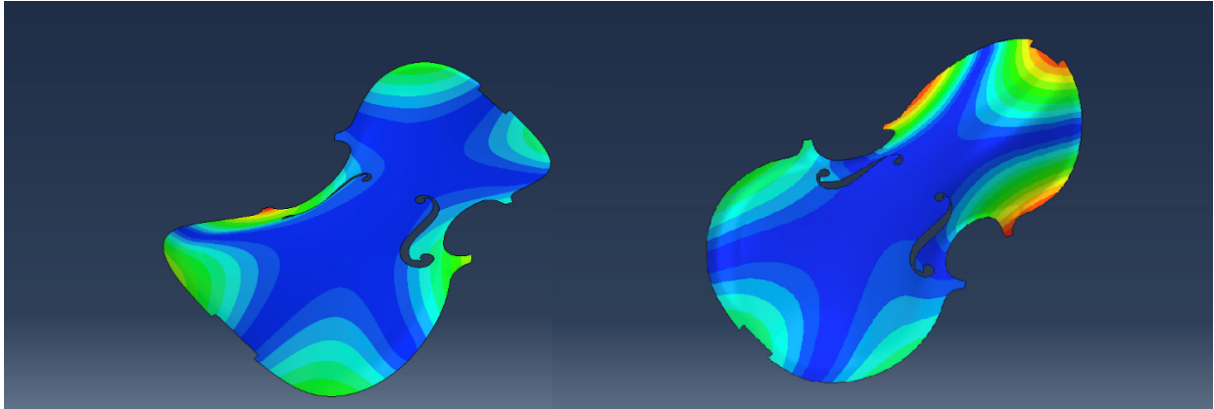
Figure 5.12: Modal shape for the 4th mode of vibration for the top plate. To the left with accelerometers and to the right without accelerometers.
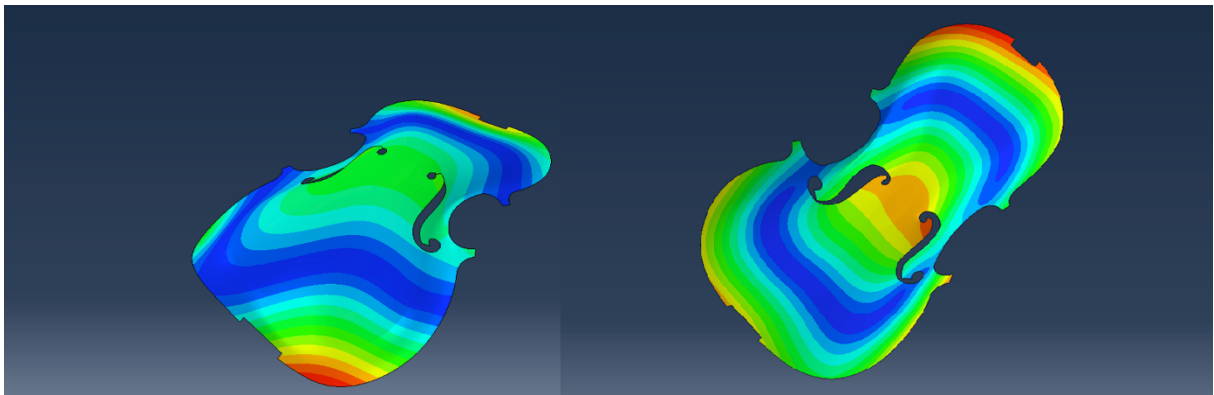
Figure 5.13: Modal shape for the 5th mode of vibration for the top plate. To the left with accelerometers and to the right without accelerometers.

Auto MAC values for the plates from the modal analysis including the accelerometers (Figure 5.14 to Figure 5.15).
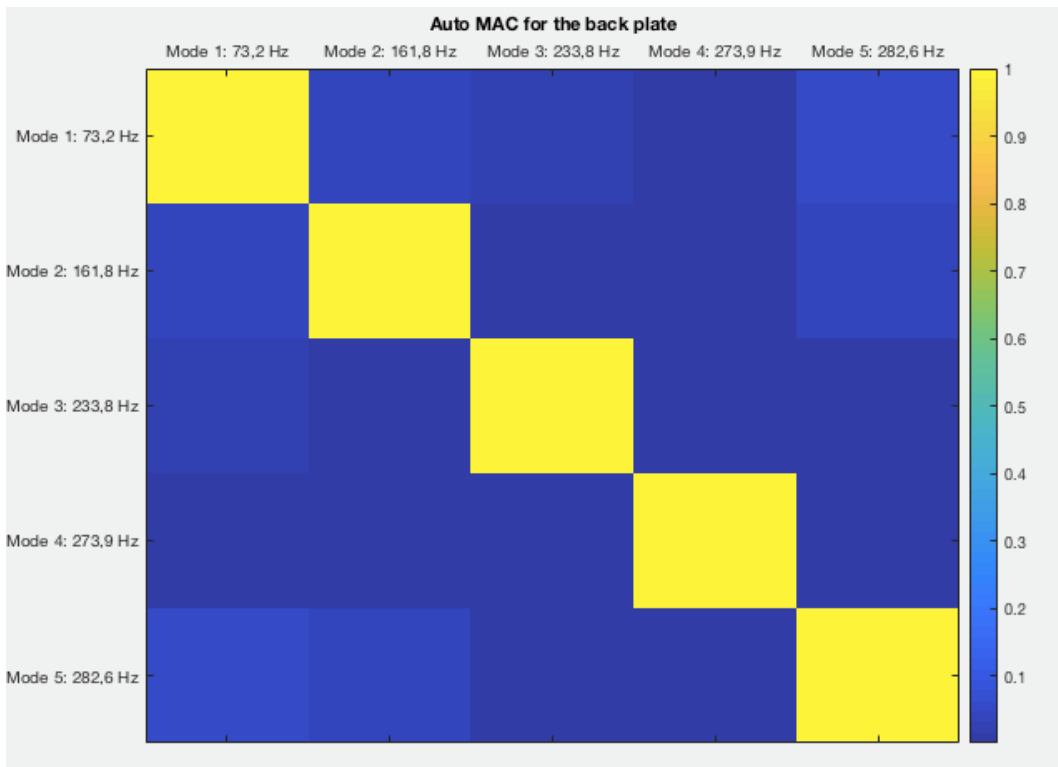
Figure 5.14: Auto MAC of the first five modes of vibration for the top plate including accelerometers.
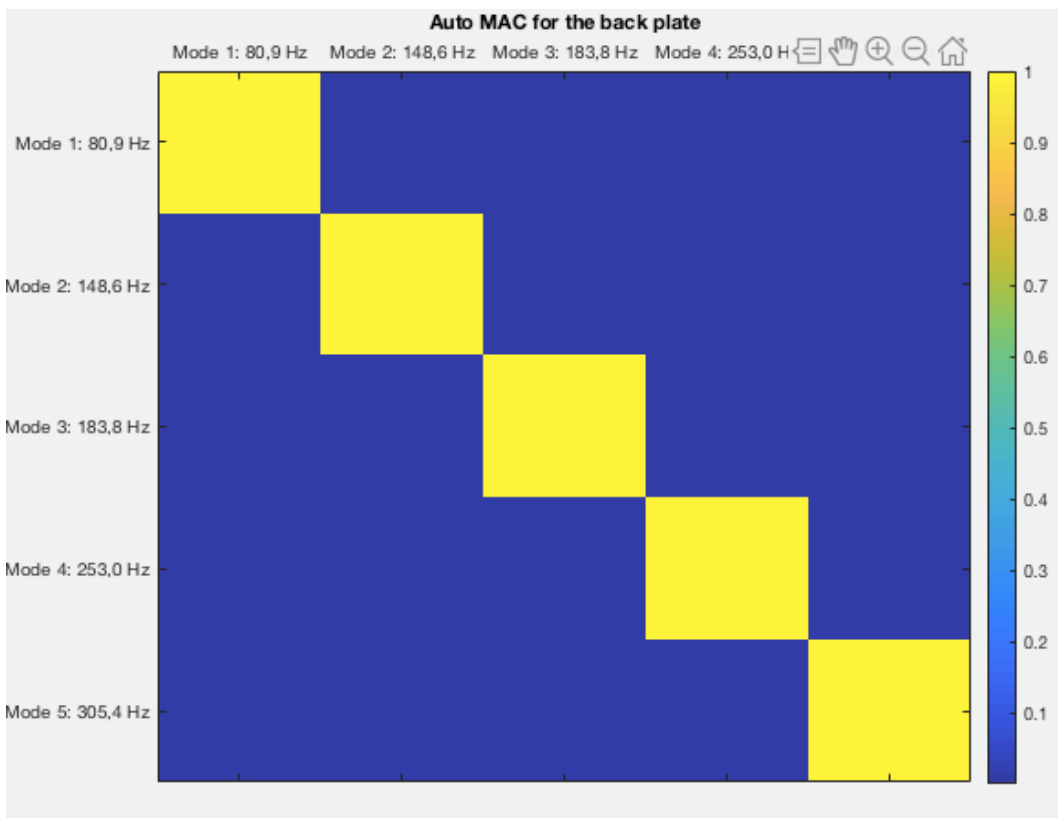
Figure 5.15: Auto MAC of the first five modes of vibration for the back plate including accelerometers.

5.5 Discussion

The strength parameters affecting the different modes of vibration did not correspond to the parameters from the study performed by Molin, et al (1988) fully. The main difference was that all parameters affected all modes more than anticipated. For example, G_{LR} had a larger impact on mode 2 than expected. Parameters in the out of plane direction had a small affect the results, because of plane stress conditions. Meaning that the resulting strength parameters acting in the transversal direction are more difficult to assess.

The calculated eigenmodes of both the top plate and back plate correlated reasonably well with the experimental modal analysis, both in terms of mode shapes and corresponding natural frequencies. For the top and back plate the deviation from the measured natural frequencies were ±5 % and ±7 % (Table 5.3 and Table 5.4) which is in line with what similar studies have achieved (Pyrkosz, 2013) (Lu, 2013). However, an interesting observation which holds for both the top and the back plate is that the first modes occurs at too low frequencies whereas the higher modes at too high. The fact that the deviation between the measured frequencies and the ones generated by Abaqus appears to not be random suggests that there remain parameters or interactions unaccounted for in the FE-model. A possible explanation to this could be that the relative thickness of one region off a plate to others are incorrect. Modes involving bending or torsion of a specific area of the plate would be disproportionally affected by a change of thickness in that area. The effects of variations of thickness in violin plates is further studied by Molin, et al (1988).

If one compares the modal shapes that include the mass from the accelerometers (Figure 5.4 to Figure 5.13) with the modal shapes from the experimental modal analysis (Figure 4.7 to Figure 4.9 and Figure 4.13 to Figure 4.15) it's clear that the shape is very similar, i.e. the same modal shapes appears in both analyses. This is a good indication that the correct modal shapes were obtained in the experimental modal analysis and that the experiment was successful. The modal shapes without accelerometers are more symmetrical and more similar to shapes found in past studies (Lu, 2013) (Pyrkosz, 2013) (Gough, 2015), compared to the results from the experimental modal analysis this also holds for the 4th and 5th modal shape. It's clear that the effect of the accelerometers on the 4th and 5th modal shape is large.

The material parameters chosen to obtain the modes largely falls within the span presented in Table 3.3 and Table 3.4. One exception being the Young's modulus in the radial direction which have a slightly higher value than proposed in past studies. The natural frequencies without accelerometers (Table 5.5) are within reasonable limits compared to previous studies (Gough, 2015) also indicating that the results are reasonable.

6 FE-model of the complete violin

With material properties determined, analyses of the complete instrument are possible. The first goal of the analysis of the complete violin is to add tension to the strings. Before tensioning the strings, interactions have to be set between the parts in the complete geometric model and a mesh needs to be applied.

6.1 Material properties

Material properties have been determined for the plates (Table 5.2). The same properties are used for all the parts modelled with maple and spruce (Table 3.1). For the parts modelled with ebony and pine the values from Table 3.5 are used.

The G-, D- and A-string is modelled as gut core strings with steel windings wrapped around them and the E-string as a steel wire. The values are collected from Knot, et al (1989) and are presented in Table 6.1. Non-structural mass is added to the G-, D- and A-string to take the steel windings into consideration. It is assumed that the winding does not contribute to the stiffness of the string. It's added as mass per length.

Table 6.1: Material parameters of the strings (Knot, et al., 1989).

String	E [GPa]	ν [-]	ρ [kg/m^3]	Non-structural mass [g/m]
G	30	0,4	1200	3,314
D	30	0,4	1200	1,352
A	30	0,4	1200	0,557
E	195	0.28	7700	-

6.2 Interaction

The goal with the interaction between the parts is to obtain a behaviour as close to a real violin as possible. A poor choice in constraints between the parts can lead to numerical difficulties in the analysis, this is considered when choosing the constraints.

Most of the parts in the violin are glued together, a behaviour that is easily modelled using a tie constraint. With a tie constraint one can choose which DOFs to tie together by defining a master and a slave region. The tie constraint is used between the following parts:
- Upper saddle to the neck
- The fingerboard to the neck
- The Neck to the top end block
- All blocks to the ribs
- Bridge to the top plate (rotations are not constrained)
- Sound post to plates (rotations are not constrained)
- Bass bar to top plate.
- Lower saddle to top plate
- Strings to upper saddle, bridge and tailpiece (rotations are not constrained)

The box structure is created by merging the ribs, top plate and back plate together into a single part.

The tailpiece is connected to the lower saddle through a link multi-point constraint (MPC). This constraint enforces the distance between a control node on the lower saddle and slave nodes at the end of the tailpiece. This setup provides a rotational joint between the tailpiece and the lower saddle. A continuum coupling constraint was added between the control node of the saddle-tailpiece link MPC and surrounding nodes on the saddle ridge to avoid excessive stress concentrations. This constraint type redistributes the forces acting on the control node to nearby nodes within a defined influence radius. The weighting method for the redistribution is chosen as linearly declining with distance from the control node.

The tail loop is important to balance the string tension acting on the lower saddle. This is done by adding a second link MPC constraint between the pin and the back of the lower saddle. The constraint setup connecting the tailpiece, lower saddle and pin is displayed in Figure 6.1.
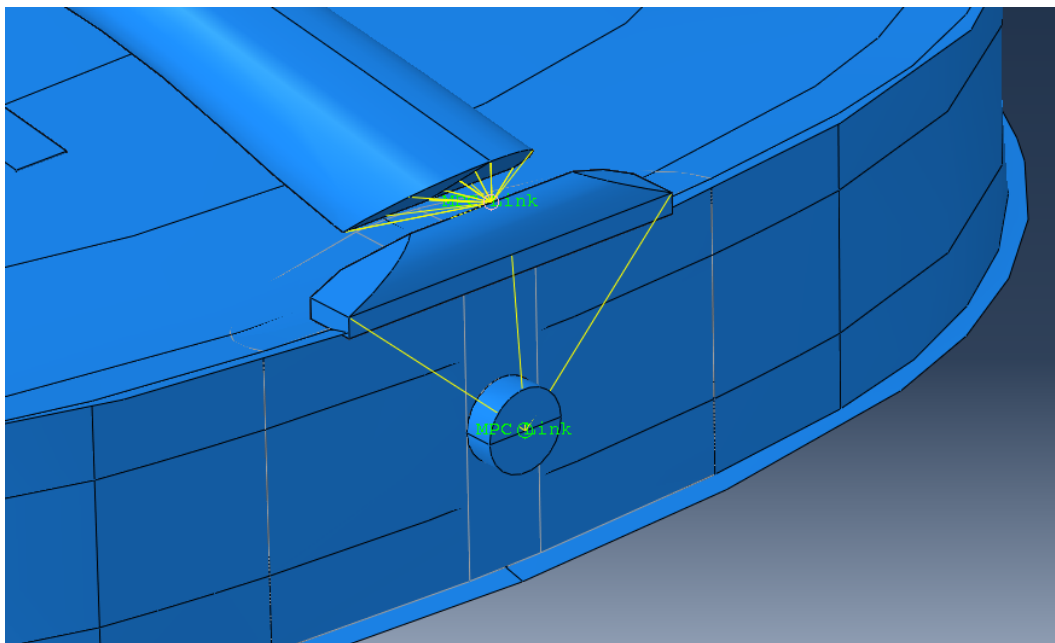
Figure 6.1: Link MPC constraints connecting the tailpiece, lower saddle and end pin.

6.3   Mesh

When creating the mesh, the goal is to get a smooth mesh where the size of the elements is similar for the whole model. If possible, structured mesh is used. In some parts, where the geometry is complicated swept and free meshing is used. The elements used and the number of elements for each part is presented in Table 6.2. The following element types are used in Abaqus:

C3D8R – 8-node solid brick element with reduced integration.

S4R – 4-node shell element with reduced integration.

B31 – 2-node Timoshenko beam element.

Table 6.2: Type and number of elements for the complete model.

Part	Type of element	No. of elements
Upper saddle	Solid	80
Neck	Solid	4059
Fingerboard	Solid	2364
Bridge	Solid	4532
Blocks	Solid	5047
Violin box*	Shell	26431
Bass bar	Solid	546
Tail piece	Solid	5591
Sound post	Solid	2646
Lower saddle	Solid	255
End pin	Solid	492
Strings	Beam	576
Total:		52619

* Includes the plates and the ribs

The mesh of the complete violin model is presented in Figure 6.2.
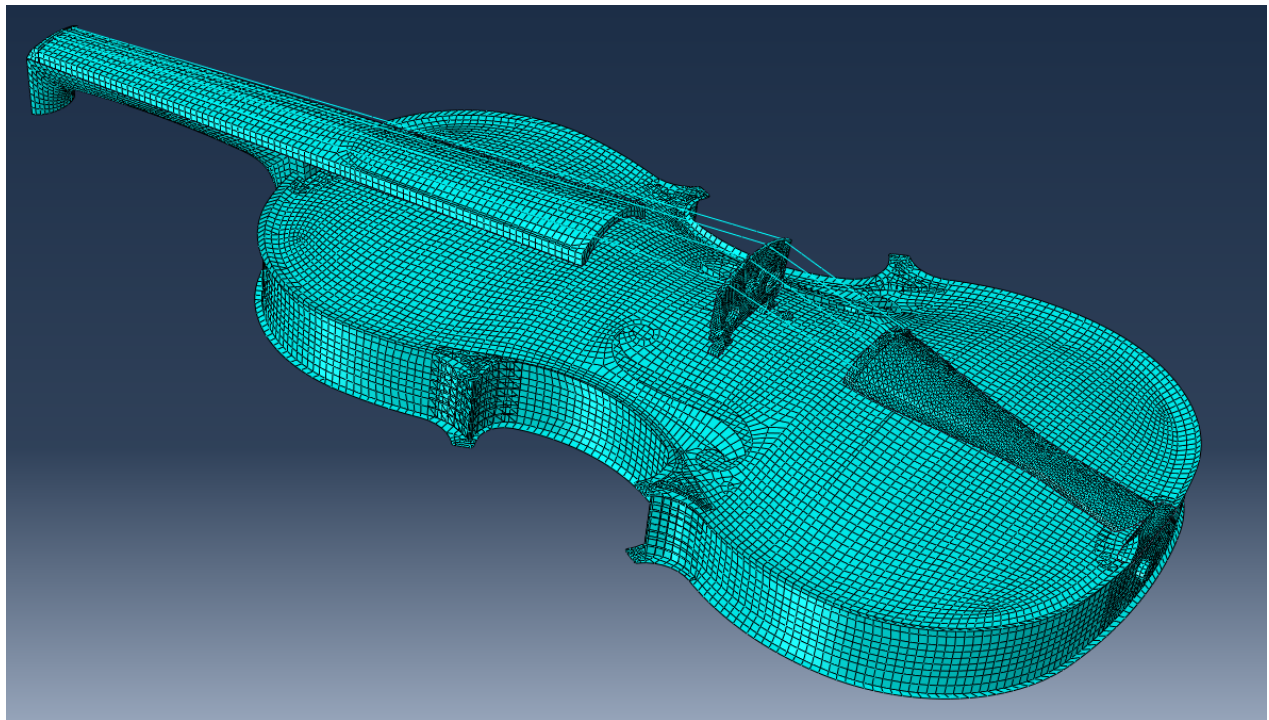
Figure 6.2: Mesh of the completely assembled violin.

6.4 String tension

By adding the strings to the violin model and applying the pre-stress linear FEM is no longer sufficient. Some theory regarding non-linear FEM is necessary.

6.4.1 Non-linear FE theory

When the strings are attached to the instrument a linear FE-formulation is not enough to obtain adequate results. In theory this means that there is no longer a linear relationship between force and displacements. In the case of the violin the pre-stress caused by the strings create non-linear deformation in the violin corps. In linear FE-theory the stiffness of the system is calculated only once, in the initial state, see equation (5.1). In the non-linear case the stiffness is updated and calculated in the current state.

There are different methods for solving non-linear FE equations. The default method for solving non-linear geometry in Abaqus is by using a *full Newton-Raphson algorithm*. It's an iterative procedure where the equilibrium equations (5.1) are solved at each iteration. The algorithm is based on equilibrium between external and internal forces. The equilibrium is described with a residual, $\boldsymbol{r}$.

$$\boldsymbol{r} = \boldsymbol{f}_{int} - \boldsymbol{f}_{ext} \quad (6.1)$$

The load or displacement is added in steps until the whole force or displacement is applied to the system. At each step iterations are performed until the residual equation is fulfilled (6.1) to a threshold. The residual equation is updated by modifying the tangential stiffness matrix, $\boldsymbol{K}_t$. The iterative process is described in Figure 6.3 (Ristinmaa, 2019).
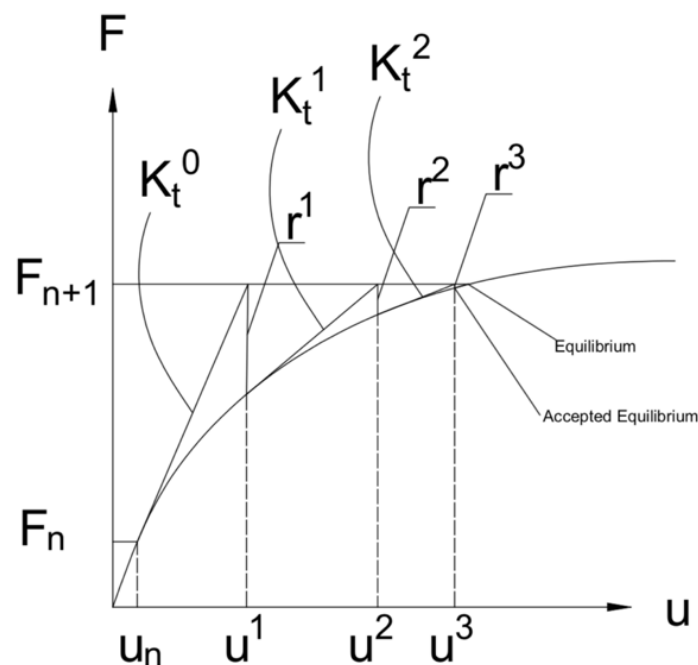
Figure 6.3: The iteration procedure described. A small increase in force is applied, up to $\boldsymbol{F}_{n+1}$. Iterations are applied by modifying $\boldsymbol{K}_t$ until the threshold of equilibrium is fulfilled by calculating the residual using equation (6.1).

70

The Newton-Raphson scheme for an increase in load is presented below (Ristinmaa, 2019). The same scheme applies for a change in displacement.

Newton Raphson Algorithm

- For load step $n = 1 \dots n_{max}$
  - Increase the load by ΔF: $F = F + \Delta F$
  - Initiate u_n
  - Loop while the residual equation (6.1) is not fulfilled $r > r_{tol}$
    - Calculate K_t
    - Calculate displacement increment: $K_t \Delta u = -r$
    - Update displacement. $u = u + \Delta u$
  - End iteration
- End load step

There is no need to calculate K_t at each iteration. In a *modified Newton Raphson algorithm* K_t is calculated once and then used in every iteration. This will require more iterations, but each iteration step is faster to calculate since the calculation of K_t require a lot of computational power.

The Newton-Raphson algorithm, where there is a continuous increase in increment is not sufficient around turning points, i.e. where K_t changes sign. It will lead to snap throughs, see Figure 6.4. This problem can be avoided by using a *constrained path following method* where neither the displacement nor the force is controlled. The method is not explained here. For more information regarding the Newton Raphson algorithm with constrained path following one is referred to *Introduction to Non-linear Finite Element Method* (Ristinmaa, 2019).
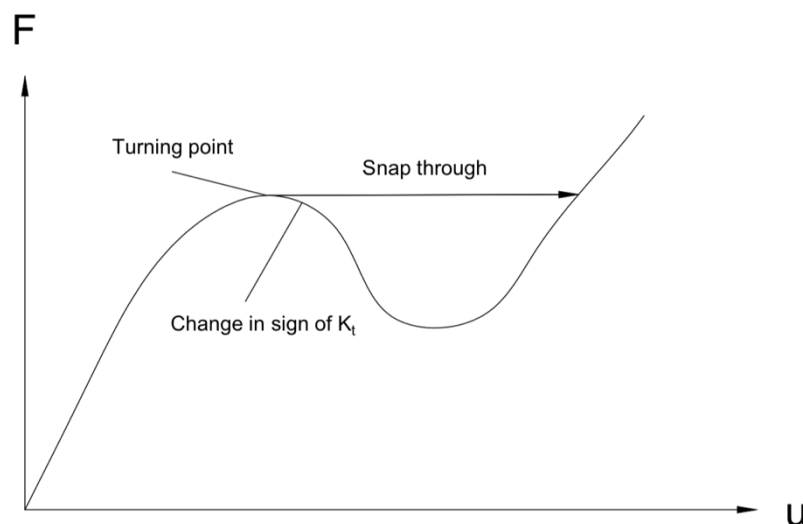
Figure 6.4: By increasing the load turning points will lead to snap throughs and parts of the equilibrium curve will go undetected. It can be solved by using a path following method where neither the force nor the displacement is modified.

6.4.2 Modelling string tension in Abaqus

To achieve the effect off string tension in the FE-model a number of different strategies were considered. Ultimately, defining stress as a predefined field assigned to the strings proved to be the easiest and most stable method. Other methods evaluated were assigning a bolt load to each string to mimic the right string force or defining a thermal expansion coefficient for the strings to control the strain by changing temperature.

Because of the different materials and cross-section of the strings, the value of the predefined stress fields needs to be tailored to each string. Further, the stresses in the strings will change as static equilibrium is calculated for the model as the stress in one string will influence the stress in the other strings. To achieve proper string tension at static equilibrium the stresses were changed, and equilibrium calculated iteratively until the right values were obtained.

To avoid stress concentrations and excessive deformations at the nodes connecting the strings to the rest of the violin, continuum coupling constraints were added at the connection points.

6.4.3 Boundary conditions

To avoid numerical issues with the solver while running the pre-stressed model certain boundary conditions were needed. The Abaqus solver would calculate a number of negative eigenvalues at string nodes which indicates the occurrence of bifurcations. To avoid this issue the process of applying tension to the strings were divided into two calculation steps. First local coordinate systems were defined for each string which allowed the movement of each string to be restricted in all directions except axial, after which static equilibrium is calculated. In the second step the boundary conditions on the strings were removed and a new static equilibrium could be calculated which represents the actual pre-stressed state of the model without displacement constraints.
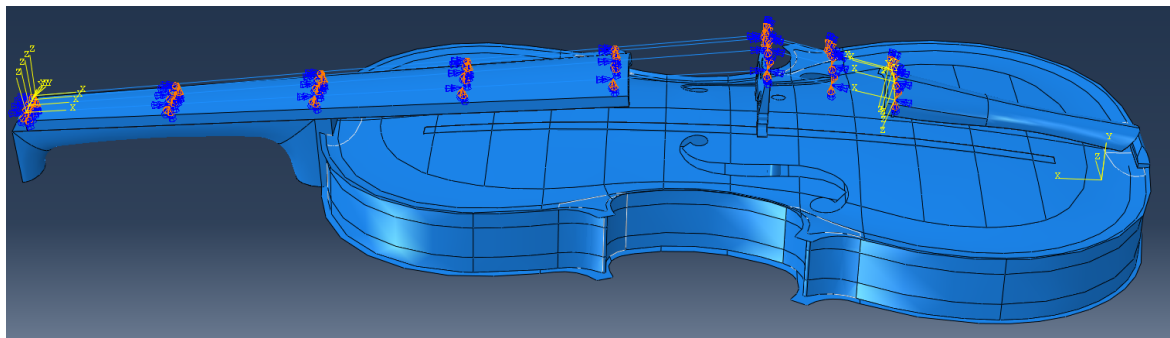
Figure 6.5: First step. Tension is applied to the strings. The strings are allowed deform axially.
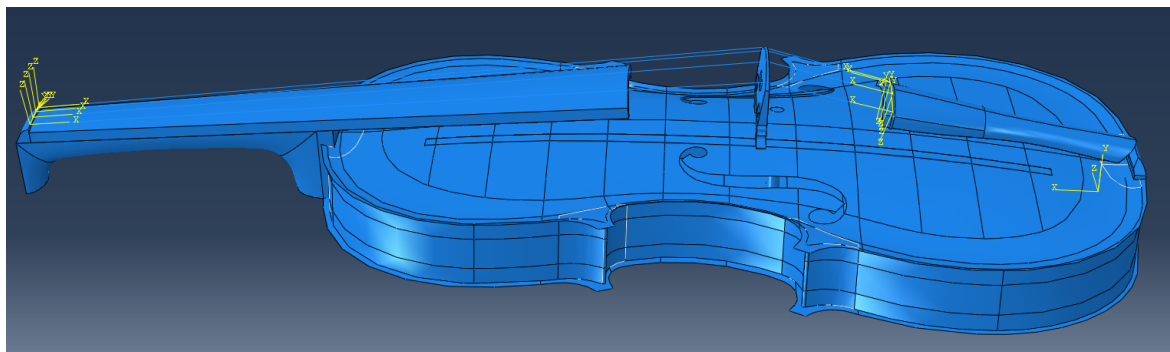
Figure 6.6: Second step. The boundary conditions from step one are removed. Violin is allowed to deform freely from the tension applied to the strings.

6.4.4 Tuning the strings

To evaluate whether correct string tension is achieved the violin is tuned by preforming a modal analysis on the pre-stressed model. The G, D, A and E string of a real violin is usually tuned to 196, 294, 440 and 659 Hz respectively (Riechers, 1928). The predefined stress fields for the strings were adjusted so that the first bending mode of each string occurred at those frequencies.

Figures of the modal shapes for the 4 strings were saved and stored. Von Mises stress fields and in plane strains of the two plates were calculated as well as the deflected shape of the violin box.

6.5 Results of pre-stressing the strings

The predefined stress fields required to tune the violin strings, and the resulting string force is presented in Table 6.3 together with the frequency for the 1st bending mode for each string.

Table 6.3: Predefined fields are added to find the 1st bending mode of each string.

String	Predefined Stress field [MPa]	String Force [N]	1st bending mode [Hz]
G	363	60,8	195,2
D	500	58,5	295,4
A	1750	132,5	439,1
E	2640	85,1	659,9

Modal shapes for the 1st bending mode for each string is displayed in Figure 6.7 and Figure 6.8.
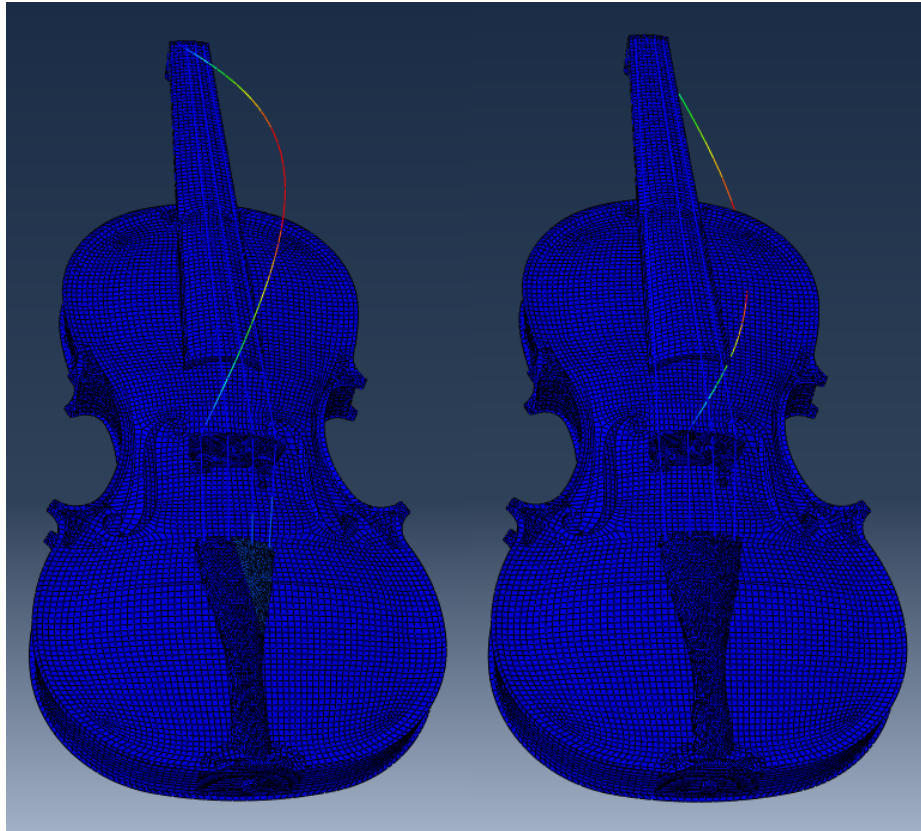
Figure 6.7: First bending mode of the G- and the D-string.
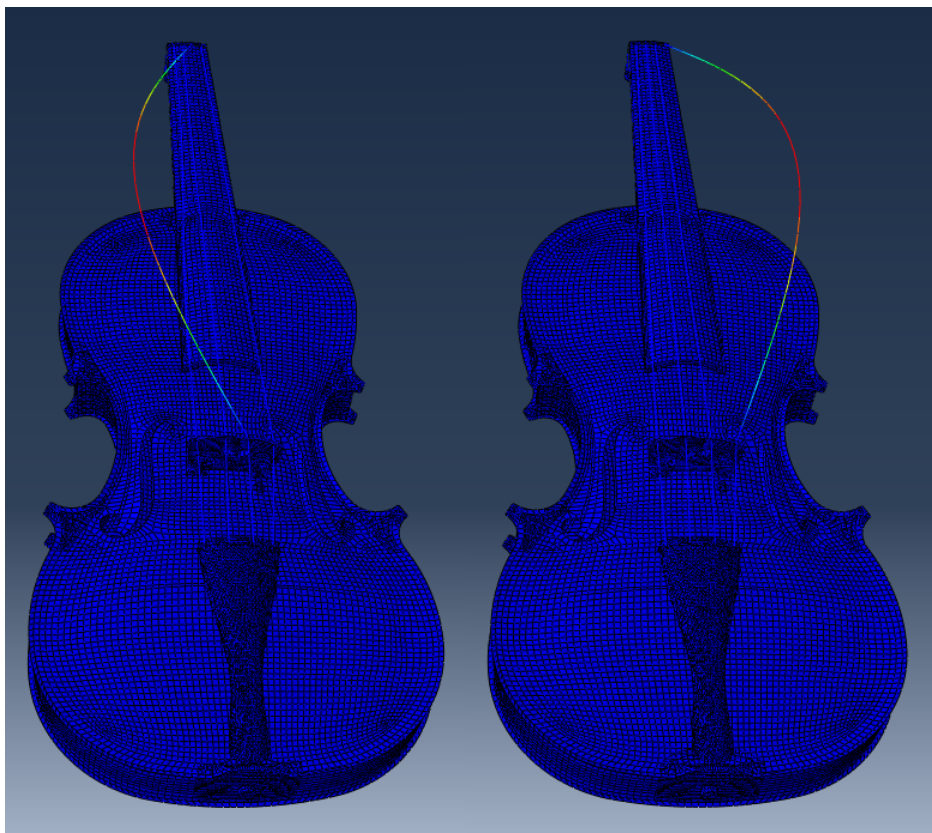
Figure 6.8: First bending mode of the a- and the E-string.

The resulted Von Mises stresses in the plates caused by the stresses in the strings is displayed in Figure 6.9
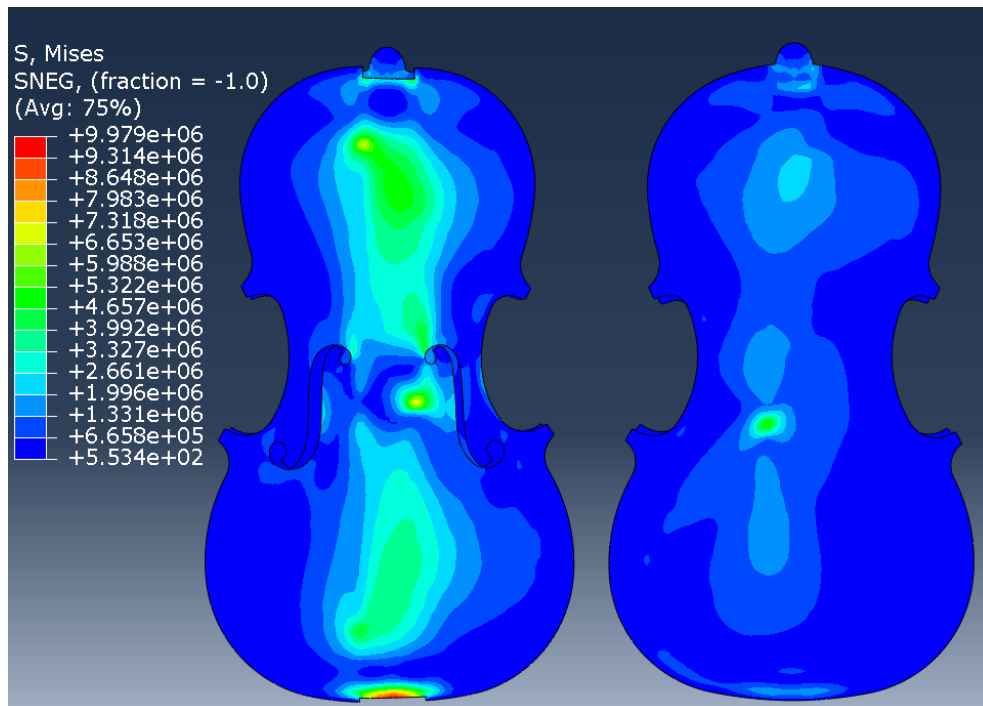
Figure 6.9: Von Misses stresses on the back- and top plate caused by the tensioning of the strings.

The maximum in plate strain caused by the tension in the strings is displayed in Figure 6.10
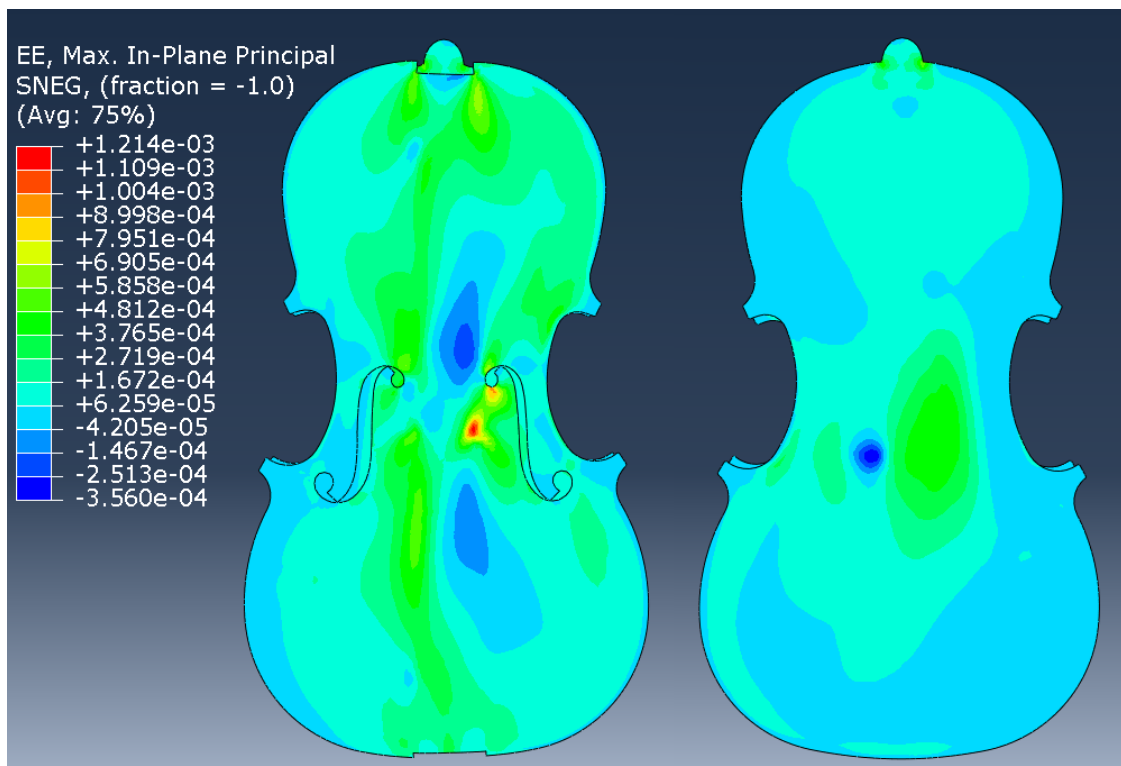
Figure 6.10: Elastic strain on the back- and top plate caused by tensioning of the strings.

Deformation fields for the violin plates in out of plane direction. (Figure 6.11).
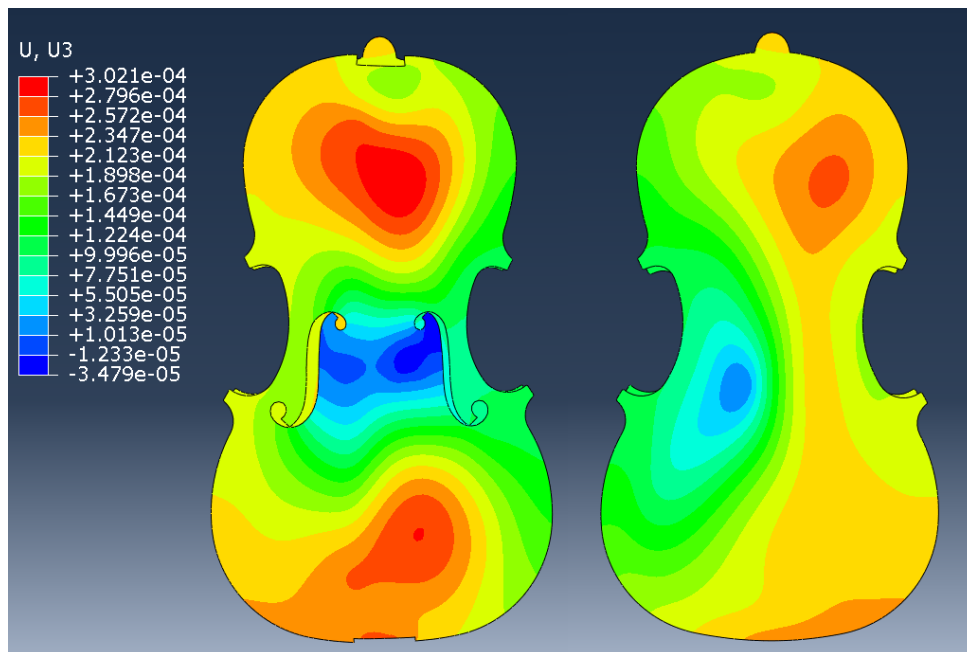
Figure 6.11: Deformation field of the tensioned violin viewed from top and back.

An exaugurated deformed shape (scale factor of 100) of the violin box is presented in Figure 6.12
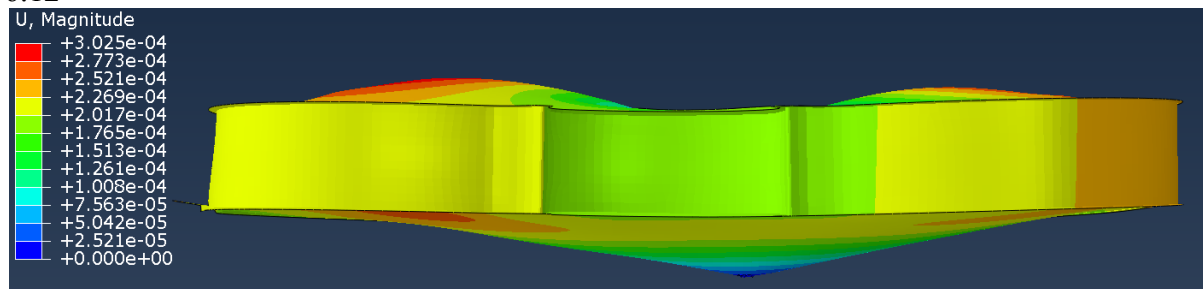
Figure 6.12: Deformed shape of the pre-stressed violin box with the deformations scaled by a factor of 100.

In both Figure 6.11 and Figure 6.12 the deformations are presented in reference to the sound post, meaning the sound post is considered stationary while the violin deforms around it.

6.6   Discussion of results

Adjusting the tension stress of the strings individually proved to be an effective way of tuning the strings to the right frequency. Tensioning the beams increases the stiffness in transverse direction resulting in higher natural frequencies. Through the iterative process of adjusting the tension of one or two strings at a time and calculating the resulting string modes the right tuning was achieved rather quickly.

When calculating the string modes, it was noted that the first bending mode always appeared two times at approximately the same frequency. The difference lied in the mode shape of the box-structure. The two modes of the G-string and the D-string involved either a rocking motion of the centre bout or a longitudinal twisting of the centre bout. The A-string modes involved rocking up and down of either the left or right C-bout. The E-string modes involved rocking up and down of the centre bout or transversal twisting of the centre bout.

Figure 6.9 shows that the stresses are higher in the top plate compared to the back plate overall. This is because the stresses from the strings are transferred through the bridge directly to the top plate and then to the back plate through the sound post and the ribs.

There are some interesting stress concentrations. The highest stress concentration in the top plate is caused from the bridge under the treble foot, below the E-string. The stresses in the E-string is larger compared to the other strings (Table 6.3) which could cause the higher stresses. The location of the bass bar, below the bass foot (under the G-string) could be a reason for the stresses being lower at the other feet, since it stiffens up that part of the top plate. The stresses in the sound post are high, which was expected since it connects the plates together, this is especially noticeable in the back plate. At the upper bout of the top plate there is a stress concentration at the top of the bass bar. Stresses are also high at the lower saddle, probably because the stresses from the strings are transferred from the tail piece to the lower saddle to a small area. The same reasoning applies to the top of the plates where the neck is connected.

The deformation of the violin plates and the violin box is displayed in Figure 6.11 to Figure 6.12 with reference to a node at the bottom edge of the top plate. The deformation of the box is what's expected from adding tension to the strings. The neck and lower saddle "pull" the bouts up. The lower and upper bout deforms around the middle part, i.e. the bouts deform in one direction and the middle part in another.

7 FE-analyses on the complete violin

With the strings attached and tuned the model is complete and analyses can be performed. The first analysis done is applying creep effects to the violin to study how the deformations change over time. The results from the creep analysis is used to study the change of a geometric property called straight tangent lines (STL). The second analysis performed is a steady state analysis where the strings are pulled to mimic the behaviour of the violin when it's being played.

7.1 Implementing creep on the violin

As discussed in chapter 3.1 creep is a very complicated phenomena that depend on various factors, leading to it being difficult to model, especially long-term creep. In this section a method of analysing creep in Abaqus is presented. The creep model is then added to the complete violin model to study how creep deforms the violin. A specific focus is put to study the change of STLs in a long-term perspective.

7.1.1 Modelling creep in Abaqus

Abaqus differs between a time-hardening version and a strain-hardening version of creep. Time-hardening is only recommended to use when the stress is relatively constant over time, which is a valid assumption for the violin since the stresses caused by the strings should not vary much with time (Dassault Systèmes, 2012). Therefore, only the time-hardening power-law is considered. The time-hardening power-law is in Abaqus expressed as:

$$\dot{\bar{\varepsilon}}^{cr} = A\tilde{q}^n t^m \quad (7.1)$$

$\dot{\bar{\varepsilon}}^{cr}$ is the uniaxial equivalent creep strain rate, it's expressed as:

$$\sqrt{\frac{2}{3}\dot{\varepsilon}^{cr} \cdot \dot{\varepsilon}^{cr}} \quad (7.2)$$

$\tilde{q}$ is, in the case of anisotropic material, the Hill's anisotropic equivalent deviatoric stress and t is the total time. A, n and m are constants.

Tissaoui (1996) performed experimental tests both on short term and long-term creep for different types of wood, including southern pine, Douglas-fir, yellow poplar and Parallam. The long-term creep tests were fitted to power laws, like equation (3.2) to find expressions for long term creep. Also, FE-analyses in Abaqus were performed. The results of this study are used as in data in the violin FE-model. What's provided from Tissaoui (1996) is the correlation between experimental tests and values of the constants, A, n and m for wood, equation (7.1).

The parameters are added as material properties in the *property module*. The factors include:
- Power law multiplier, A
- Equivalent stress order, n
- Time order, m

In Abaqus creep is added as a viscous step in the *step module*. Factors to decide are total time of the step and the increment step, i.e. at what times equilibrium is to be calculated.

7.1.2   Straight tangent line

An interesting aspect to consider, using the violin model created is whether luthiers during the 17th and 18th century created the arching shape of their plates in a way where STLs were present, or if it's an effect of creep in the wood over a long time. For a description of the geometric shape of the violin plates including the STLs the reader is referred to chapter 2.2.

To get a definite answer to if this was an aspect considered 300 years ago is of course impossible without more information of the techniques used during this time. But with the possibility of performing analyses that include creep effects, the state of STLs over time can be studied. This will give an indication if STLs are a phenomenon considered by old luthiers or a geometric property developed over time.

The idea behind the STLs is that they, if present in the plates, the centrelines of the outer and inner STLs on the plates compose the framework of a four-sided octahedron, see Figure 7.1. Such a structure is efficient at carrying loads applied at the apex, i.e. where the bridge is located. It can be argued that making use of an efficient load carrying structure in the design of the plates allows for the use of thinner plates without compromising the overall strength of the structure. Assuming that the robustness of the framework keeps the STLs relative stationary one would predict to see larger deformations in the sides of the framework.
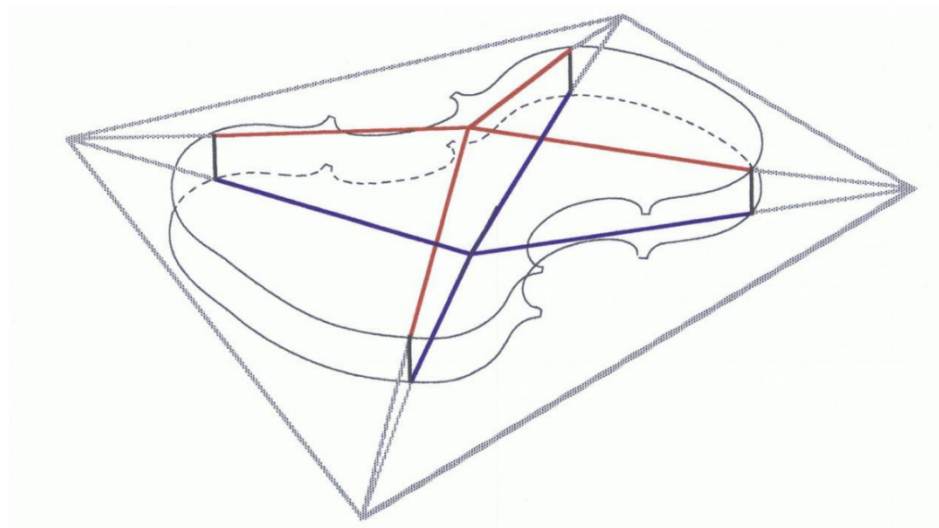
Figure 7.1: Framework created by STLs (Zuger, 2012a).

If one considers the deformations of the plates by the tension of the strings (Figure 6.11) with the STLs in mind it appears that upper and lower bout deflects positively while the side bouts deflect negatively. This indicates that a rotation of the STLs around their longitudinal axis has taken place in order to facilitate the deflections caused by the static string-loads.
The deflecting areas largely correspond to the sides of the STL framework, lending credence to the idea that the STLs indeed effects the load paths and deflections of the structure.

7.1.3   Applying creep to the violin model

Creep parameters are added as material properties in the *property module*. Input parameters are collected from Tissaoui (1996). Mean values for Douglas-fir from 4 different samples is

calculated from tests performed in compression. The same values of parameters are set for all parts modelled with maple and spruce. Creep in other parts are neglected (Table 7.1).

Table 7.1: Material parameters used to model creep added in the property module (Tissaoui, 1996).

A	4,08E-13
n	1
m	-0,98499

The creep steps are added after the pre-stressing step, i.e. strings are pre-stressed and equilibrium in the system is calculated and then the creep step is added. The time set for the creep analysis is 100 years. 3 creep steps are used in total. The first step is for the first 30 days. The second step from 30 days up to 1 year. The third step is between 1 and 100 year. For all steps of the analysis the increment step is set to 10, i.e. 10 equilibriums are calculated for the first 30 days, then 10 equilibriums between 30 days and 1 year and lastly 10 equilibriums between 1 year and 100 years. The creep effects are assumed to be greatest at the beginning. Non-linear geometry is used in all steps.

The calculation steps to perform the creep analysis on the complete violin are as follows:
- Static general steps: Calculate the pre-stressed state of the model
- Viscous steps to model creep. One step for each time period. All steps are divided into 10 increments.

7.1.4 Results of creep analysis
Figure 7.2 and Figure 7.3 displays a time series of the creep strain in the top and back plate after 30 days, 1 year and 100 years. The lines drawn onto the plots are the STLs.
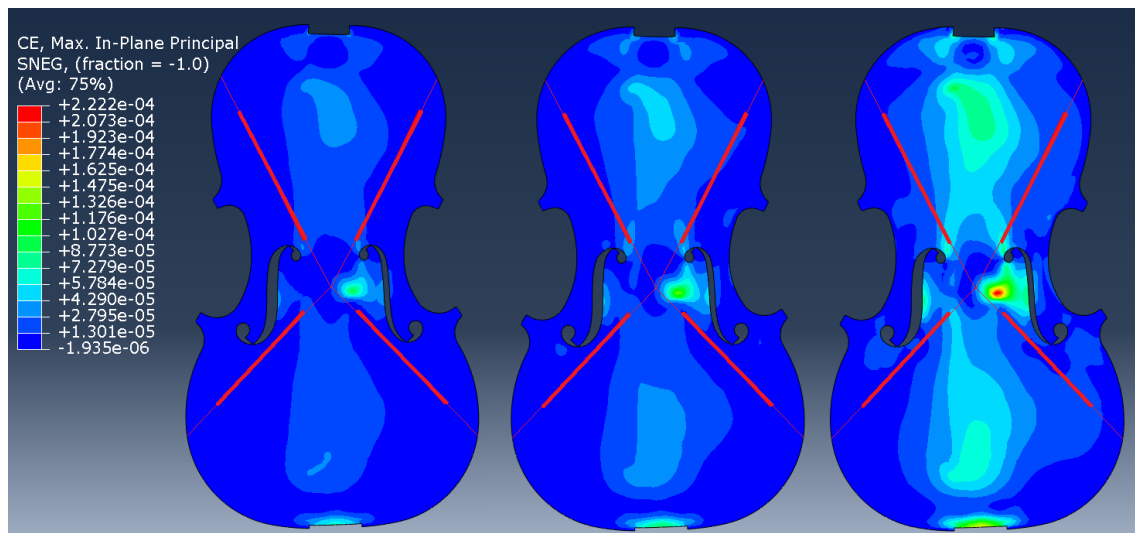
Figure 7.2: Maximum in plane creep strain for the top plate. From the left: 30 days, 1 year and 100 years. The red lines are the STLs.
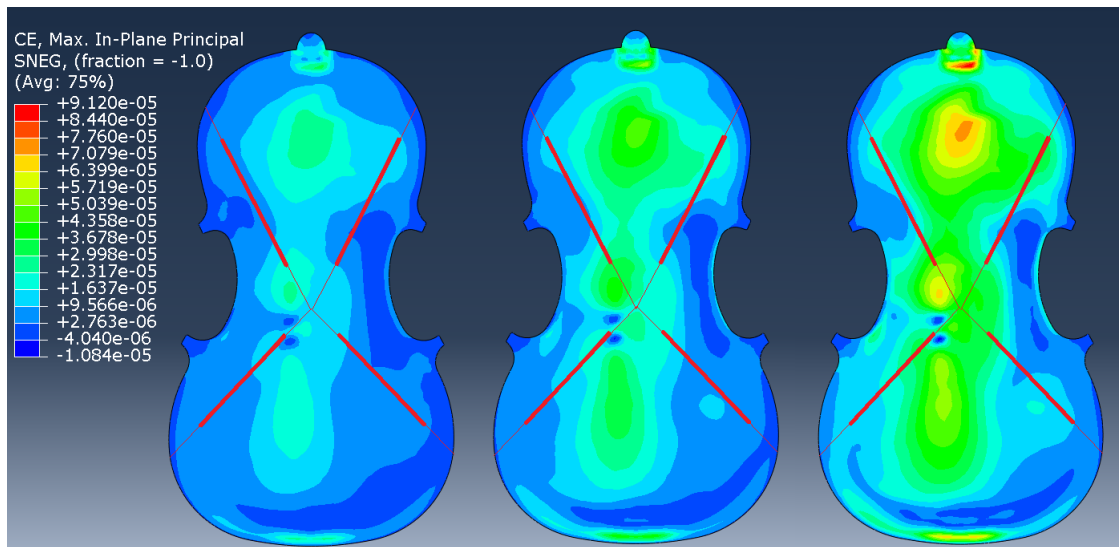
Figure 7.3: Maximum in plane creep strain for the back plate. From the left: 30 days, 1 year and 100 years. The red lines are the STLs.

Figure 7.4 displays the creep strain as a function of time for one element in each plate. The location of the elements is at the upper bout at the longitudinal centre line for both plates.
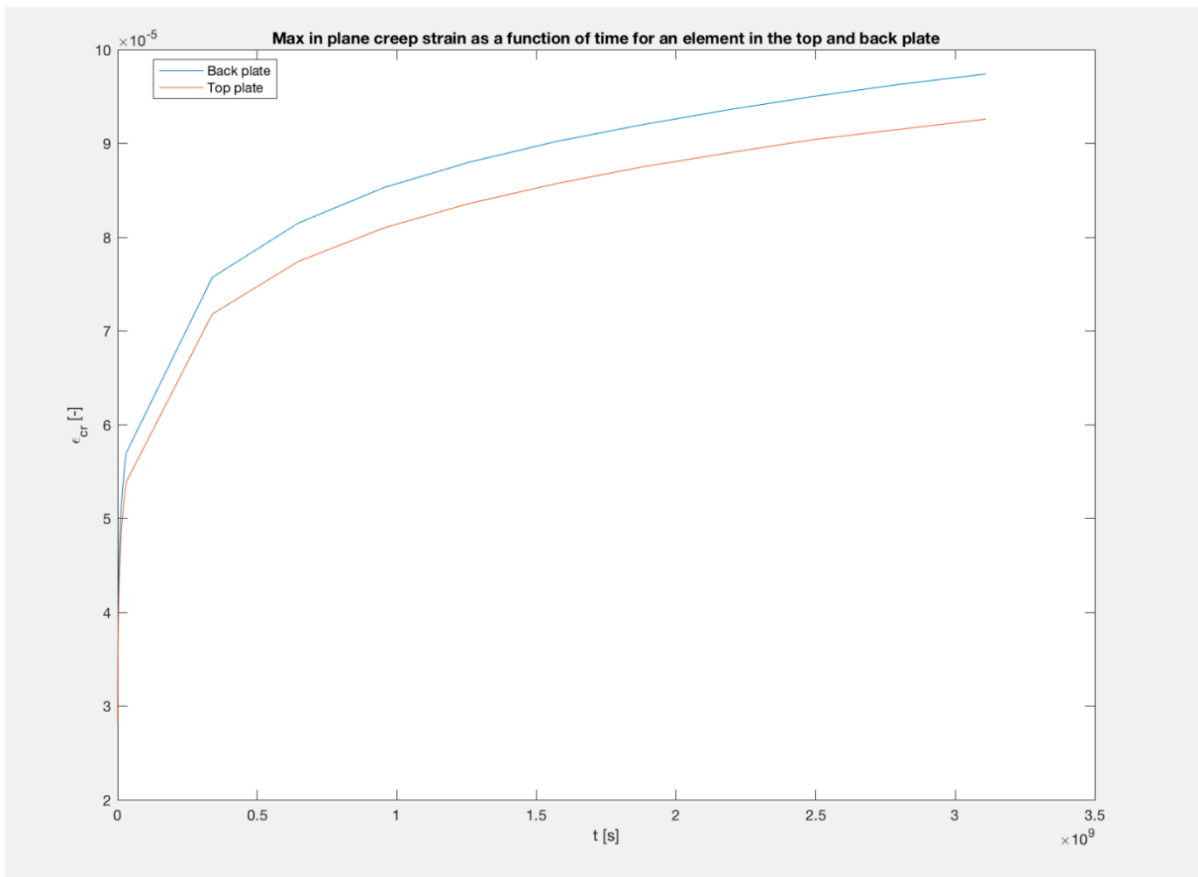
Figure 7.4: Creep strain as a function of time for one element in each plate.

Figure 7.5 and Figure 7.6 displays a time series of the deformations caused by creep in the top and back plate after 30 days, 1 year and 100 years. The lines drawn onto the plots are the STLs.
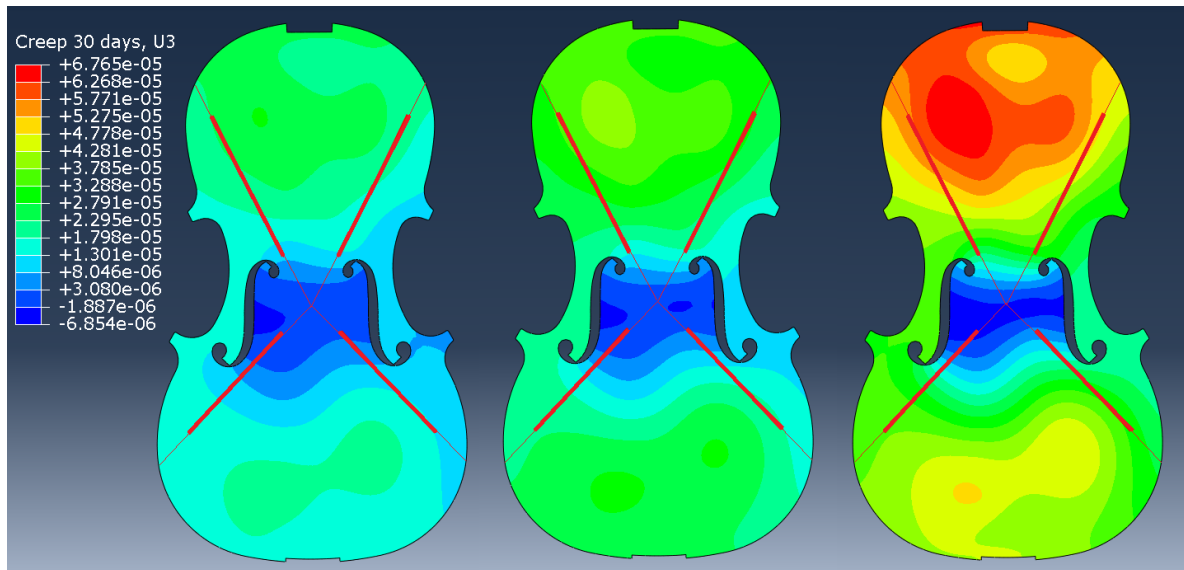
Figure 7.5: Deformation in out of plane direction for the top plate. Form the left: 30 days, 1 year and 100 years. The red lines are the STLs.
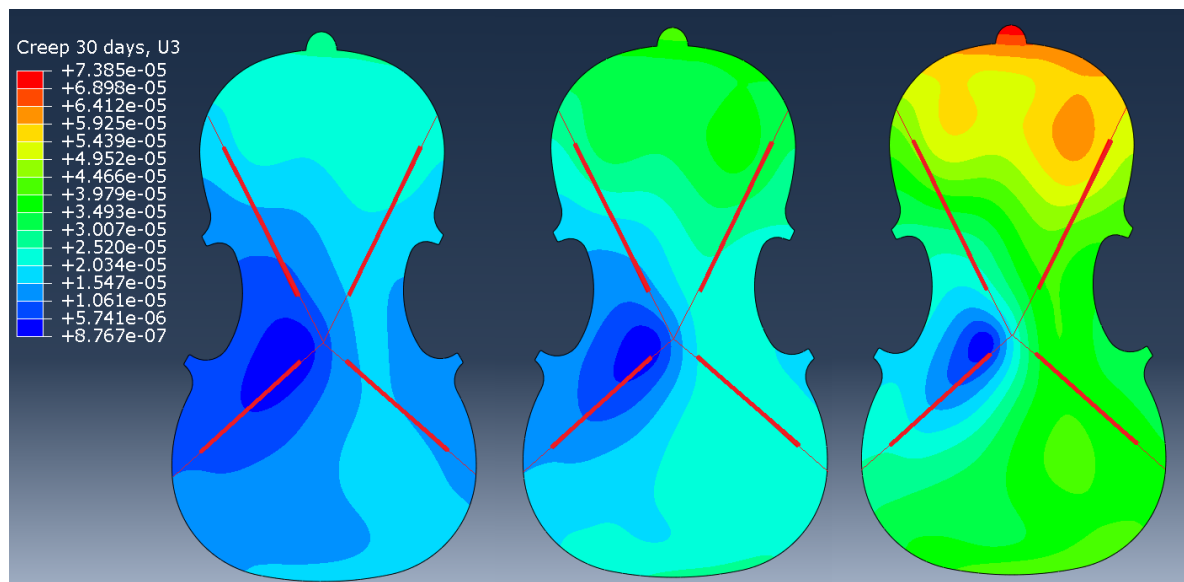
Figure 7.6: Deformation in out of plane direction for the back plate. Form the left: 30 days, 1 year and 100 years. The red lines are the STLs.

7.1.5 Discussion of creep results

From how the creep strain evolve over time (Figure 7.2 and Figure 7.3) it's clear that the creep strain does have an effect on the plates in the same regions as the strain caused by the tension in the strings, which was expected. If one compares the creep strain to the strain caused by tensioning the strings (Figure 6.10) it's evident that the creep strain compared to the strain caused by tensioning the stings is not major. The instrument deforms more from the strings than it does by creep after 100 years with the creep model used.

Figure 7.4 displays that a lot of the creep strain takes place during the first year which was expected. An interesting aspect is that the curves do not flat out even after 100 years.

This analysis has shown a possible method for modelling creep in a complete violin model by using a time hardening power law in a long-time perspective. To be able to validate the results

more research is necessary. The parameters used (Table 7.1) would have to be modified to accurately describe maple and spruce used in violins. This could be accomplished with experimental tests on equivalent wood specimens as done by Tissaoui (1996). The effects on the results is difficult to foresee. But one aspect that probably would stay the same are the regions affected by creep (Figure 7.2 and Figure 7.3), while the value of strain would differ. Another aspect to consider would be to include more complicated creep models by taking into account creep in the secondary phase (equation 3.3). By doing this more accurate results after a long time might be possible.

To get an insight in how modifying the parameters in Table 7.1 would affect the results it's easier to look at the curves in Figure 7.4, which follow the typical shape of power laws (equation 3.1) (Wadsö, 2018). Tissaoui (1996) used three different sets of parameters when computing the effect of creep on a dome structure built up by wood frames. The results showed a large difference in vertical displacements, but the shape of the curves is more or less the same. The expected results with other parameters are thereby an offset of the curves in Figure 7.4.

Another important aspect is the moisture level. Violins are always kept indoors in favourable climate. The long-term creep tests performed by Tissaoui (1996) were conducted in a room with 12 % moisture content, which would be a reasonable place to keep a violin.

The creep along the STLs (Figure 7.2 and Figure 7.3) is not large which indicate that creep does not affect the STLs substantially. It's low enough that it's not certain that it would be noticeable. The magnitude of the creep deformation is displayed in Figure 7.5 and Figure 7.6. A possible outcome of the analysis was that there would be a clear creep deformation forming around the lines, making the lines more distinct, which is not the case. This would have indicated that creep in old violins were a reason for the forming of the STLs. To get a clearer understanding on if STLs are a product of the methods used by luthiers in the 17th century, or a result of creep deformation, different arching shapes and geometry has to be analysed and compared.

7.2   Steady state analysis

The goal of performing the steady state analysis is to study the behaviour of the violin box when the strings are pulled. Since the sound from the violin is caused by vibrations of the violin box, the volume change of the violin plates over a frequency range is studied. The analysis is performed with a modal steady state analysis, each string is exited at a position where the bow would be used.

To perform a modal steady-state analysis the modes of the system needs to be extracted beforehand. A linear perturbation frequency step was added before the steady state steps to calculates all modes in the span 50-1000 Hz based on the pre-stressed state of the violin. These modes are used in the steady-state step to calculate the steady-state amplitude of the system through superposition techniques. Structural damping of 5% was added to all participating modes.

The calculation steps necessary to perform the modal steady-state analysis in Abaqus are as follows.
- Static general steps. Calculates the pre-stressed state of the model
- Linear perturbation frequency. Extracts all modes in the frequency span 50-1000 Hz.

- Steady-state modal. Calculates the steady-state response to an 1N G-string excitation.
- Steady-state modal. Calculates the steady-state response to an 1N D-string excitation.
- Steady-state modal. Calculates the steady-state response to an 1N A-string excitation.
- Steady-state modal. Calculates the steady-state response to an 1N E-string excitation.

To judge the change in volume of the violin box-structure the mean displacement of the top and back plate was calculated from the steady-state analysis. A difference in mean displacement of the top and back plate would indicate a change in volume of the box structure. The mean values are calculated from a set of approximately 1000 nodes each from the top and back plate.

7.2.1   Physical behaviour of the strings
By stroking a string with the bow, the string is pulled along due to the friction between the string and bow. As the string deforms the tension increase and ultimately the string will slip from the bow and rebound. The bow can now catch the string again and the process is repeated in a periodic manner for the duration of the bow stroke. When the bow catches the string, it creates a kink in the string which travels from the bow through the wire and is reflected at the upper saddle. When the kink returns to the bow the tension in the string causes the string to slip from the bow. This interaction causes what's called a Helmholtz motion of the string (Wolfe, u.d.). For the stick and slip interaction to occur properly, appropriate force needs to be applied to the string by the player, which depends on the tension of the string, the friction between the string and the bow and how close to the bridge the string is played.

A study performed by Askenfelt (1986) where bow force was measured using specialized bows, found the bow force to typically vary between 0,5 and 1,5 N. Based on that study a force of 1 N was used to excite the strings during the steady-state analysis.

7.2.2   Implementing a force on the strings
In a steady-state analysis preformed in Abaqus any concentrated load added to a node in the system is assumed to vary sinusoidally in the frequency span defined for the analysis step (Dassault Systèmes, 2012). The stroke of a bow can be modelled by adding a partition to the wire structure representing the string between the fingerboard and the bridge. The node at the partition is assigned a concentrated load in the direction a bow stroke would have. As Abaqus interprets the applied force as a sinusoidal force the strings also takes on a sinusoidal shape when excited. A true Helmholtz motion of the strings could thus not be achieved.

7.2.3   Results of steady state analysis
Mean displacements for the violin plates in the out of plane direction, over the frequency range when the strings are exited are presented in Figure 7.7 to Figure 7.10. Mean displacement is calculated from a subset of 1000 nodes on the top and back plate.
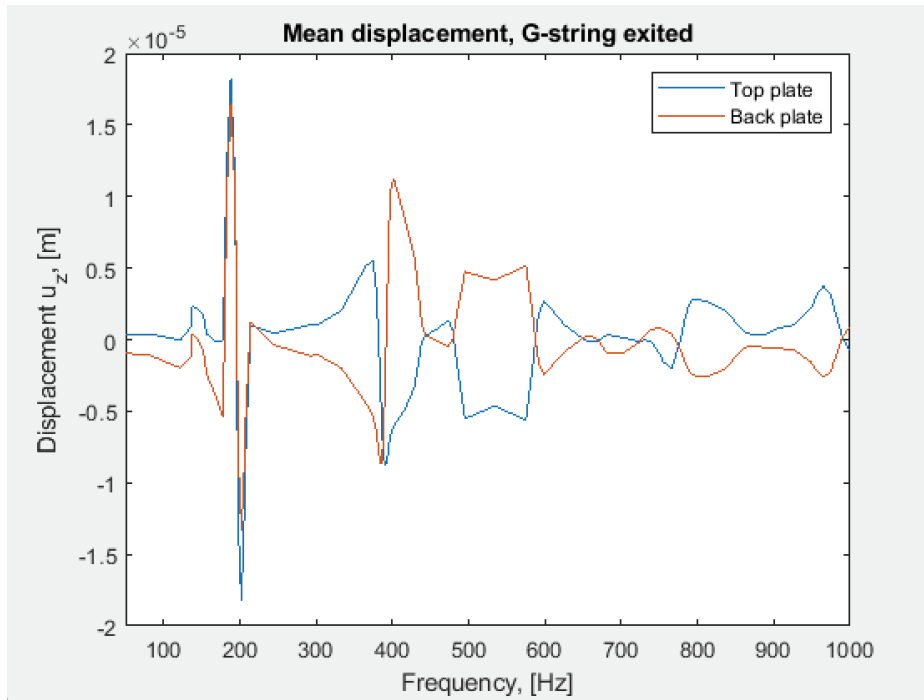
Figure 7.7: Mean displacement over the frequency range when the G-string is exited.
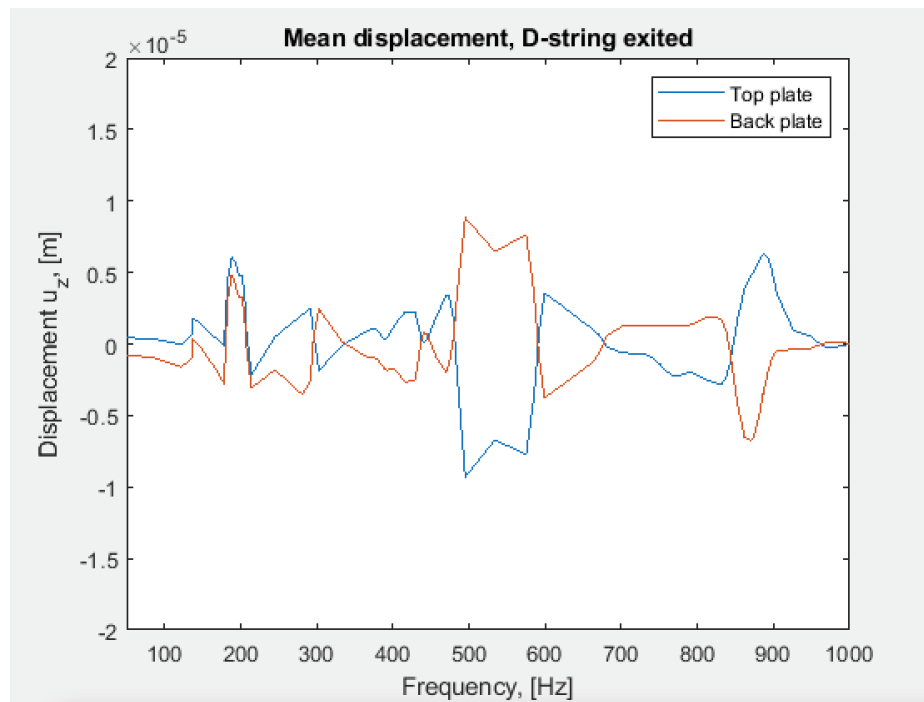
Figure 7.8: Mean displacement over the frequency range when the D-string is exited.
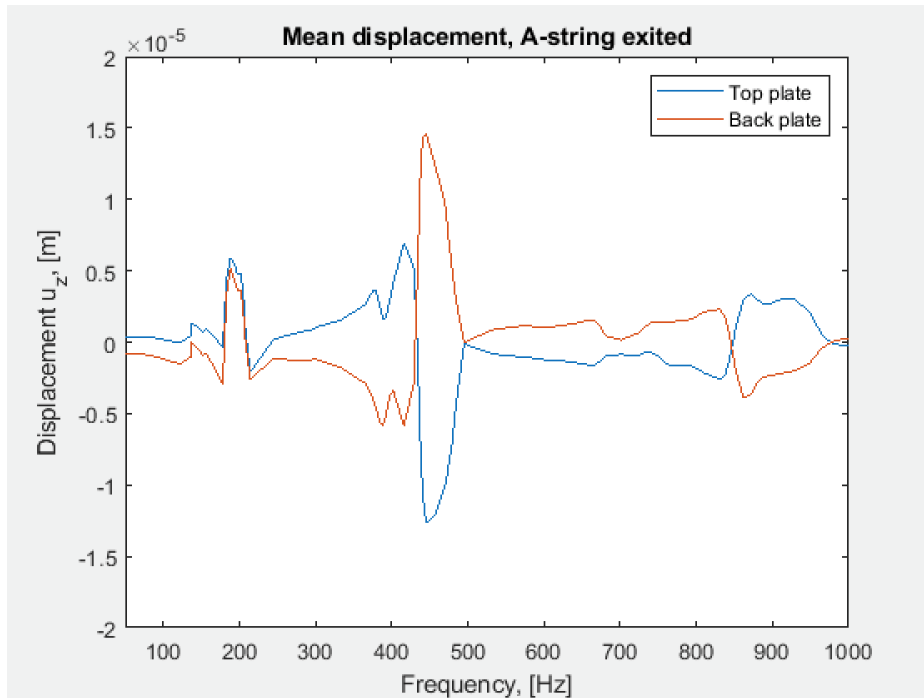
Figure 7.9: Mean displacement over the frequency range when the A-string is exited.
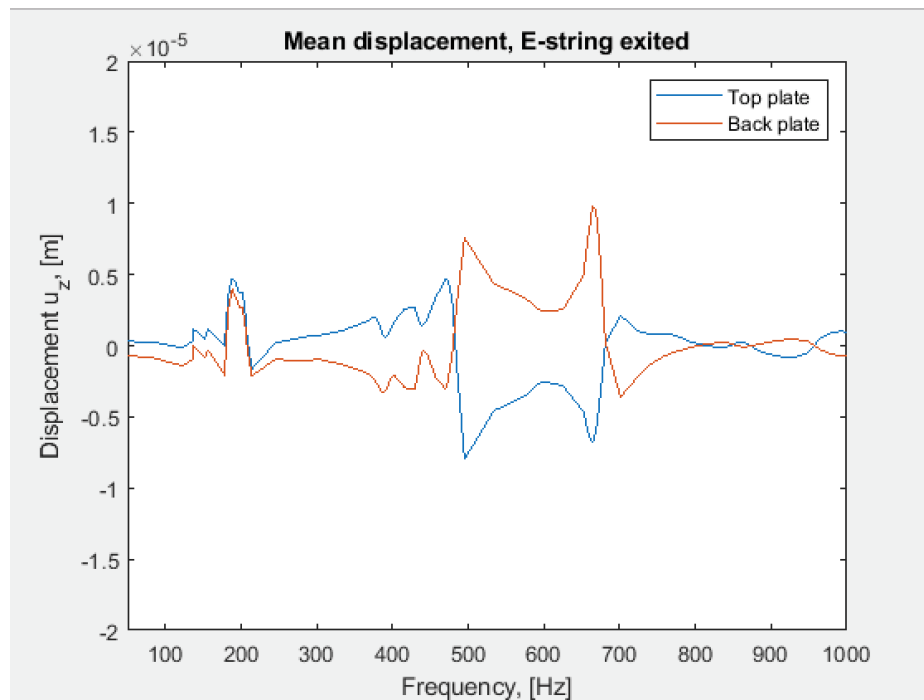
Figure 7.10: Mean displacement over the frequency range when the E-string is exited.

7.2.4   Discussion of steady state results

The plots in Figure 7.7 to Figure 7.10 reveal frequency spans where the relative mean displacement between the top plate and back plate are large, indicating large volume changes in the box structure. It is also noted that for all plots the displacements at the lower frequency range (50-180 Hz) the relative displacement is small. This span is followed by a frequency range (180-215 Hz), where the plates vibrates in phase. After this the plates displace out of phase in the remaining frequency span. All plots show areas where the relative displacement of the plates is especially large.

8 Conclusions

The objective of this project to create a FE-model of a complete violin with pre-stressed strings has been fulfilled. The violin plates were calibrated successfully based on the modal characteristics measured from two violin plates provided by R. Zuger. The material parameters used for the plates are probably close to the real ones since the experimental modal analysis correlated very well to the analysis of the FE-model. To further verify the behaviour of the complete model, experimental modal analysis of a complete instrument would be necessary.

The plate materials, spruce and maple are used for the majority of the violin parts. Since it is recommended that the violin parts of the same material are gathered from the same specimen, the behaviour of all spruce and maple parts should at least resemble those of the plates. It is not guaranteed though, as stated in chapter 3, specimens gathered from the same source can present different material properties. Experimental modal analysis of the complete instrument would also lead to the possibility of determining the material properties of the parts modelled with other material parameters. The conclusion is that the created FE-model should behave closely to a real instrument built with the same plates. It is, however, a question how the connections behave. In the model, all parts are modelled as being rigidly tied together. In the real structure the parts are glued together that can result in a joint with lower stiffness.

A model of a complete violin has been developed which can be used for further studies regarding geometric and dynamic properties. In an effort to show the capabilities of the model, studies have been performed to analyse the behaviour of the complete instrument, including steady state analysis and creep analysis.

The analyses were performed successfully, but to get a better understanding of the properties influencing the results more extensive analyses are needed with more specified input data. To obtain more accurate results for long term creep more complicated creep models should be investigated. In regard to the steady state analysis values for the modal damping has to be examined combined Helmoltz motion of the string force. The main issue with the analyses are that there is no possibility for verification of the results. This would require experimental tests performed on the complete violin.

The geometric property studied in this project was change of STLs in a long-time perspective, but with the complete model in place it is possible to study other geometric properties. One difficulty when performing analyses with the goal to study geometric properties is that to observe the implications the geometry has to be modified, which would mean changing the geometry of the model.

Building the geometric model of the complete violin was a more difficult task than anticipated which had implications on the time frame of the project. Building a violin is hard, in real life as well as creating a geometric model. Small adjustments in the geometry had large implications when assembling the complete instrument. The time spent on creating the geometry had implications on performing extensive analyses on the complete model.

8.1 Further studies

One constant issue with the analyses performed on the complete violin is verification of the results, which would require more in-depth, time consuming studies with the possibility of comparing results. Proposed further studies are thereby more specific analyses on the complete model to research the behaviour of the instrument more accurately.

- Perform experimental modal analysis on a complete violin to determine the modal characteristics of the full instrument.

- Perform studies to obtain damping parameters for the violin. Model the correct string force with Helmoltz motion. With accurate damping parameters and the correct motion shape a more accurate steady state analysis is possible.

- Study creep for actual violin parts. Performing more complicated creep analyses to get a better understanding of the violins behavior over time. This includes experiments to obtain creep parameters specifically for spruce and maple.

- Studies regarding the impact of geometric properties on the harmonic content. By modifying geometrical parameters, like arching shape, thickness, etc. a deeper understanding of the importance of certain factors is possible. This type of information could help violin makers create better instruments.

9 Bibliography

Askenfelt, A., 1986. Measurement of bow motion and bow force in violin playing. *The Journal of the Acoustical Society of America ,* 80(4), pp. 1007-1015.

Bretos, J., Santamarıa, C. & Moral, J. A., 1999. Vibrational patterns and frequency´ responses of the free plates and box of a violin obtained by finite analysis. *The Journal of the Acoustical Society of America,* 105(3), pp. 1942-1950.

Brüel & Kjær, 2008. *PRODUCT DATA Miniature Impact Hammer – Type 8204.* [Online]
Available at: https://www.bksv.com/-/media/literature/Product-Data/bp2077.ashx
[Accessed 10 April 2020].

Brüel & Kjær, 2018. *PRODUCT DATA Piezoelectric Accelerometer Types 4507 and 4508.* [Online]
Available at: https://www.bksv.com/-/media/literature/Product-Data/bp1841.ashx
[Accessed 10 April 2020].

Buksnowitz, C. et al., 2007. Resonance wood [Picea abies (L). Karst.]. -evaluation and prediction of violin makers' quality – grading. *The Journal of the Acoustical Society of America,* 121(4), pp. 2384-2395.

Burström, P. G., 2007. *Byggnadsmaterial.* 2:3 ed. Lund: Studentlitteratur.

Carlö, J. A. & Sanborn, G., 1965. *Fiolbyggnadskonsten.* Göteborg: Christerssons Tryckeri.

Chopra, K. A., 2015. *Dynamics of Structures.* 4th ed. s.l.:Pearson Education Limited.

Curtin, J., 2006. Tap Tones and Weights of Old Italian Violin Tops. *Violin Society of America Papers,* 1(2).

Dagnell, J. & Sarnell, S., 1988. *Bygg din egen fiol.* Västerås: ICA bokförlag.

Dassault Systèmes, 2012. *Abaqus/CAE User's Manual.* [Online]
[Accessed 2020].

Døssing, O., 1988a. *Structural Testing Part I: Mechanical Mobility Measurements.* [Online]
Available at: https://www.bksv.com/media/doc/br0458.pdf
[Accessed April 2020].

Døssing, O., 1988b. *Structural Testing Part II: Modal Analysis and Simulation.* [Online]
[Accessed April 2020].

Fu, L., Zhang, A. & Jia, R., 2014. *New Devices or Testing Effective Material Properties of Free Violin Plates.* Beijing, The 21st International Congress of Sound and Vibration.

Gough, C., 2015. Violin plate modes. *The Journal of the Acoustical Society of America,* 137(1), pp. 139-153.

Knot, G. A., Shin, Y. S. & Chargin, M., 1989. A Modal Analysis of a Violin. *Finite Element in Analysis and Design,* 5(3), pp. 269-279.

Loen, J. S., Borman, T. M. & King, A. T., 2005. Path through the woods. *The Strad,* Volume September 2005, pp. 68-75.

Lu, Y., 2013. *Comparison of Finite Element Method and Modal Analysis of Violin Top Plate,* Montreal, Canada: s.n.

Manege, A. U., 2018. *Hammer Impact Considerations.* [Online]
Available at: https://www.crystalinstruments.com/blog/2018/11/27/hammer-impact-test-considerations
[Accessed April 2020].

Marshall, K. D., 1985. Modal Analysis of a Violin. *The Journal of the Acoustical Society of America,* 77(2), pp. 695-709.

Molin, N. E., Lindgren, L.-E. & Jansson, E. V., 1988. Parameters of violin plates and their influence on the plate modes. *The Journal of the Acoustical Society of America,* 88(1), pp. 281-291.

Ottosen, N. & Petersson, H., 1992. *Introduction to the Finite Element Method.* Harlow: Pearson Education Limited.

Pástor, M., Binda, M. & Harčarik, T., 2012. Modal Assurance Criterion. *Procedia Engineering,* Volume 48, pp. 543-548.

Persson, K., 2000. *Micromechanical modeling of wood and fibre properties,* Doctoral Thesis: Lund University.

Pyrkosz, M. A., 2013. *Reverse Engineering the Structural and Acoustic Behavior of a Stradivari Violin,* Michigan Technological University: s.n.

Radeş, M., 2010. Performance of Various Mode Indicator Functions. *Shock and Vibration,* Volume 17, p. 474.

Richardson, M. H., 1986. *Global Frequency & Damping Estimates from Frequency Response Measurements.* Los Angeles, CA, U.S., 4th IMAC Conference.

Richardson, M. H. & Formenti, D. L., 1982. *Parameter Estimation from Frequency Response Measurements using Rational Fraction Polynomials.* Orlando, FL, U.S., 1st IMAC Conference.

Richardson, M. H. & Formenti, D. L., 1985. *Global Curve Fitting of Frequency Response Measurements using the Rational Fraction Polynomial Method.* Orlando, FL, U.S., 3rd IMAC Conference.

Riechers, A., 1928. *Violen och dess byggnad.* Stockholm: Gottfr. Johanssons Musikförlag.

Ristinmaa, M., 2019. *Introduction to Non-linear Finite Element Method.* Division of Solid Mechanics Lund University: s.n.

Ross, R. J., 2010. *Wood handbook: wood as an engineering material,* Forest Products Laboratory: Centennial ed. General technical report FPL; GTR-190. Madison, WI: U.S. Dept. of Agriculture, Forest Service.

Sproßmann, R., Zauer, M. & Wagenführ, A., 2017. Characterization of acoustic and mechanical properties of commontropical woods used in classical guitars. *Results in Physics,* Volume 7, pp. 1737-1742.

Stoel, B. C. & Borman, T. M., 2008. A Comparison of Wood Density between Classical Cremonese and Modern Violin. *PLoS ONE 3(7): e2554.*

Swedish Wood, 2015. *Design of timber structures: Structural aspects of timber construction.* Stockholm: Swedish Forest Industries Federation.

Tissaoui, J., 1996. *Effects of Long-Term Creep on the Integrity of Modern Wood Structures.,* Dissertation: Virginia Tech.

Waddle, J., Rossow, S. & Sirr, S., 2014. Climate Conundrum. *The Strad,* Volume April 2014, pp. 61-63.

Wadsö, L., 2018. *Construction Materials Science.* Lund: s.n.

Wolfe, J., n.d. *Bows and strings.* [Online]
Available at: https://newt.phys.unsw.edu.au/jw/Bows.html
[Accessed May 2020].

Wolfe, J., n.d. *How does a violin work? - An introduction to violin acoustics.* [Online]
Available at: http://newt.phys.unsw.edu.au/jw/violintro.html
[Accessed March 2020].

Yamaha, n.d. *How a violin is made: Selecting the right piece of wood.* [Online]
Available at: https://www.yamaha.com/en/musical_instrument_guide/violin/manufacturing/
[Accessed 24 April 2020].

Zuger, R., 2012a. *Making the Violin Geometric Arching Shape and A Method of Thickness Graduating Plates,* Bjuv: s.n.

Zuger, R., 2012b. *The impact of Arching Shape on Structural Deflections,* Bjuv: s.n.